ABSTRACT

Title of Dissertation:	FEEDBACK-CONTROLLED BIOELECTRONIC HYBRID SYSTEM ENABLED BY ELECTROGENETIC CRISPR
	Sally Patricia Wang, Doctor of Philosophy, 2023
Dissertation directed by:	Professor William E. Bentley, Fischell Department of Bioengineering

With the rise of concepts like the "internet of things" and the advances in electronic technologies, our lives have now been occupied with smart devices that easily communicate with one another. These devices, however, lack the ability to freely exchange information with the world of biology, since electronics and biology possess very different communication modalities. Recently, the field of "electrogenetics" was introduced by enlisting redox mediators like hydrogen peroxide as a novel signaling medium to facilitate the connection between electronics with biology. In this dissertation, we expanded the electrogenetic framework and established a complete network of Bio-Nano Things, which collectively allowed automated, algorithm-based feedback control of electrogenetic CRISPR activity. First, we engineered the abiotic/biotic interface in order to improve information transfer between electronics and biological systems. Inspired by nature, we created an "artificial biofilm" that immobilized living cells on the surface of the electrode by electrochemically assembling bacteria and thiolated polyethylene glycol (PEG-SH) to form a thin film. We then endowed the PEG-SH hydrogel with redox capabilities via conjugation to generate

an interactive material that can autonomously synthesize hydrogen peroxide to initiate communication with a bacterial population. Additionally, a polycysteine-tagged *Streptococcal* protein G was introduced for PEG-SH hydrogel surface decoration to enable the recognition of cells and other biological molecules. Next, we developed *oxyRS*-based electrogenetic CRISPR to broaden the bandwidth of electrochemical signaling, allowing multiplexed transcriptional regulation on various genetic targets. These include two crucial quorum sensing genes that controlled the relay of electrochemical signals to a broader yet selective audience of microbial populations through quorum sensing communication. We then integrated the engineered interface with eCRISPR-mediated transcriptional regulation to present "Biospark", a full electrogenetic system including custom-made hardware and software, for algorithm-governed automated control of gene expression. Finally, we demonstrated a network of Bio-Nano Things by connecting the Biospark system with another custom bio-electrochemical device and even users to achieve remote feedback control of eCRISPR activity and more importantly, multidirectional communication between living systems regardless of physical distance. Together, we believe this work represents a huge leap toward making "smarter" devices and networks that can seamlessly guide biological processes with electronic input and can spawn various applications in the fields of biotechnology.

FEEDBACK-CONTROLLED BIOELECTRONIC HYBRID SYSTEM ENABLED BY ELECTROGENETIC CRISPR

by

Sally Patricia Wang

Dissertation submitted to the Faculty of the Graduate School of the
University of Maryland, College Park, in partial fulfillment
of the requirements for the degree of
Doctor of Philosophy
2023

Advisory Committee:
Professor William E. Bentley, Chair
Professor Gregg Duncan
Professor Greg F. Payne
Professor Nam Sun Wang
Professor Srinivasa Raghavan, Dean's Representative

Dedication

To mom and dad, 你們可以來接我放學回家了<3

Acknowledgments

First and foremost, thank you Dr. Bentley for all your scientific guidance, warm encouragement, and witty comments. Thank you for all the freedom you have given me to fail, to learn, to grow as a scientist, and to discover how to be an engineer.

I'd also like to thank all my committee members: Dr. Duncan, Dr. Payne, Dr. Wang, Dr. Karlsson, and Dr. Raghavan for your insights into my dissertation and proposal.

Thank you to all the past and present Bentley lab members, all of whom I will try my best to give my gratitude below:

To Chen-Yu Tsao- thank you for taking me under your wings and being my mentor in both science and life during my Ph.D. journey. Thank you for always responding to my SOS messages and never failing to come up with a solution.

To Jinyang- thank you for introducing me to the world of electrochemistry and involving me in a lot of your projects that most of this work stems from. And thank you just for being a good friend.

To my collaborators Chen-Yu Chen and John- thank you for allowing me to work with you, for your patience, and for your immense contributions to my dissertation work.

To Kristina and Eric- thank you for being the best 'senpai's in Bentley lab. I am so grateful for all the help, guidance, and encouragement you have given me. I will also cherish our lively scientific (in most times, non-scientific) discussions and all the good times we spent together in lab, in TCM, or in that heated pool at Orlando Hilton (#ACSSpring2019).

To David- You joined at a time when I was constantly doubting myself and felt extremely lost. Thank you for instilling a lot of confidence in me.

To Dana- thank you for being my ride-or-die and lab spouse for the past five years. Without you, I could probably be a hundred times more productive in lab but will also not gain all the crucial knowledge on trash TV shows and F1 racing. I will miss our Britney Fridays greatly.

To Rahma, Kayla, Monica, Nick, Briahnna, and Ben- thank you for joining to do cool science with us! Shoutout to Rahma who helped me a lot with another project that did not make it into this dissertation.

To Futoon- thank you for trusting me enough to become my mentee, a member of our F1/baking/HBO shows gang and most importantly, a great friend.

To Kimberly- what are the odds to meet someone randomly in class (and lab) and turns out you both went to the same concert in Taiwan back in 2014? Thank you for all the times we got quality boba and tacos together.

And thank you to all the other great people I met in this program. Special shout out to Divya who "made" me go to the gym and be healthy for a whole semester.

To all friends I made in Maryland, especially my flatmates in Mazza, the "Maryland girl squad", the "Cheapers", my baseball fan buddies in Miner St., and Janus- we all came to this place knowing no one, but you guys have become my family here. Thank you for your support, encouragements, laughter and all the good times.

To all my friends and family in Taiwan- knowing that y'all have my back gave me the courage to pursue this degree halfway across the world. Thank you.

Finally, to the three people who also resides in Hotel 72-1 3F-1- I am extremely grateful to be raised by two amazing scientists and proud to be the 3rd doctor in this household (it's your turn now bro?). Thank you for everything. I love you.

Table of Contents

List of Tables

List of Figures

Chapter 1. Connecting the disparate worlds of biology and electronics

ⓘThis chapter is partially adapted, with permission, from the book chapter: **Wang, S.**; Payne, G. F.; Bentley, W. E. Repurposing *E. coli* by Engineering Quorum Sensing and Redox Genetic Circuits**.** *Gene Expression and Control*, IntechOpen. 2019

1.1 Introduction

Recent feats in engineering communication between electronic devices and sensors provide us with a plethora of new "smart" technologies that greatly benefit our daily lives. For example, Internet of Things (IoT), an emerging paradigm that connects electronic devices and sensors through the internet, has revolutionized our current lifestyle. Dazzling technologies that used to only exist in science fiction films like smart cities, smart homes, pollution and energy consumption control, agriculture automation, and smart transportation are now a reality due to IoT (1). Although these achievements make our lives immensely easier, these networks still struggle to connect humans/living organisms or artificial nano-biological functional devices (e.g., engineered bacteria, human cells, nanobiosensors) to the vast IoT due to disparate modalities in communication between the electronics and biological systems. To establish such a heterogeneous and collaborative network, new communication conduits must be created since conventional electromagnetic techniques for the electronics are either not feasible for the size- and energy-constrained biological systems or not performing well *in vivo* due to physical constraints (2-4). Molecular communication, on the other hand, is one of the promising techniques to enable biology-electronics communication, as it is already utilized by natural biological systems in an incredibly energy-efficient and

robust manner (5). In this chapter, we summarize the recent approaches that aim to bridge the communication gap between electronics and biology, from rewiring native molecular/biochemical communication to several novel physical methods based on electromagnetic waves, in hopes to achieve electrically probing, interrogation, or control of biological systems.

1.2 Biochemical Molecular Communication

1.2.1 Direct Electron Transfer

While most technological devices rely on electron flow, nature designed the cell membrane to be an insulator that restricts the flow of charged species. This has made it significantly challenging to introduce a biocompatible pathway for transferring electrons across the membrane without disrupting the cell. Remarkably, a limited set of bacterial species, named exoelectrogens (6), are discovered to possess the ability to directly transfer electrons to electrodes. These include *Shewanella putrefaciens* (7), *Geobacter sulfurreducens* (8), *Rhodoferax ferrireducens* (9), or even an evolved consortium of facultative anaerobes (10) (consisting of *Alcaligenes faecalis*, *Enterococcus gallinarum, Pseudomonas* and more). These dissimilatory metal-reducing bacteria have evolved mechanisms to use electrodes as electron acceptors and for anaerobic respiration (11, 12). One of the best-understood electron transfer pathways belongs to that of *Shewanella oneidensis* MR-1 and is comprised of c-type cytochromes that are responsible for shuttling electrons from cytoplasmic and inner membrane oxidizing enzymes toward the cell surface during anaerobic respiration. Previous studies suggest that this pathway consists of an inner membrane tetraheme

cytochrome CymA, a periplasmic decaheme cytochrome MtrA, outer membrane decaheme cytochromes OmcA and MtrC, and an outer membrane β-barrel protein MtrB (13-17). Through a series of intermolecular electron transfer events from quinol to either MtrC and/or OmcA, this pathway is proposed to move electrons from the intracellular quinol pool to extracellular metal oxides, such as Fe_2O_3 (s). One major and direct application of these electron-generating species is, conceivably, generating electricity. They serve as the workhorses in many microbial fuel cells (MFC), as reviewed in (18, 19), providing alternate solutions to energy production and waste treatment to address the current global energy crisis. As the field of synthetic biology matures, it continues to provide more sophisticated tools to engineer living cells as a material for advanced biological systems and applications. Researchers are now able to rewire native extracellular electron transfer (EET) pathways to generate current as an output to be directly integrated with electronic systems, creating bioelectronic living sensors (20-22) or controlling microbial electrosynthesis and electrofermentation (23). Conversely, these pathways can be modified and ported to other chassis endowing non-exoelectrogens with new functions related to electron transfer. For example, a portion of the extracellular electron transfer chain of *S. oneidensis* MR-1 was reconstituted into the model microbe *Escherichia coli* to create a conduit for electronic communication from living cells to inorganic materials (24). Living conductive materials can also be engineered by employing native and or rewired EET pathways, as reviewed by Bird *et al.* (25).

Intracellular electron transfer pathways, contrary to the extracellular pathways, are common and have vital importance in biological systems. Essential biological

functions such as cellular respiration (26), DNA repair (27), and activation of sensory proteins (28). Through synthetic biology, direct and dynamic control over these electron transfer pathways has led to progress in metabolic engineering for chemical synthesis (29, 30). Recently, dynamic control over energy flow in metabolism was enabled by the creation of electron ferredoxin logic gates that utilize various inputs to control energy flow through a synthetic electron transfer pathway required for bacterial growth (31). Coupling this feature with the reconstituted *S. oneidensis* electron transfer pathway and endogenous sulfur assimilation proteins, Atkinson *et al.* (32) achieved real-time environmental biosensing of chemicals with an *E. coli* biosensor that generates electron flow to an electrode upon detecting thiosulfate. These living electronic sensors provide a platform that can be expanded for continuous environmental sensing and potential integration with IoT to allow alerts and smart pollution control.

1.2.2 Optogenetics

Light represents an alternative modality to interface biological systems with electronic networks since light-sensitive proteins and bioluminescent/fluorescent proteins are now routinely used in many biotechnological systems. Optogenetics combines optical and genetic techniques to design and apply light-sensitive proteins in order to control cellular processes within living organisms. Often plant-derived, light sensitive proteins such as channelrhodopsins, halorhodopsins, and other LOV domain proteins can also be found in unicellular organisms (e.g., bacteria and archaea) or higher animals (33). Upon illumination with a specific wavelength, the light-sensing domains undergo a conformational change that leads to association/dissociation with

an interaction partner or partial folding/unfolding of the protein structure, which in turn controls downstream biological processes. Optogenetic control systems resemble electronics in several ways, for example, it is highly spatiotemporal and allows for often reversible on/off manipulation of biological processes (34, 35). Light is also easily controllable and programmable through microchip controllers and optical filters, allowing direct integration with existing paradigms for electronic devices (36, 37). Recent endeavors demonstrated the translation of electronic commands into biological optogenetic responses through engineering far red/green light-triggered engineered cell systems (38, 39). The engineered optogenetically-controlled cells can produce a variant of human glucagon-like peptide 1 (shGLP-1) or mouse insulin for diabetes treatment when given a wireless electromagnetic signal that encoded the details (e.g., duration, brightness) of illumination.

While the majority of applications were originally developed in eukaryotes, optogenetics increasingly finds its way into prokaryotic (or yeast) systems to facilitate drug production/delivery, biosensing, and biomanufacturing (40). When combined with electronics, real-time and remote feedback control of cell cultures can be achieved through optogenetics regulation, as reviewed by Liu *et al.* (41). These hardware-integrated platforms enable feedback control over bacterial growth rate (42, 43), consortia composition (44), unfolded protein response in yeast (45), and gene expression in mammalian cells (46).

In addition to optogenetics, which uses light as an input, light can also be an output signal produced by biological systems to be easily fed into electronic devices via existing hardware like phototransistors or photomultiplier tubes. Following the

initial discovery of green fluorescent protein (GFP) in jellyfish *Aequorea victoria*, GFP has been widely used as a reporter for monitoring dynamic processes in biological systems (47); and likewise for bioluminescent proteins LuxCDABE (48). As a proof of concept, Mimee *et al.* (49) presented a luminescence biosensor for heme that is housed in an ingestible micro-bio-electronic device (IMBED) and demonstrated accurate diagnosis of gastrointestinal bleeding in swine. In **Chapter 5**, we also presented a bioelectronic system that employs green fluorescence as the representation of gene expression for automated feedback control of CRISPR activity.

1.2.3 Redox electrochemistry

As discussed in **Section 1.2.1**, while there are no freely moving electrons exist within biological systems, native electron transport chains transfer electrons with the help of redox molecular mediators (e.g., NADPH) and metalloproteins (e.g., iron-sulfur cluster containing proteins) (50). The dual nature of redox reactions combines the unique characteristics of both biological and electronic networks (51), therefore enabling electron-based communication that is transduced between both domains through ‘‘redox channels’’. As electrons pass through the redox molecules, their oxidative states and unique structures change accordingly, thus determining their interactions with receptors and sensor proteins. That is, we can electronically interpret or actuate the structural changes of these molecules through standard electrochemical techniques and subsequently initiate or diminish molecular communication. We argue that by harnessing native redox mechanisms, many approaches can be spawned to allow the control of biorecognition and associated genetic machinery (52) via electronic signals.

Owing to the dual nature of redox communication, researchers have engineered ways to exploit redox reactions for bridging electronic input to biological systems and translating biological output to electronics. Practicable methodologies that enable bio-to-electronics connectivity, as extensively reviewed by VanArsdale *et al.* (53), include clever ways to electrochemically detect many native redox molecules produced and generated by cells (including exoelectrogens), probe the state of complex materials and biological systems, and decode biological reporter gene activity. In this section, we focus on methods based on native redox signaling that are developed to transform electronic input into a signal recognizable by biological systems, and in turn, achieve electrogenetic control (54). First, two vital oxidative stress protein sensors, SoxR and OxyR, and their corresponding signaling pathway will be introduced.

1.2.3.1 SoxR: [Fe-S]-cluster based, superoxide/nitric oxide stress sensor.

The *E. coli soxRS* system enhances the production of ~45 proteins in response to superoxide exposure, including those in detoxification (*sodA*, manganese superoxide dismutase), DNA repair (*nfo*, endonuclease IV), maintaining cellular reducing power (*zwf*, glucose-6-phosphate dehydrogenase) and central metabolism (*fumC*, superoxide-stable fumarase C and *acnA*, aconitase A). The *E. coli* SoxR protein exists as a homodimer that contains one [2Fe–2S] cluster per subunit. During aerobic growth, up to 95% of SoxR is held in the reduced ($[2Fe–2S]^{1+}$) state. Upon sensing conditions that promote the production of superoxide, SoxR is oxidized to ($[2Fe–2S]^{2+}$) clusters and it leaves the *soxR/S* promoter region (P*soxRS*) to activate the expression of transcription factor SoxS. SoxS, unlike SoxR, when bound to P*soxRS* initiates the expression of the proteins listed above located downstream of the promoter (55).

1.2.3.2 OxyR: thiol-based, peroxide stress sensor.

OxyR, the hydrogen peroxide sensor, and transcription regulator, belongs to the cohort for combating oxidative stress and is perhaps the model for bacterial redox sensors considering its widespread occurrence in Gram-positive and Gram-negative bacteria (52). Although OxyR acts as a repressor in some bacteria, in *E. coli* and most species it is an activator that recruits RNA polymerase (56). Consisting of an N-terminal DNA-binding domain and a C-terminal regulatory domain, OxyR forms an intramolecular disulfide bond between residues C199 and C208 in the regulatory domain that introduces large structural changes upon binding hydrogen peroxide (henceforth, peroxide or H_2O_2) (57, 58) (**Figure 1**). The structural changes within the regulatory domain of each monomer in turn induces the overall structural change of the tetramer, resulting in the occupation of four consecutive major grooves of DNA (59, 60). Once the oxidized OxyR binds to the promoter region of *oxyRS*, it then recruits RNA polymerase and activates the transcription of the downstream gene *oxyS*. Remarkably, OxyS is a small regulatory RNA that mediates the activation or repression of several crucial transcription factors including *fhlA* (61), *rpoS* (62), and *nusG* (63). In addition to *oxyS,* OxyR globally regulates the activation or repression of over 40 genes, including several detoxifying enzymes such as hydroperoxidase I (*katG*) and alkylhydroperoxide reductase (*ahpCF*) (56).

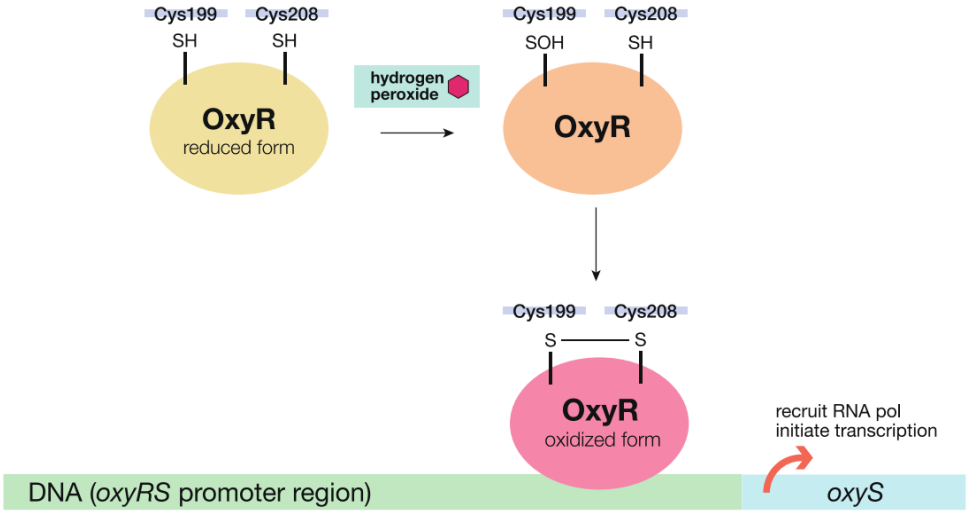

Figure 1.1 Molecular mechanisms of the OxyR transcriptional activator.

Transcriptional activator OxyR in *E. coli* contains two conserved cysteine residues, Cys199 and Cys208, in the C-terminus regulatory domain. Once exposed to hydrogen peroxide, Cys199 is oxidized to sulfenic acid, which can then react with Cys208 to form an intramolecular disulfide bond. This disulfide bond formation within the monomer results in a structural change in the whole OxyR tetramer, which allows more occupation and higher affinity to the *oxyRS* promoter region. Once the oxidized OxyR is bound, it will recruit RNA polymerase to initiate the transcription of the downstream small regulatory RNA *oxyS*.

1.2.3.3 Development of Electrogenetics

We believed that the first intended attempt at controlling gene expression through electronic means, while being indirect, belongs to this synthetic, mammalian electro-genetic transcription circuit (64). By linking the electrochemical oxidation of ethanol to acetaldehyde, an applied voltage was shown to trigger the acetaldehyde-inducible gene expression circuit. A more direct methodology recently appeared in which the engineered genetic circuit responds directly to the electrode-oxidized signal molecule, opening an entirely new modality for bioelectronic control (65). Using pyocyanin as the redox mediator, it is responsible for translating electrical signals into a biochemical redox signal that, in turn, can be sensed by SoxR and initiate the expression from the *soxS* promoter. Strikingly, gene expression controlled by this device is functionally reversible on relatively short time scales (30–45 min). It was also found to be quite robust, as oscillatory behaviors were shown over many cycles. Accordingly, electrogenetic systems will require that an entirely new 'suite' of genetic elements be developed that respond to and coordinate these environmental cues. In (65), the expression of AHL-synthesizing enzyme LasI was electronically actuated, resulting in electronic control of QS behavior of nearby cells. Analogously, motility regulator CheZ was also electronically stimulated demonstrating the electronic initiation of cell motility. In (66), Bhokisham *et al.* coupled *soxRS*-based electrogenetics with CRISPR transcriptional regulation and enabled signal amplification, noise attenuation, and spatiotemporal information processing. Furthermore, Lawrence *et al.* (67) redesigned the P*soxS* promoter and demonstrated electrochemical activation of gene expression

under aerobic conditions using a modular bio-electrochemical device. These studies in cooperation continue to improve the ever-developing electrogenetic systems.

Recently, Terrell *et al.* employed H_2O_2 signaling and *oxyRS* regulon to create an electronically controlled biological local area network (BioLAN) (68). Peroxide, as the redox signal, can be generated directly from an electrode and without mediators to carry information to bacteria that are attached to the electrode by surface engineering. The initiated genetic response, when coupled with a second, recognition-based redox event, propagates and validates information flow between the electronic system and a consortium of engineered microbes. Jointly, BioLAN can reliably facilitate on-demand bioelectronic communication and concurrently perform programmed tasks. In **Chapters 3 and 5**, we also demonstrated novel approaches to allow or expand electronic-to-bio communication based on H_2O_2 signaling and *oxyRS* regulon.

1.3 Physical Electromagnetic Nanocommunication

Other non-MC (molecular communication) nanocommunication modalities were also being proposed by researchers to compensate for several drawbacks of molecular communication such as low communication rate, non-linearity, and molecular interference (69). Many of the novel approaches, including nanocommunication enabled by THz-band electromagnetic waves, acoustic waves, and Forster Resonance Energy Transfer (FRET) were reviewed by (5). Improvements that are intentionally made for bridging biological systems in traditional electromagnetic communication are also paving ways for highly energy-efficient and secured transmission of information. For example, human body communication (HBC) takes advantage of the high-water content of human bodies and uses it as a medium for low-

loss transmission, enabling energy-efficient communication means for wearable technologies (70). To enhance transmission security, Das *et al.* (2) presented "Electro-Quasistatic Human Body Communication" (EQS-HBC), a method for localizing signals within the body using low-frequency carrier-less (broadband) transmission. Other various forms of HBC were introduced in (71). As wearable devices slowly become a necessity in our daily lives, we imagine more advancements in this field will continue to emerge.

1.4 Conclusion

In this chapter, we introduced and discussed a variety of approaches for connecting the seemingly disparate worlds of electronics and biology. This conduit is vital to building a complete Bio-Nano Things framework that, we believe, can spawn many revolutionary applications in the medical, environmental, and biomanufacturing fields. As a rising and interdisciplinary research area, we envision many novel and creative ways will soon join the growing repertoire described here to facilitate the development of new technologies that can greatly benefit our lives.

Chapter 2. Quorum Sensing Communication: Molecularly Connecting Cells, Their Neighbors, and Even Devices

ⓘThis chapter is adapted, with permission, from the publication: **Wang, S.**; Payne, G. F.; Bentley, W. E. Quorum Sensing Communication: Molecularly Connecting Cell, Their Neighbors, and Even Devices. *Annu. Rev. Chem. Biomol. Eng.* 2020. 11:11.1–11.22

2.1 Quorum Sensing: History and Background

Although they are considered primitive, microbes have been found to be social creatures, just like humans. Whereas we use words and body gestures, gregarious bacteria converse through secretion and perception of small signal molecules. Greenberg and colleagues termed this phenomenon quorum sensing (QS). Hints of microbial social interaction through extracellular molecules had been found in early studies in which scientists discovered that both (a) luminescence in two species of marine bacteria (72, 73) and (b) genetic competence in *Streptococcus pneumoniae* (74) required production of hormone-like small molecules. The big breakthrough in QS studies came with two landmark discoveries: One identified the genes that control (luxI, luxR) and produce (lux) luminescence in *Vibrio fischeri* (75, 76), and the other unveiled the QS-signal molecule to be N-(3-oxohexanoyl)-l-homoserine lactone (3OC6-HSL) (77). Soon after, the dawn of genomic profiling allowed the discovery of an explosion of systems that are homologous to the lux QS system in different species (78, 79). Since then, many and widely disparate scientific efforts have been dedicated to understanding how bacteria communicate.

2.2 Quorum Sensing Systems and Networks

In general, QS bacteria produce and release chemical signal molecules termed autoinducers (AIs), the external concentrations of which increase as a function of increasing cell-population density within a particular niche. Once the bacteria detect that AIs have reached a threshold concentration, they will respond by altering their gene expression and behavior. AIs, playing a vital role in QS, are the cues by which QS bacteria communicate and synchronize particular behaviors on a population-wide scale, thus gaining the ability to function as multicellular ororganisms. In this section, two well-characterized QS systems and their signals, receptors, mechanisms of signal transduction, and target outputs are reviewed.

2.2.1 AI-1, LuxI/R System

For most QS systems in Gram-negative bacteria, the LuxI/R system of V. fischeri (**Figure 2.1a**) serves as an underlying paradigm (80). In this system, proteins LuxI and LuxR control expression of the luciferase operon (*luxICDABE*) required for luminescence. *luxI* encodes for an AI synthase that produces the acyl-homoserine lactone (AHL) autoinducer N-3-oxododecanoyl HSL (3OC6-HSL). Following its production, the AHL will accumulate - its concentration increasing as the cell density increases. Upon reaching a critical level, LuxR, the cytoplasmic AI receptor/DNA-binding transcriptional activator, will bind to AHL, and this complex will initiate the expression of the luciferase operon. This actuates a positive feedback loop, as *luxI* is encoded in the operon, and soon the environment is flooded with AHL, which, in turn, switches all bacteria nearby to the QS-active, light-shedding mode (81). All other LuxI/R systems share a general mechanism: LuxI homologs synthesize AHL as AIs, and LuxR homologs recognize, specifically, their cognate AHL. This specificity makes

LuxI/R QS systems ideal for enabling intraspecies communication. In Gram-positive bacteria, such as the aforementioned *S. pneumoniae*, the modified oligopeptides are used as AIs, and the two-component-type membrane-bound sensor histidine kinases are used as receptors. Like the Gram-negative LuxI/R system, each Gram-positive bacterium uses a signal different from that used by other bacteria, and the cognate receptors are exquisitely sensitive to the signals' structures. Because AHLs from different species have been characterized extensively, they can be used for synthetic cell – cell communication. In addition, components of the LuxI/R system can be used as modules within heterologous gene circuits, as they are often ported to non-native strains. Particularly important, the broad class of signals comprising the AHLs freely diffuse through Gram-negative membranes so that active signal transduction motifs are not needed for synthetic communications systems. Also, bacteria rarely rely on one exclusive LuxI/R QS system but often employ multiple signaling systems in parallel. This biochemical diversity of AHL signaling pathways can be leveraged for circuits controlled by combinations of unique signals (82). Together, these characteristics make the LuxI/R system particularly attractive to fields like synthetic biology, as they can be translated to function in engineered systems and environments.

2.2.2 AI-2, LuxS System

The LuxS/AI-2 system (**Figure 2.1b**) was first observed in yet another bioluminescent marine bacterium, *Vibrio harveyi*, which can communicate via multiple QS signals, including those secreted by other species (83). The QS signal AI-2, which is actually a family of cyclic furanones (84), serves as the "bacterial Esperanto" (85), as it can be generated by more than 80 species of both Gram-negative and Gram-

positive bacteria (81, 86). During central metabolism, the reactive methyl moieties of S-adenosylmethionine are transferred to various substrates, yielding by-product S-adenosylhomocysteine (SAH). LuxS-containing bacteria have two enzymes (Pfs and LuxS) acting sequentially to convert SAH to adenine, homocysteine, and the signal molecule, 4,5-dihydroxy-2,3-pentanedione (DPD). This, in turn, is exported and cyclized to AI-2, enabling both the synthesis of AI-2 and the detoxification of the toxic by-product SAH (87).

Remarkably, AI-2 is found to be actively transported into the cell by the luxS-regulated (Lsr) transporter in Enterobacteriaceae and several other taxa (88, 89). In *Escherichia coli*, the AI is imported by the Lsr transporter (LsrACDB) and in turn, is phosphorylated by LsrK to AI-2P. As AI-2P binds LsrR, it relieves the repression of LsrR on the *lsr* genes and accelerates AI-2 intake. Interestingly, through modeling and experimental studies, alternative, less prominent routes of AI-2 synthesis (90) and uptake (91, 92) have been postulated. Also interestingly, LsrACDB is also regulated via glucose and cyclic AMP/cyclic AMP receptor protein, as well as other common carbon sources (91, 93). Based on these discoveries, the LuxS/AI-2 system has two noteworthy features: (a) the desynchronization of the LuxS/AI-2 QS system caused by AI-2 intake via the *lsr* operon, which allows the display of bimodal Lsr signaling and fractional induction (94), and (b) the ability to endow cell population–dependent behavior while interacting with central metabolism and regulating cell fitness through the intracellular activated methyl cycle and intervention of the aforementioned S-adenosylmethionine metabolism pathway. Moreover, in **Figure 2.1b**, we also show that the AI-2 uptake mechanism (Lsr) is phylogenetically dispersed among Gram negatives

and Gram positives (89). That is, although bacteria possessing the AI-2 signal transduction mechanisms are believed to have the ability to sense the general bacterial population density in a multispecies consortium, this diversity suggests the ability to self-report. The prevalence of LuxS among bacteria (and AI-2 in proximal microenvironments) has fueled speculation about the role of AI-2 as a QS-signal molecule, yet its diverse uptake and signal translocation mechanisms enable species-specific ability to respond to AI-2. Interestingly, some question whether AI-2 and the LuxS/AI-2 QS system can be defined as a true interspecies QS-signaling pathway, or in some cases a non-QS-related cue (95), but this system possesses many attributes and components that can be rewired and incorporated into engineered systems.

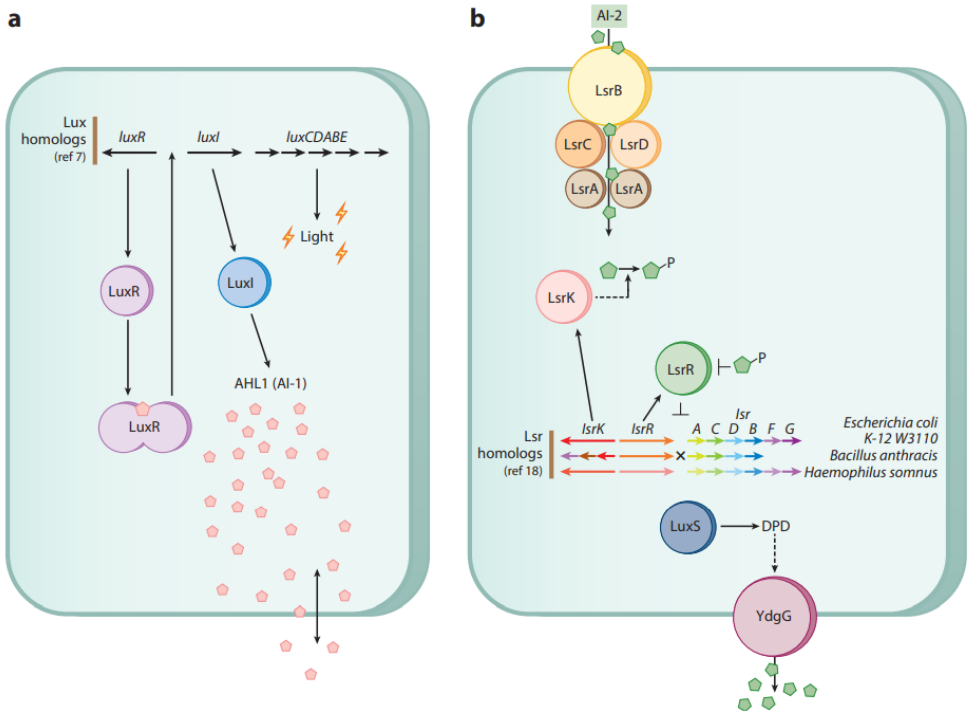

Figure 2.1 Canonical quorum sensing (QS) systems.

(a) QS in *Vibrio fischeri*. Pink pentagons denote the acyl-homoserine lactone (AHL) autoinducers (AIs) that LuxI produces (3OC6-homoserine lactone). Transcriptional regulator LuxR modulates the expression of AHL synthase, LuxI, and the lux operon, leading to luciferase-mediated light emission. Homologous lux-like systems are described in Reference 7. **(b)** Regulatory mechanisms of the LuxS/AI-2 circuit in *Escherichia coli*. AI-2 (green pentagons) is imported into the cell by the Lsr transporter (LsrACDB) and is then phosphorylated by LsrK. When AI-2P binds LsrR and releases LsrR from the promoter region (thus modulating Lsr gene expression), AI-2 uptake is increased. LuxS produces DPD, the precursor to AI-2. The AI is exported by YdgG (TqsA). Lsr homologs and their organizational structures are found in both Gram-positive and Gram-negative bacteria (89).

2.2.3 Global Quorum Sensing Regulons

The prevalence of genomic fingerprinting has revealed that QS can control gene expression in a global manner. QS mutants of *S. pneumoniae* and related *Streptococci* show defects in multiple pathways, including biofilm formation, acid tolerance, bacteriocin production, and virulence (78). *E. coli*, too, have been reported to elicit broad QS activities. For example, the quantity and architecture of biofilms are regulated by lsrR/K, as well as the generation of several small RNAs (96, 97). Transcriptome analyses of an *E. coli luxS* mutant, which showed that 242 genes (5.6% of the whole genome) exhibited significant transcriptional changes upon a 300-fold AI-2 signaling differential (79, 92, 98), suggest that QS coordinates the control of a large subset of genes. Although we are not entirely certain whether these *luxS* mutant phenotypes are a result of the lack of QS signaling or may simply be due to metabolic perturbations, these findings surely demonstrate that QS allows bacteria to alternate between distinct genome-wide programs by activating numerous genes both directly and indirectly. For example, AI-2 also serves as a chemoattractant for *E. coli* (99, 100). Chemotaxis studies have revealed that both LsrB and Tsr, a serine chemoreceptor, are involved in AI-2 sensing (101). As a signal molecule, AI-2 is not a nutrient, unlike other known chemoattractants of *E. coli*; therefore, chemotaxis toward AI-2 may not involve the narrow dose ranges that are characteristic of most indirectly binding chemoattractants (102). This provides opportunities to enable programmed motility toward user-selected features on nearby surfaces. Antigen 43–dependent autoaggregation of *E. coli* is also mediated by AI-2. Hence, the AI-2 chemotactic response will lead to active aggregation,

and in turn, autoaggregation enhances AI-2-mediated signaling, and subsequently, biofilm formation and stress resistance (103).

Since long before the formal recognition of metabolic engineering in 1991 (104), scientists and engineers had been developing microbial strains for the production of valuable chemicals. The emergence of metabolic engineering and synthetic biology was predicated on the multidimensional value associated with biological synthesis processes for chemical products—a natural progression was the desire to program cells to carry out these functions. QS regulons, having the potential to connect inter- and intraspecies communication systems with genome-spanning regulatory processes, dramatically simplify what otherwise might be the de novo engineering of gene circuits (105, 106). QS serves as an excellent platform for many technologies, particularly if one understands the regulatory reach of the genetic circuits. In the past two decades, the rewiring of native QS networks has enabled novel ways to engineer cell behavior, exemplified by such advances as programmed population controllers (107), synchronized genetic clocks (108), and population-based autonomous gene actuators (109, 110). These studies have set the stage for the future development of a variety of innovative biotechnological applications, which are discussed in the following sections.

2.3 Manipulation of Quorum Sensing Systems: Endowing Cells with New Function

Owing to their diversity and versatility, QS systems are perfect candidates as platforms for facilitating the endowment of bacterial strains with unique and increasingly complex functions. In this section, we explore recent endeavors to excerpt

QS mechanisms and pathways to enable cells with advanced functions for various applications.

2.3.1 Biosensing and programming population-wide behavior

Whole-cell biosensors, as the name suggests, are native or engineered cells that detect and report on a target or condition of interest (111, 112). Biocompatible and renewable, they make good substitutes for current chemical or electrical sensors. Originally, cells that elicit QS behavior were simply rewired to detect their own autoinducers (113) (**Figure 2.2a**). This was typically accomplished by the deletion of the terminal autoinducer-synthase gene and replacing the native QS-induced gene system with a reporter gene. Perhaps the most well-characterized and used sensor is the *V. harveyi* strain BB170, of Bassler and co-workers (114). While developed over two-decades ago, these biosensor cells continue to benefit science; for example, they are frequently utilized in studies to probe for new QS inhibitors (115-118). Analogously, by fusing QS promoters with fluorescence genes, *P. aeruginosa* were given the ability to report on the genetic expression of four QS networks (119). Owing to the wide diversity of natural QS systems, various pathogens and infection markers can also be detected by engineered QS-based biosensors (120-122). These bacterial 'sentinels' were further enhanced to perform with higher sensitivity (123) or to encode and distribute therapeutic payload upon detection, which will be discussed in the following section.

QS-based biosensors are also employed to probe pollutants (i.e., heavy metal ions) in the environment, in which the positive feedback loop of LuxI/R system is used for signal amplification (124, 125). On top of enhancing signal amplitude, QS circuits

have been shown to resolve some common problems met by biosensors. Genetic noise, or specifically variation in phenotype between cells, can be assisted by QS systems (126, 127). Early work showed that by coupling LuxI/R circuitry to the expression of a toxic protein (CcdB), it was possible to program population dynamics irrespective of the variability in individual cells (107). With the same notion in mind, a synchronized genetic clock was engineered based on both the LuxI/R system and the QS system of *Bacillus thuringiensis* (108). Here, colony-level synchronized oscillation could diminish single-cell variability and increase the sensitivity and robustness of the response to external signals. These frontier endeavors have paved the way for building better, more effective macroscopic biosensors. Interestingly, one further study chose to dwell on the heterogeneity observed within bacterial populations that, despite the group showing collective behavior, could still be observed. In this work, a stable quorum wherein a specific fraction of the whole exhibits the desired collective behavior is generated – say a group of cells was programmed to have 65% of the total population to express DsRed, a red fluorescent protein (128). This was done by manipulating the native *E. coli* AI-2 transduction cascade along with an autoinducer signal amplification vector that makes the strain hypersensitive to AI-2, therefore it overexpresses the marker protein and with this QS mechanism leads a subgroup of cells to exhibit the same behavior. More than an AI-2 biosensor, we believe studies like this also anticipated many future works to focus on intentional control of group behavior, which will be discussed later in this article. Owing to the development of the many tools of synthetic biology, QS components and signaling mechanisms have helped to streamline biosensor development. The adaptable and well-defined nature of QS systems will

surely continue to benefit the improvement of biosensors, even broadening their capabilities.

2.3.2 Therapeutics: QS-regulated sense-and-kill probiotics

In an extension of previous work (129), Hwang *et al.* (130) have endowed probiotic *E. coli* strain Nissle 1917 to seek the pathogen through AI (3OC12HSL)-regulated motility; induce self-lysis (driven by lysin E7); and release pyocin c5, an anti–P. aeruginosa toxin (**Figure 2.2b**). The engineered strain exhibits *in vivo* prophylactic and therapeutic activity against *P. aeruginosa* during gut infection. Recently, BeQuIK (Biosensor Engineered Quorum Induced Killing), a newly proposed design that aims to combat recalcitrant biofilms, adopted the same sense-and-kill premise but with a twist for aiding in the targeting and penetration of biofilms (131). Biofilms are 3D structures in which a cluster of bacteria resides within a self-produced matrix primarily composed of proteins, polysaccharides, and extracellular DNA (132). Mature biofilms are notoriously difficult to penetrate or degrade. Because the formation of biofilms is governed by QS activity, the "sense-and-kill" system can be adopted to clear these three-dimensional structures, yet success depends on localization of the engineered *E. coli*, since this system relies heavily on the diffusion of autoinducers. Better eradication of biofilms could perchance be achieved through surface display of one or more biofilm-targeting "nanobodies" (Nb), which are single-domain antibodies derived from the heavy chain antibodies of camelids (133), to recognize and bind to components of the extracellular polymeric substance (EPS) or biofilm-mediated proteins. Additionally, fusing one or more biofilm-degrading enzyme domains to the

Nbs would possibly allow for more effective diffusion of autoinducers for activating the killing mechanism as well as better permeation of the therapeutic agents.

2.3.3 Therapeutics: QS-regulated *in situ* production and delivery

It is perhaps inevitable that some bacteria would evolve to preferentially grow in environments that harbor disease, and hence these cells may serve as a natural platform for the development of engineered therapies (134-136). *Salmonella*, for instance, are one of the ideal candidates because they preferentially accumulate in tumors, actively penetrate tumor tissue, and can be engineered to produce anticancer drugs in situ (137-140). Notably, however, nonspecific expression can damage healthy tissue. Engineering QS signaling offers the opportunity to restrict expression of the therapeutic compounds to relevant body sites. For example, the LuxI/R QS system was excerpted to build a density-dependent switch in *Salmonella* so that the engineered bacteria express the to-be-delivered proteins only in tightly packed colonies within tumors (141). This proof-of-concept study using an *in vitro* 3D tumor-on-a-chip device and in vivo mouse models showed that QS *Salmonella* specifically initiates green fluorescent protein expression within cancerous tissue while remaining uninduced in liver; hence, this study provided a road map for limiting systemic toxicity caused by unwanted expression in healthy tissues. In addition, such therapies could also benefit from bacteria that are programmed to maintain relatively low overall colonization levels in the body while continually producing and releasing cytotoxic agents (142, 143). Using coupled positive and negative feedback loops that had previously been used to generate robust oscillatory dynamics (108, 144), Din *et al.* (145) constructed a synchronized lysis circuit to allow engineered *Salmonella* to deliver therapeutic cargo

and lyse synchronously at a threshold population. In this system, both *luxI* and *hlyE* (which encodes haemolysin E, an antitumor toxin) were constitutively expressed. As the AIs slowly built up to reach a threshold level, the bacteriophage lysis gene (φX174E) was induced, thus triggering cell lysis and simultaneously releasing the therapeutic toxin.

Alternatively, targeted therapeutic cargo delivery has also been made possible in *E. coli* via incorporation of the native AI-2/Lsr signaling pathway (146) (**Figure 2.2b**). Here, bacteria were modified to enable programmed motility, sensing, and actuation based on the density of user-selected features on nearby surfaces. Specifically, bacterial enzymes LuxS and Pfs were introduced onto cancerous eukaryotic cells as a nanofactory, where they were used to synthesize chemoattractant AI-2. That is, the LuxS-Pfs fusion protein also contained a bacterial protein G domain that enabled the assembly of targeting antibodies. After expression and purification from *E. coli* and incubation with an antibody targeting epidermal growth factor receptor (which is upregulated on cancer cells), these nanofactories were used to synthesize AI-2 on the cell surfaces at EGFR sites, thus directing engineered *E. coli* to swim toward the cancer cell line (SCCHN). Once in place, the same AI-2, which is differentially accumulated above cancer cells, enabled QS computation to induce red fluorescent protein (RFP), a marker for therapeutic or other compounds.

2.3.4 Biosynthesis

Metabolic engineering often takes inspiration from natural regulatory mechanisms in microbes and repurposes them to maximize productivity; QS systems offer many suitable components that can be exploited for this purpose. One of the more

severe problems met by the most productive metabolic engineering methods is the heavy metabolic burden that accompanies the genetic modification. Because QS networks can report the metabolic state of a bacterial population and the metabolic burden is self-indicated by this network (98), Tsao *et al.* (109) created a system in which the system itself can autonomously induce protein expression and achieve metabolically balanced coordination through rewiring native AI-2/LuxS QS circuitry in *E. coli*. Further, a LuxI/R-based, semiautonomous induction circuit was assembled in *E. coli* and employed for isopropanol production (147); it was later modified to create a fully self-induced system for synthesis of a biofuels compound, bisabolene (148). These approaches allow cells to grow with less metabolic burden in early stages and transition to a production mode after the population growth phase has completed. Notably, these systems can ensue without exogenous addition of inducers or perhaps even user input. Compared with other strategies exploiting dynamic pathway engineering, QS-based regulatory mechanisms provide process- and pathway-independent control of the metabolic state, which makes them highly applicable to different bioprocesses. That said, there remains a general lack of quantitative understanding of exactly how much burden the additional QS logic gates bring to these engineered systems; perhaps computational modeling or fundamental understanding of resource competition within cells could bring about a more robust, productive cell factory in the future.

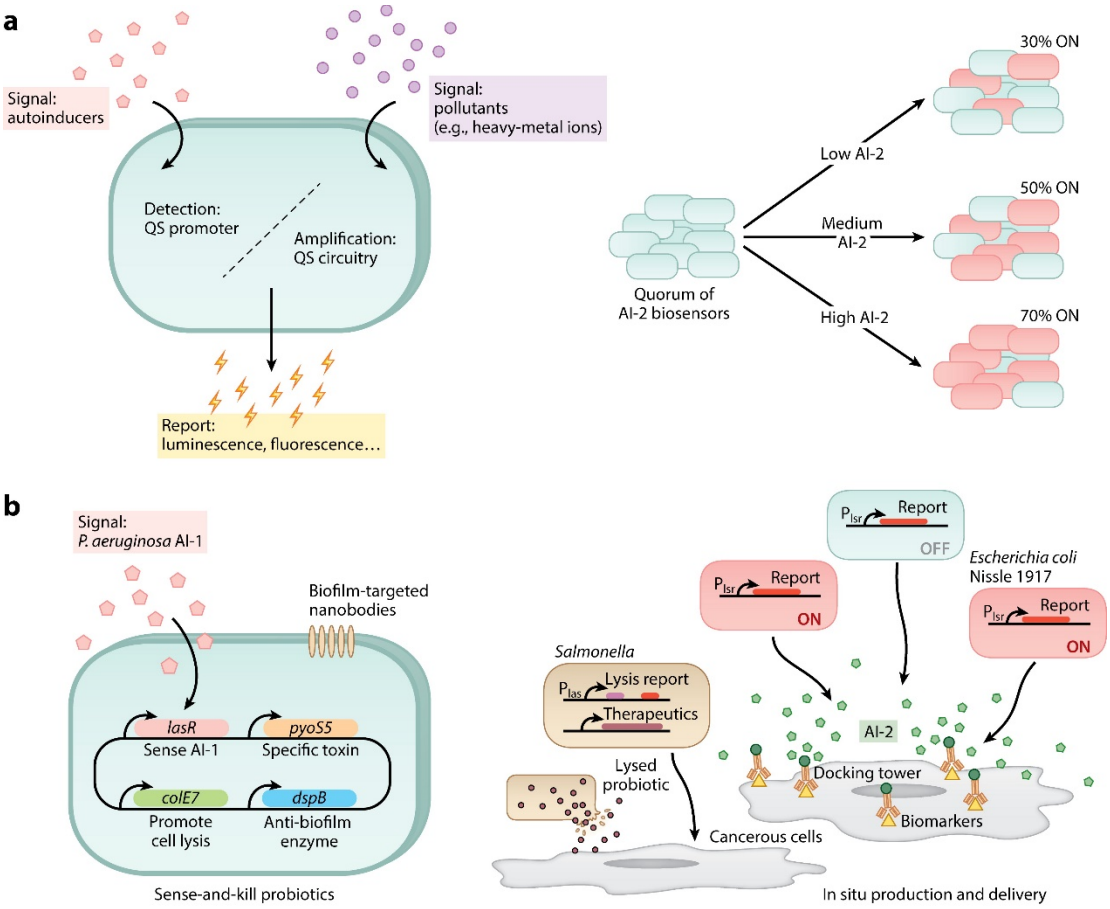

Figure 2.2 Quorum sensing (QS)-enabled cell functions.

(a, left) Paradigm of QS biosensors. A wide range of signals can be detected and amplified through QS circuitry and reported via optical or biological means. (right) A quantified quorum of biosensors is engineered to respond to different levels of signal and produce a collective response. **(b)** Examples of QS therapeutics. (left) Sense-and-kill probiotics (green) can sense pathogenic signals, specifically acyl-homoserine lactone (AHL) produced by pathogens, and express toxin (pyocin S5) and cell-lysis proteins (lysin E7) to eliminate *Pseudomonas aeruginosa*. Anti-biofilm enzyme (DspB) and biofilm-targeted nanobodies can be incorporated to facilitate biofilm penetration.

These smart probiotics can either autoaggregate toward tumor cells (e.g., *Salmonella*) or be programmed to actively seek target cells. (right) Nanofactories consisting of Pfs, LuxS, protein G, and anti-EGFR antibody will specifically bind to selected biomarkers (EGFR) and produce AI-2. Probiotics (*Escherichia coli* Nissle 1917) recognize and then chemotax toward AI-2 (produced by targeted cells). Upon arriving at their destination, smart probiotics use the same AI-2 level to report (via red/green fluorescence) (green/red, *E. coli*) or lyse when the population threshold is reached and release genetic-encoded cargo (tan, *Salmonella*).

2.4 Manipulation of QS Systems: Opening Lines of Communication

In the previous section, we witnessed how QS regulons could be taken apart and reassembled into novel genetic circuits and how these endow cells with various advanced functions. These strategies mostly made use of the QS information/control paradigm in which cells autonomously regulate gene expression after detecting self-generated or synthetically produced molecular cues in their immediate microenvironments. Most often these systems have employed diffusible AIs, such as the large family of AHLs. That said, QS derives from its well-established function as a means for conveying and coordinating social behavior (149, 150); hence, it is also expedient to apply and further engineer QS systems to do what they do best: launch and promote communication between groups of bacteria.

2.4.1 Microbial Consortium: A Prospective Platform

As the saying goes, "Two heads are better than one." Microbial consortia have long proven their abilities to outperform single microorganisms at multiple tasks, as evidenced by the evolutional development of natural communities. The gut microbiota, for example, plays multiple vital roles in human health, from regulating metabolism to influencing the immune system and even guiding maturation of the enteric nervous system, all while varying in composition across time, location, and individuals (151, 152). Besides their versatility, native consortia (such as the gastrointestinal microbiome) are also robust; they respond to environmental challenges, display cooperation and exchange of public goods, and communicate (chemically or physically) between species. In light of these beneficial traits, microbial communities present themselves as an attractive platform for synthetic biologists who aim to modify microorganisms for

biotechnological applications. From an engineering perspective, the division of labor, in which different populations are charged to perform different tasks, represents a key to overall effectiveness. Some potential advantages born by such a division of labor include improving functionality via specialization, reducing metabolic burden via function distribution, and reducing engineering complexity (153). Within consortia, complex tasks can be segmented, and each part can be delegated to a subpopulation. This allows subgroups to specialize and together display sophisticated multifunctionality that cannot be achieved in a single clonal population. Because cells are now completing only part of the overall function, they can be relieved from the responsibility of carrying all the modified genetic machineries and hence ameliorate their heavy metabolic burden. Lastly, compartmentalizing cellular processes into different populations increases modularity. Therefore, engineering design becomes more facile, as each module (or subpopulation) can be tuned, modified, or even replaced in a plug-and-play manner (154). That said, synthetic microbial communities are significantly more complex to engineer than monocultures. With each additional member, the size of the interaction matrix increases geometrically, so that the transition from static monoculture to dynamic consortia presents a new challenge for us to conquer. In the following sections, we discuss how QS networks may contribute to the synthetic biology toolbox that assists in the construction and deployment of synthetic microbial communities.

2.4.2 Engineering QS-based communication

Brenner *et al.* (155) first demonstrated a synthetic coculture composed of two engineered *E. coli* strains that were able to communicate bidirectionally and reach a

consensus (see the middle panel of **Figure 2.3**). Two populations conversed through secretion and detection of 3-oxododecanoyl-HSL (3OC12HSL) and butanoyl-HSL (C4HSL), which are AIs made by enzymes LasI and RhlI, respectively, from the QS networks of *P. aeruginosa*. In this consortium, one population relied on the signal from the other population to activate gene expression, and a consensus could be attained when both populations reached their cell-density thresholds. Remarkably, the responses were sustained for up to several days when the consortium was cultured as a biofilm. This success took scientists one step closer to engineering a living film—the consensus response could potentially be replaced into an enzyme and prodrug pair or two inactive fragments of a toxin. Complex metabolic tasks could be divided into two or more, and the intermediate pieces could be assembled to reach a consensus. Soon after, the concept of synthetic consortia with bidirectional communication became a paradigm for many similarly programmed consortia. Balagaddé *et al.* (156) reported an artificial ecosystem that aims to mimic the canonical predator–prey systems in terms of logic and dynamics. Here, communication was fostered by *lux* and *las* QS networks, and similarly the two populations regulated each other's gene expression via QS-rewired circuits. The predator population could kill the prey population by secreting AIs, which, in turn, induced a killer protein (CcdB) expression within the prey; meanwhile, the prey revived the predator, in which the killer protein was constitutively expressed, but with an induced antidote protein (CcdA). Recently, it was proposed and modeled in silico that this predator-and-prey architecture, or a slightly altered version in which two groups rescue each other, could turn into a population-controlled consortium (157, 158). A similar *lux*-based population control strategy was later

applied to a synthetic three-species consortium for vitamin C fermentation (159). A subsequent study built a symbiotic microbial ecosystem with the aid of *lux* and *rhl* QS networks to examine the interplay between the environment and the ecosystem (160). Many population dynamics, such as extinction, mutualism, and commensalism, can be observed by tuning different levels of environmental factors (represented in this work by antibiotics) and initial cell densities. Genetic oscillations, previously made possible in monocultures, were now shown to be generated by an activator and repressor coculture (161). Two strains conversed through QS networks: *rhl* (from *P. aeruginosa*), providing the additional positive feedback loop, and *cin* (from *Rhizobidium*), providing the additional negative feedback loop, with both containing an inherent AiiA-mediated negative feedback loop. Experimental and modeling data together had shown that this network topology displays more robust oscillations than those generated by just one negative feedback loop. AHL-mediated communication can also be coupled with AI-2 signaling to create an autonomously regulated consortium (162). In particular, this system consists of two populations of *E. coli*, one of which generates AHL based on nearby AI-2 levels, and the AHL concentration, in turn, affects the growth rate of the other population, resulting in a change in coculture composition. Subsequent programming enables composition trajectories and control. Together, these studies portend the engineering of complex synthetic populations, perhaps bacteria in combination with tissues and even organs composed of multiple cell types.

Co-cultured cellular networks can also serve as effective biosensors. Terrell *et al.* (163) described assembly of a nano-guided QS information processor, which included two cell populations that independently interrogate natural microbial

communities and autonomously generate information about QS activity by accessing AI-2. They were used to eavesdrop on the dialogue initiated by Gram-positive *Listeria innocua* in complex media. Populations displayed either red or green fluorescent proteins on their outer surfaces and were designed to detect lower and higher levels of AI-2, respectively. With the help of streptavidin-binding protein that was expressed on their outer surfaces and exogenously added magnetic nanoparticles, both populations reported on AI-2 secreted by *L. innocua* and were binned by their fluorescence responses. The magnetic nanoparticles enabled an unbiased collection of the sensing cells and at the same time focused the signal responses. This multidimensional setup combined biotic and abiotic features for the active probing of molecular space and translated the molecular dialogue into light signals that were easy to bin and interpret. The success of these studies has proven QS-based communication to be an effective, modular, and robust icebreaker for initiating communication in a microbial society.

2.4.3 Engineering a microbial consortium: challenges.

Despite their utility for engineering microbial consortia, QS systems have several drawbacks that limit their use as field-deployable communication networks. First and foremost is the crosstalk (see challenges in **Figure 2.3**) between different QS networks at both the promoter and signal levels (164). Signal crosstalk occurs when a receptor can bind its noncanonical AI. For example, LuxR is known to bind 3OC12HSL, the AI native to another QS system, the *las* system. Promoter crosstalk occurs when activated receptors can bind a noncanonical promoter. For instance, Brenner *et al.* (155) encountered this issue when pairing QS networks *rhl* and *las*. Specifically, high levels of activated LasR were found to initiate the *rhl* promoter. A combination of signal and

promoter crosstalk is also possible, whereby a receptor that is activated by a noncanonical AI binds to a noncanonical promoter.

That said, if parts are well-characterized, such crosstalk can be harnessed to create unique dynamic circuits. Initially, most endeavors were made to avoid crosstalk; for example, a positive feedback loop on the I proteins was incorporated into the design of the bidirectional communication circuit to mitigate promoter crosstalk between *lasR* and *rhl* (155). However, it is critical that additional QS systems with complete orthogonality be developed. Via rational promoter and protein engineering, Scott & Hasty (164) adapted two new QS systems, the *rpa* system from *Rhodopseudomonas palustris* and the *tra* system from *Agrobacterium tumefaciens*, into *E. coli* to expand upon the extensively used *lux* and *las* systems. Notably, engineered *rpa* and *tra* systems displayed complete orthogonality, while signal and promoter orthogonality was observed between *rpa*/*lux* and *tra*/*las* QS systems, respectively. Another recent study systematically characterized six commonly used QS systems, the *lux*, *las*, *tra*, *rpa*, *rhl*, and *cin* networks, and developed a software tool that automatically identifies combinations of receptors and AIs that behave orthogonally within a given AI concentration regime (165). The software predictions were carefully validated through experimental characterization of synthetic *E. coli* consortia that, in turn, implemented three orthogonal communication channels: *rhl*, *lux*, and *las*. The use of different classes of QS systems, such as the AI-2/LuxS system or Gram-positive signaling oligopeptide systems, in parallel with the lux-like systems has also demonstrated orthogonality (94, 166).

Another challenge in consortia engineering would be the presence of cheaters in a microbial community (see *challenges* in **Figure 2.3**). Microbial social cheaters rely on public goods or other beneficial collective actions to survive, but they do not contribute. These noncooperating populations pose a potential threat to the robustness of consortia. Studies have shown, however, that native consortia can stably maintain coexistence with and prevent proliferation of these external populations compared with high-fitness monocultures that are more prone to be exploited by cheaters (167). While it was postulated that employing QS could also be a way to reward cooperators and thus aid in eliminating cheaters (168), QS was also shown to be exploitable in many laboratory cultures (169). One illustrative case concerned the opportunistic pathogen *P. aeruginosa*, which relies on QS to induce the production of extracellular proteases that are required for growth on proteins. It was observed that QS mutants were able to survive when in coculture with QS-competent cells (170). This phenomenon subsequently led to an ongoing debate as to why there remain numerous functional QS systems that are maintained in nature, especially if QS systems are so easily exploited or circumvented. Policing, the ability of cooperators or hosts to hinder the fitness of cheaters, could be one of the possible reasons; this idea was used to introduce the concept of punishing freeloaders (171). Majerczyk *et al.* (172) described how QS regulation of pairs of genes coding for toxins and toxin immunity serves as a policing mechanism. In *Burkholderia thailandensis*, those that are QS competent deliver toxins to other individuals. Although the QS-competent cells are immune, QS mutants are not. Perhaps this scheme can be incorporated into future circuit and consortium designs to help create more robust communities that repress or eliminate social cheaters.

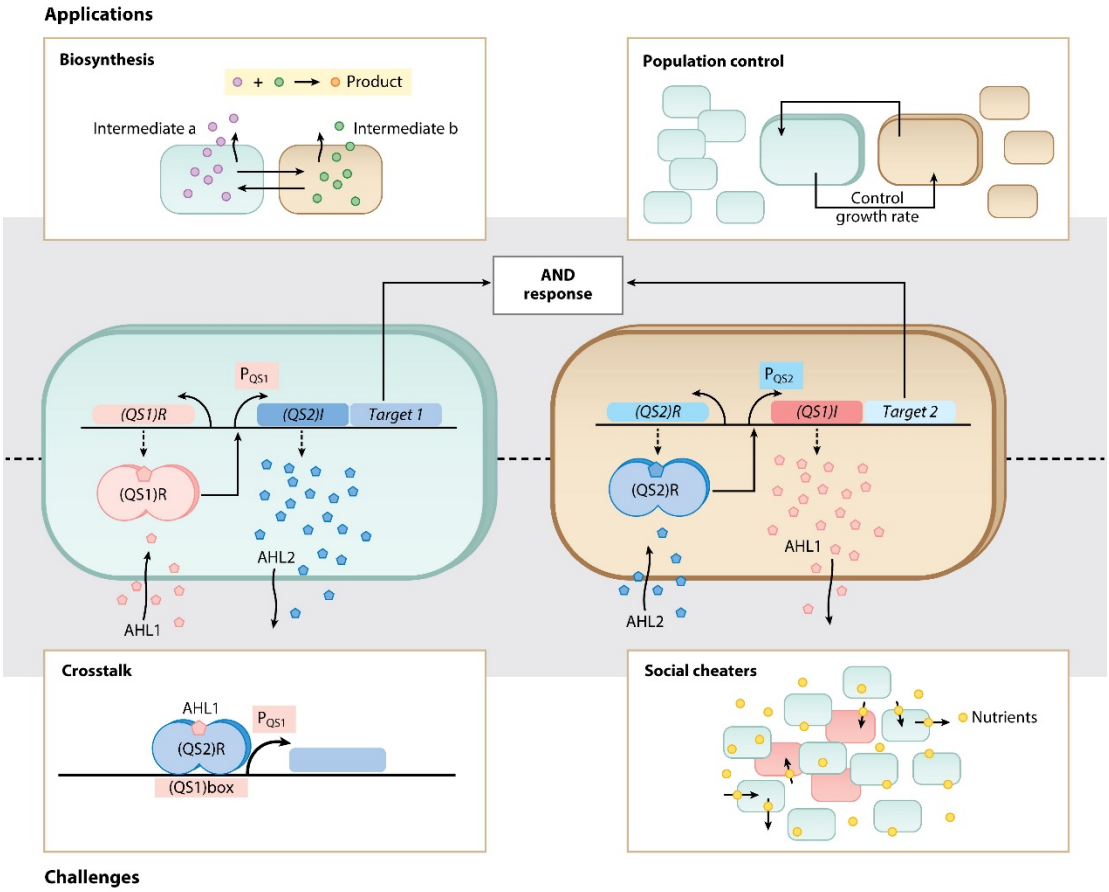

Figure 2.3 Applications and challenges of quorum sensing (QS)-based synthetic consortia.

The middle images provide an example in which QS-communicative consortia are used to provide a collective response. Population 1 (green) expresses regulator (QS1)R and secretes AHL2 and target 1 under the control of promoter PQS1, which activates upon AHL1-bound QS1R. Population 2 (tan) does the reverse. Because one population makes the required signal for the other's gene expression, both cells and genetic circuits are needed to generate a response. Hence, this is an AND logic switch. Such synthetic consortia can be applied to metabolic engineering for distributing tasks among multiple

strains (top left). Such a system can be fine-tuned by controlling the growth rate of one of the populations relative to the other (top right). Challenges must be overcome, however, for these systems to work effectively. One involves signal crosstalk (bottom left), and another, social cheaters (bottom right).

2.5 Interkingdom Consortia: Engineering Communication Networks

As described earlier, the AI-2/LuxS system was shown to be distinct relative to the *lux* systems in many Gram-negative bacteria, and it has been dubbed the bacterial Esperanto since a plethora of both Gram-negative and Gram-positive bacteria have been reported to synthesize AI-2 and putatively use AI-2 as a signal molecule. Because this LuxS-mediated AI-2 synthesis system is so widespread, it is only natural to think of its perception as a way of delineating its role as a signal molecule. That is, there is significant diversity in the uptake/signal transduction systems across many genera, including Gram positives and Gram-negatives. The canonical *lsr* operon, found in *E. coli*, consists of the genes noted in **Figure 2.1b**. Quan & Bentley (89) showed how some of these genes (e.g., *lsrRK*, *tam*) are absent in some strains, whereas their order and regulatory regions are different in others, providing great diversity in the way AI-2 is perceived. The net result of this is that evolutionary pressures may have led to distinct patterns by which AI-2 could be taken up or processed and thereby used as a signal molecule. This is completely orthogonal to its synthesis as a metabolic by-product. As such, it may be possible that next-generation antimicrobials could be created by intercepting intra- and interspecies bacterial communication for the creation of smart, disease-fighting bacteria. Instead of targeting the viability of pathogenic strains, interruption of their communication is proposed, as there may be less selective pressure to develop resistance if instead one targets the mechanisms that key pathogenicity (173). This idea is not new for small-molecule drugs, but to our knowledge not as mediated by bacteria. Because it is an AI, inhibition of the signal AI-2 could possibly lead to decreased virulence in a variety of bacterial species. Many

parts of the AI-2/LuxS system, from signal generators (Pfs and LuxS) to signal receptors (LsrK, LsrR), are likely targets for inhibition, especially because many synthesized AI-2 analogs are available for quorum quenching (116-118, 174). For example, commensal *E. coli* were engineered to increase AI-2 levels in the mouse gut. During streptomycin-induced dysbiosis, these AI-2-producing *E. coli* promoted gut colonization by *Firmicutes* over *Bacteroidetes* (175), whereas added streptomycin massively favored the *Bacteroidetes* and inhibited *Firmicutes*. This offered an exciting possibility that by altering AI-2, one could ameliorate the effect of an applied antibiotic on microbiota-derived functions. This success suggests that continued efforts to engineer strains with the intent to bias microbiome signaling (123) will surely emerge. Additionally, AI-2-producing *Ruminococcus obeum* were also shown to be vital for defeating *Vibrio cholerae* infection and facilitating recovery (176). *R. obeum* restricted colonization of *V. cholerae* through upregulation of the *luxS* gene to produce more AI-2, and in turn, AI-2 displayed QS-mediated repression of several *V. cholerae* colonization factors. Whereas AI-2 signaling was found to be critical in native gut environments, LuxI/R-type systems have not been detected in the normal, healthy gut. This provides another possible opportunity to interrogate and manipulate communication for positive gain. A recent study constructed an information-transfer system to probe whether the *lux* QS system can be repurposed into a functional, artificially established language in the mammalian gut (177). Both interspecies and intraspecies communication were made possible despite some complexities in in vivo studies. Together, these studies promise to underpin many valuable uses of QS

networks in the future to either promote or interrupt communication, not just at the species level but to affect a whole microbiome.

2.5.1 Interkingdom and beyond.

QS bacteria are also observed reaching out to eukaryotes. Indeed, QS-communicating bacteria and their components are emerging at many interfaces, including in interactions with viruses, eukaryotic cells and organisms (e.g., plants), artificial cells, biomaterials, and even electronic devices (**Figure 2.4**). Orphan, or solo, LuxR homologs were first discovered in *Salmonella typhimurium*, a bacterium that was reported as lacking a LuxI homolog and the ability to produce AHL-type AIs. It was further discovered that an *E. coli luxR* homolog, *sdiA*, was shown to respond to mammalian host-produced small molecules (178). This discovery hinted at the possibility that LuxR homologs, instead of acting as QS receptors, were sensors of the host environment. Many orphan LuxR homologs were then found in plant-associated bacteria, regulating plant–bacterial interactions through detection of small molecules secreted by the host (179). Contrarily, host cells could respond to AIs secreted by their commensal bacteria. RNA-sequencing technology revealed that human colonic cell line HCT-8 expresses inflammatory cytokine interleukin 8 in response to AI-2 secreted by nonpathogenic *E. coli* (180). Surprisingly, Silpe & Bassler (181) recently revealed that vibriophage VP882 can respond to a *V. cholerae*–produced QS AI (DPO). Once bound to DPO, the phage QS receptor $VqmA_{Phage}$ in turn activates the phage lytic program. Activated $VqmA_{Phage}$ can even recognize the host *vqmR* promoter and influence its QS behavior. This is the first case reported to show that viruses can eavesdrop on their hosts and decide their actions based on what they have heard.

Finally, when considering more biotechnological objectives, we note that QS systems have also enabled cell signaling to pass from biological niches to abiotic and even microelectromechanical systems. Although this could be the topic of a far more extensive review, we note a few examples that are logical extensions of the above work in that the molecular components of AI-2 QS are abstracted and put in play to mediate bio-/device signaling. For example, to understand the interplay between QS signal molecules and human epithelial cells, a nanofactory consisting of the two terminal AI-2 synthases, Pfs and LuxS, and a targeting antibody was created and electro-assembled into microfluidic devices, where it was used to capture cells and stimulate their QS responses (182, 183). Analogously, the construct was loaded onto receptor molecules of human intestine epithelial cells, where they stimulated QS activity among nearby commensal *E. coli* (183, 184). The same enzyme construct was later shown to be grafted onto spider silk and subsequently wound into place in a microfluidic device, where its molecular signaling activity could be localized with minimal machine guidance or intervention (185). In another example, Lentini *et al.* (186) engineered minimal artificial cells capable of expressing AI-2 synthesizing fusion protein HLPT (His_6-LuxSPfs-Tyr_5) (182), wherein newly synthesized AI-2 was proven to induce luminescence in nearby cells. The same HLPT fusion was shown to be electrically assembled onto gold electrodes, where its activity was controlled electrochemically (187) by simply applied voltage and redox actuation. In all these systems, AI-2 is synthesized in carefully controlled environments and in ways that are programmed by external inputs—some even electronic. That is, biomolecular synthesis reactions, even pathways, are carried out in well-controlled microsystems so that the kinetics and mass

transfer processes can be controlled, designed, and even optimized. Such complex microfluidic environments are recreated on chips for preclinical drug development and toxicity screening. These studies ultimately suggest that, by bridging with nonbiological materials, there are many opportunities to build novel microelectronic, biohybrid devices that can alter the complex networks of natural cells without tampering with the original genetic makeup. In turn, these can be used in drug development studies as well as detailed biological studies in which distances and dynamics are of the same scale as the cells and molecules themselves.

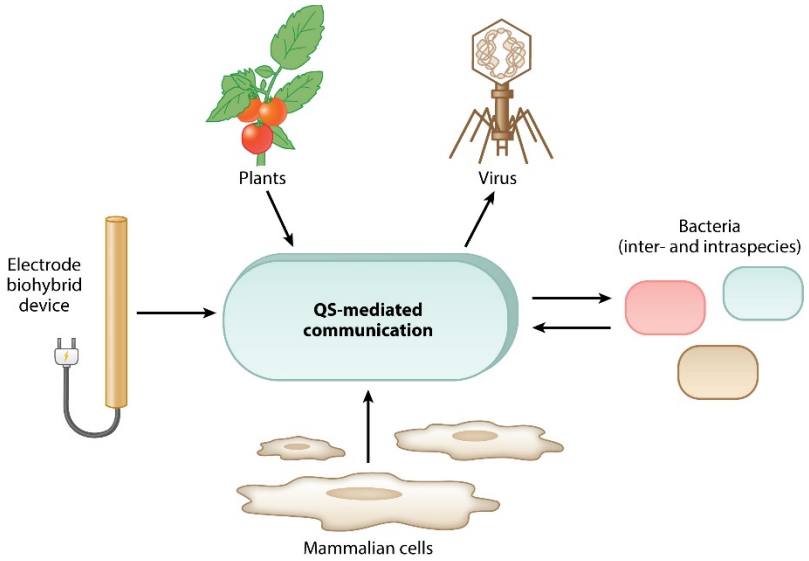

Figure 2.4 QS-mediated communication to interkingdom and beyond.

Native and engineered quorum sensing (QS)-mediated communication can be used to target a variety of areas. QS bacteria not only are observed to display both intra- and interspecies communication (right) but also are capable of interpreting signals from eukaryotes, such as plants (top left) and mammalian cells (bottom). Recently, viruses (top right) have been found to respond to and make decisions based upon host-produced acyl-homoserine lactones (AHLs). Communications between abiotic materials and QS-communicating bacteria (left) by QS-component assembly on gold electrodes or on/within artificial cells.

2.6 Conclusion and Future Outlook

QS has provided researchers with a variety of novel platforms or techniques from which to address biotechnological problems. In this article, we addressed the versatility of native QS and the numerous strategies aiming to repurpose QS systems to program the behavior of a single cell, a cell consortium, or even a microbiome. QS advances synthetic biology by offering various genetic building blocks that can be reassembled into functional circuits to regulate gene expression and biological phenotype. Owing to the engineered QS circuitry, cells are endowed with smart functions, such as user-specified sensing and reporting, in situ drug delivery, and sophisticated biosynthesis processes. Further, as researchers have attempted to build more complex functions into a single cell, they have realized that these may be too much responsibility for one microbe to carry. Hence, looking again to nature for guidance, many groups have turned to engineering multispecies consortia that are considered to be more robust than monocultures. In this way, rewired QS networks can help create a synthetic microbial community in which members actively interact with each other with end user–designed guidance. These activities feed well into the emergence of systems biology tools that enable detailed interrogation of various microbiomes. Finally, QS systems and their components can allow direct interaction with abiotic materials, creating biohybrid, microelectronic devices that may integrate with our daily lives. We believe these innovative QS-based methods will no doubt continue to generate impactful applications in the future.

Chapter 3. Engineering communication between the biotic and abiotic realms

ⓘThis chapter is partially adapted with permission, from the following publications:
(1) Li, J., **Wang, S. P.**, Zong, G., Kim, E., Tsao, C.-Y., VanArsdale, E., Wang, L.-X., Bentley, W. E., Payne, G. F., Interactive Materials for Bidirectional Redox-Based Communication. *Adv. Mater.* 2021, 33, 2007758.
(2) Li, J., Kim, E., Gray, K. M., Conrad, C., Tsao, C.-Y., **Wang, S. P.**, Zong, G., Scarcelli, G., Stroka, K. M., Wang, L.-X., Bentley, W. E., Payne, G. F., Mediated Electrochemistry to Mimic Biology's Oxidative Assembly of Functional Matrices. *Adv. Funct. Mater.* 2020, 30, 2001776.

3.1 Chapter Overview

In this chapter, we focused on engineering the interface between biotic factors and abiotic materials to facilitate information transfer between these domains. First, we developed a simple, yet controllable method for assembling live cells with thiolated polyethylene glycol (PEG-SH) to form a hydrogel that resembled the microbial biofilms found in nature. We then modified the PEG-SH hydrogel, endowing it with redox capabilities by covalently crosslinking a redox-active molecule catechol to PEG-SH. This resulted in an interactive material that can autonomously synthesize H_2O_2 as the electrochemical signaling molecule for communication with a bacterial population.

3.2 Motivation and Background

Cell immobilization provides a clever strategy to spatially fix cells on an abiotic surface to create a biohybrid "living electrode," in order to better integrate biological systems that were mostly cultured in a suspension aqueous state with electronic devices. While ideal for bacterial growth, liquid cultures are only viable for a few days and tend to be difficult to maintain and transport (188). Moreover, due to the diffusion-limiting

nature of most electronic signals (e.g., electrons or redox mediators), this also greatly benefits the signal transfer by localizing the cells at the bioelectronic interface. Many immobilization techniques have been explored, and can be roughly categorized into entrapment, adsorption, encapsulation, and containment within synthetic polymers (189, 190). To enable cell attachment on electrode surfaces, certain adsorption-based techniques initially emerge as good candidates since they are developed based on the interactions between biochemical moieties and metal surfaces. For example, both histidine and cysteine residues are known to interact strongly with gold, via its carboxylate or sulfhydryl (thiol) groups, respectively (191, 192). These findings previously birthed multiple biotechnological applications, mostly biosensors (193), enabling multimodal detection of many critical biochemical small molecules. Recently, cell-surface engineering allowed the display of specific peptides to be presented on the cell membrane. Dong *et al.* designed several gold-binding sequences to be surface displayed on *E. coli* outer membrane and demonstrated successful self-assembly of gold nanoparticles driven by metal-peptide interaction (194). Instead of utilizing sulfhydryl moieties, Terrell *et al.* surface displayed a known gold-binding peptide without cysteine and achieved direct assembly of engineered *E. coli* onto the electrode (68). However, these methods require extra genetic engineering to express non-native peptides/proteins which may add metabolic stress to the cells. On the other hand, electrofabrication is an emerging biofabrication approach that provides complementary additive manufacturing capabilities for life science applications (195-198), including bioelectronics (199-201), and regenerative medicine (202). This approach utilizes the fabricated hydrogel to entrap cells within, mimicking key features of the oxidative

assembly of tissue extracellular matrices. Here, we chose a synthetic yet biocompatible polymer PEG-SH that is commonly used in biological applications as a mimic for extracellular matrix (203) and mucin (204) for the entrapment of engineered *E. coli*. In addition to cell immobilization, soft materials were now designed to be capable of enabling "communication" between the material and biology via tailored moduli (205) or specific ligands (206) that interact with cells through mechanical modalities or distinct cell-surface receptors. Because diffusible reactive oxygen species (ROS) are major signaling molecules for redox-based communication in biological systems (e.g., gut microbiome or the rhizosphere) (207-211), we aimed to endow abiotic materials with the ability to participate in redox-based communication and induce biological responses. As nucleophiles, thiol (-SH) groups can undergo conjugation reactions with moieties like quinones that are commonly found in biological systems (212, 213). In this work, we chose to investigate the interaction between PEG-SH and the quinone-forming species catechol (214), with the focus on how catechol-conjugated PEG hydrogel promoted molecular communication with bacterial cells through ROS signaling.

3.3 Results

3.3.1 Electrodeposition of PEG-SH and living cells.

We took inspiration from bacterial biofilms found in nature and created an "artificial biofilm" to immobilize cells onto the electrode surface, generating a "living electrode". The "artificial biofilm" was generated through electrodepositing the bacteria with PEG-SH to form a cell-containing hydrogel. Specifically, cells were

mixed with PEG-SH monomer in a solution containing a redox mediator ferrocene (Fc) to facilitate the oxidation of thiol groups in PEG-SH to form disulfide bonds (**Figure 3.1a**). The ability of redox mediator Fc to oxidatively crosslink PEG-SH was then investigated through cyclic voltammetry (CV) studies. Evidence for mediated oxidation of PEG-SH was provided by CV studies with glassy carbon electrode. The CV plots (**Figure 3.1b**) showed that PEG-SH (50 mg/mL, 10 mM) was oxidized by 5 mM Fc when the working electrode was poised at + 0.5 V. The inserted image showed the PEG-SH polymer formed a hydrogel film in response to Fc oxidation reactions. To demonstrate the deposition of cell-containing PEG-SH hydrogel, we suspended MDA-MB-231 cells (3×10^5 cells/mL) into a deposition solution (50 mg/mL, 5 mM Fc) that also included the thiolated polysaccharide hyaluronic acid (HA-SH; 0.4%) to enable these cells to undergo matrix interactions in the electrodeposited hydrogel (215). Deposition was performed onto an indium tin oxide (ITO)-coated glass electrode (+0.6 V, 5 min), and after deposition these cell-containing PEG-based hydrogels were incubated for 2 days in cell culture medium and then live/dead cell assays were performed. Z-stack images were collected and the fraction of live cells per imaging plane was calculated and shown in the left plot in **Figure 3.2**. These measurements show high cell viability was observed even for cells entrapped close to the electrode surface.

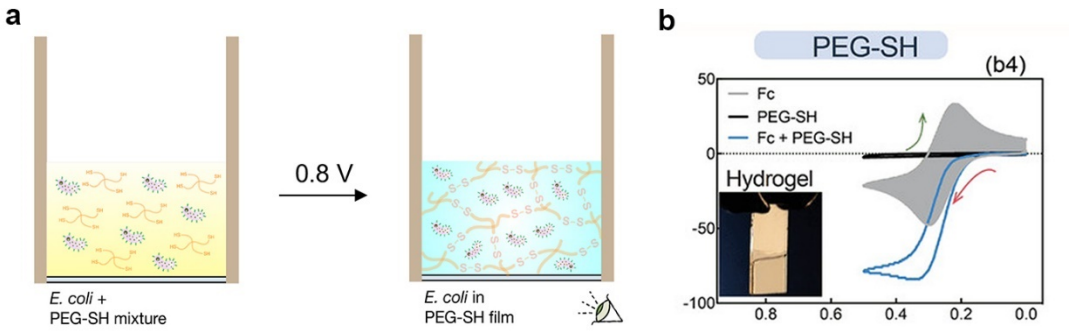

Figure 3.1 PEG-SH hydrogel and "artificial biofilm" deposition.

(a) Schematic illustration of *E. coli* and PEG-SH codeposition. An oxidizing voltage (0.8 V) is used to oxidize the thiol group in PEG-SH and initiate gelation. **(b)** CV result and gel formation photo (inserted) show that Fc can oxidize and crosslink PEG-SH.

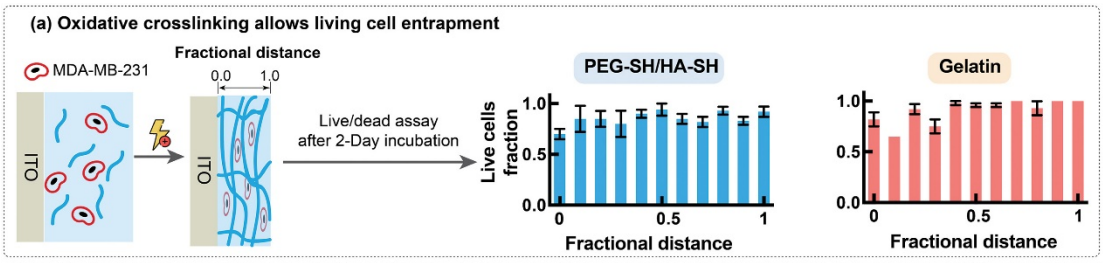

Figure 3.2 Co-deposited cells in PEG-SH films retain high viability.

The mediated oxidation of PEG-SH allows the codeposition of viable human cells.

3.3.2 Controllable fabrication of "artificial biofilm."

We further characterized cell/PEG-SH co-deposition and showed that the "artificial biofilm" can be robustly deposited in a controlled manner. First, electrodeposition of the 'artificial biofilm' can be spatially controlled. As shown by the representative fluorescence images (**Figure 3.3a)**, PEG-SH hydrogel containing SYTO 9-stained *E. coli* BL21 (+0.4 V, 2 min) was homogeneously deposited on a patterned gold electrode and the cell distribution was clearly defined by the geometry of the electrode. We then deposited the same strain onto two electrodes with different surface areas (25 mm^2 and 100 mm^2) with the same oxidation voltage and deposition time (+0.7 V, 2 min), and after deposition both "artificial biofilms" were incubated in LB media for 2 – 5 hours. Since BL21 naturally secretes the QS signaling molecule AI-2 in a constitutive manner, we collected the media during the incubation period and performed AI-2 assay to quantify its AI-2 secretion as a representative of active cell number within the "artificial biofilm". We found that the number of deposited cells also correlated with the size of the electrode (**Figure 3.3b**), suggesting it is possible to guide electrogenetic signal transduction with electrode design.

Second, 'artificial biofilms' can be controllably deposited with custom thickness by varying the deposition time. To enable optical observations, we deposited the film containing *E. coli* DH5α-sfGFP that constitutively express green fluorescent protein (GFP) on an ITO electrode and took confocal Z-stack images to estimate its thickness (**Figure 3.3c**). Our results showed that film thickness, along with the deposited cell count, highly correlated to deposition time (**Figure 3.3d**). This provided an orthogonal approach to precisely control the characteristic of this living material.

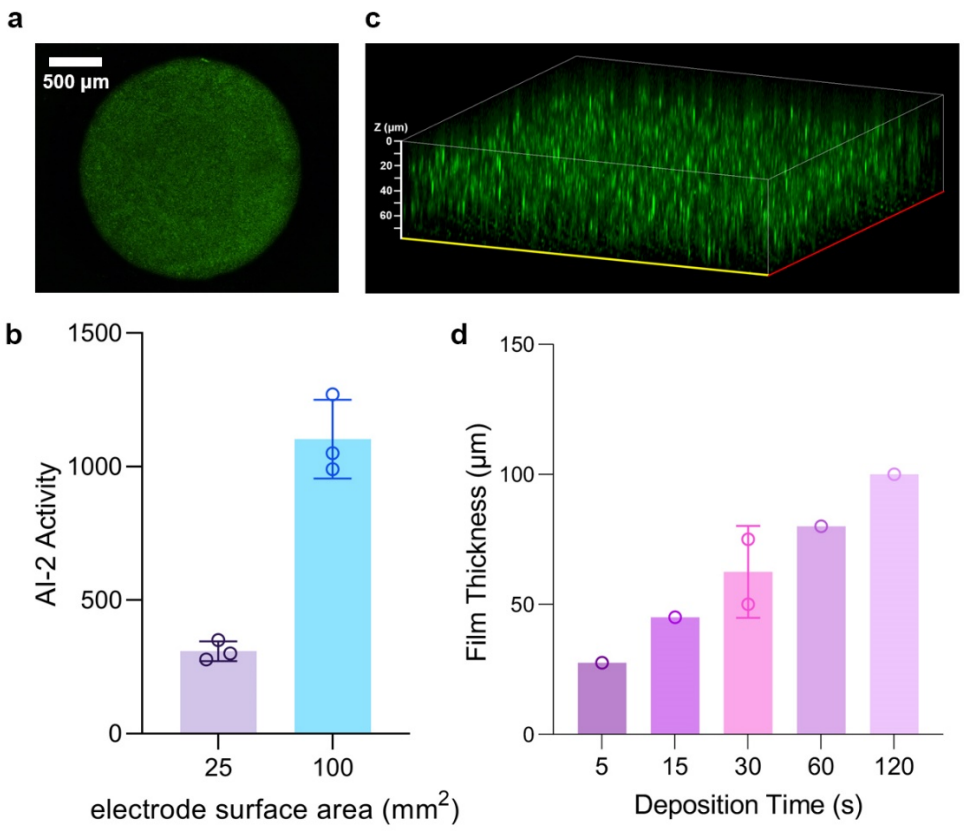

Figure 3.3 "Artificial biofilm" can be controllably electrodeposited.

(a) Fluorescence image of deposited engineered *E. coli*. *E. coli* BL21 were grown to mid-log phase and harvested via centrifugation. The harvested cultures were stained with SYTO-9 and then added into PEG-SH solution for electrodeposition. Electrode diameter = 2 mm.**(b)** AI-2 activity of BL21 cells deposited on electrodes of various sizes. **(c)** Z-stack image of the "artificial biofilm" containing engineered *E. coli* that constitutively express GFP (DH5a-sfGFP). **(d)** Thickness of the deposited "artificial biofilm" as estimated through confocal Z-stack images. Film thickness is customizable by varying deposition time. For **(b)** and **(d)**, bar height represents the mean while open circles represent individual replicates.

3.3.3 Catechol conjugation to PEG-SH film.

CV studies provided initial evidence for catechol and PEG-SH crosslinking. In **Figure 3.4a**, we saw that the control catechol solution underwent reversible electrochemical oxidation and reduction, while the mixture of PEG-SH and catechol showed comparable catechol oxidation and significantly attenuated catechol reduction. This observation suggests the oxidized quinone (Cat^{Ox}) that was generated at the electrode was consumed by reaction with PEG-SH (216). Conceivably, Cat^{Ox} reacted with PEG-SH to form Michael-type thiol-quinone adduct (217, 218). **Figure 3.4b** provided orthogonal evidence from single quadrupole electrospray ionization mass spectrometry (MS) which proved catechol can crosslink thiols through the formation of thiol–quinone adducts. From the MS results, we observed two new peaks from the reaction between catechol and cysteine, in which the peak at *m/z* 230.45 is consistent with the molecular weight of (mono)thiol-quinone adduct and the peak at *m/z* 349.2 suggests that one catechol may form adducts with two cysteines (219, 220).

Catechol oxidation was also demonstrated to cue electrodeposition of a catechol-PEG-SH hydrogel, as shown in **Figure 3.4c**, a colorless hydrogel film was formed. However, the color of the catechol-electrodeposited film changed to brown upon Ir^{4+}-oxidation and switched back to colorless upon DTT-reduction. This observation suggested that catechol-PEG-SH gel the conjugated catechol moieties remain redox-active and can be switched between reduced (catechol) and oxidized (quinone) states (221, 222).

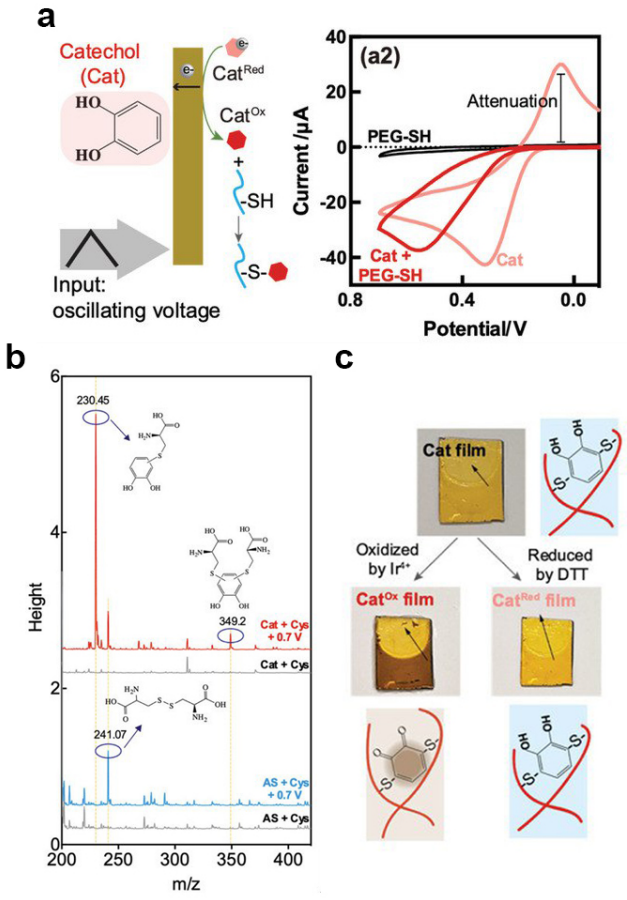

Figure 3.4 Catechol conjugation to PEG-SH hydrogel.

(a) CV with a 4-armed PEG-SH suggests catechol conjugates to the thiol. **(b)** MS with cysteine shows catechol forms thiol-quinone adducts. **(c)** Catechol-deposited films switch their redox state but do not dissolve upon DTT treatment.

3.3.4 Catechol-PEG-SH film promotes communication through ROS signaling.

The interchangeable redox state of the catechol-PEG-SH film leads to another interesting discovery. We hypothesized that this reversible redox nature would enable electron donation to oxygen for generating ROS like H_2O_2. Experimentally, we electrodeposited films onto a gold-coated wafer (+0.7 V, 20 min) and then set the film's redox state by treating with Ir^{4+} or DTT. As illustrated in **Figure 3.5**, these films were then incubated in 1 mL deionized water (room temperature), and the H_2O_2 concentrations in the solutions were then analyzed at pre-determined intervals using the ferrous-mediated oxidation of xylenol orange which generates a purple colored product with a characteristic absorbance peak at 595 nm (223). The inset images in **Figure 3.5** were taken after 24 h incubation, and quantitative results show that the reduced film (designated Cat^{Red}) progressively generates H_2O_2 (approximately 200 μM was generated after 24 h incubation), while the control films show minimal H_2O_2 production. This result demonstrated that the catechol-deposited film in its reduced state can donate electrons for generating H_2O_2.

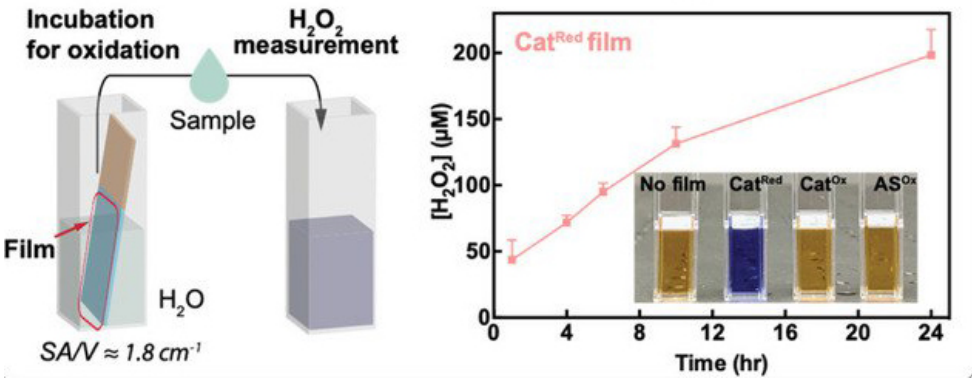

Figure 3.5 The Cat^{Red} film generates H_2O_2 in the presence of O_2.

Cat^{Red} film donated electrons to oxygen and progressively generated up to 200 μM of H_2O_2 in 24 hours.

Because H_2O_2 is an important biological signaling molecule (224), we reasoned that an H_2O_2-generating film could interact with living cells through this native biological communication modality. **Figure 3.6a** illustrated our hypothesis that a Cat^{Red} film can generate H_2O_2 to activate the redox-responsive regulon *oxyRS* in *E. coli* (52, 56, 225). To test this hypothesis, we engineered an *E. coli* reporter cell (NEB10β harboring plasmid pOxy-sfGFP) that responds to H_2O_2 by expression of the reporter protein, superfolder green fluorescent protein (sfGFP) and measured gene expression using fluorescence-activated cell sorting (FACS). Initial characterization of the H_2O_2-response of these reporter cells was provided in **Figure 3.7**. The first histogram in **Figure 3.6b** shows a large population of *E. coli* expressed relatively high levels of sfGFP after 6 h incubation with 200 μM H_2O_2. The second histogram showed the addition of the H_2O_2-degrading enzyme catalase (250 μg/mL) significantly diminished the expression level of sfGFP, confirming the activation of sfGFP expression is caused by H_2O_2.

Next, we investigated whether Cat^{Red} film can induce H_2O_2-dependent gene expression. Experimentally, we electrodeposited the films using 10 mM PEG-SH and 30 mM catechol (+0.7 V, 20 min) onto gold-coated wafer, set the redox state to the reduced state (using DTT), and then incubated the films with 1 mL H_2O_2 reporter cells (grown to mid-log phase) for 6 h. As shown by the histogram in **Figure 3.6b**, a high level of gene expression was observed when the cells were incubated with the Cat^{Red} film, while expression was significantly attenuated when the H_2O_2-degrading catalase was included in the incubation mixture. Incubation with control films (Cat^{Ox} or acetosyringone-deposited films) also showed negligible expression from the H_2O_2

reporter cells after 6 h. These results demonstrated that a catechol-deposited film that is poised in its reduced state can communicate with biology by synthesizing the diffusible H_2O_2 signal that can induce redox-responsive gene expression (e.g., to alter bacterial phenotype).

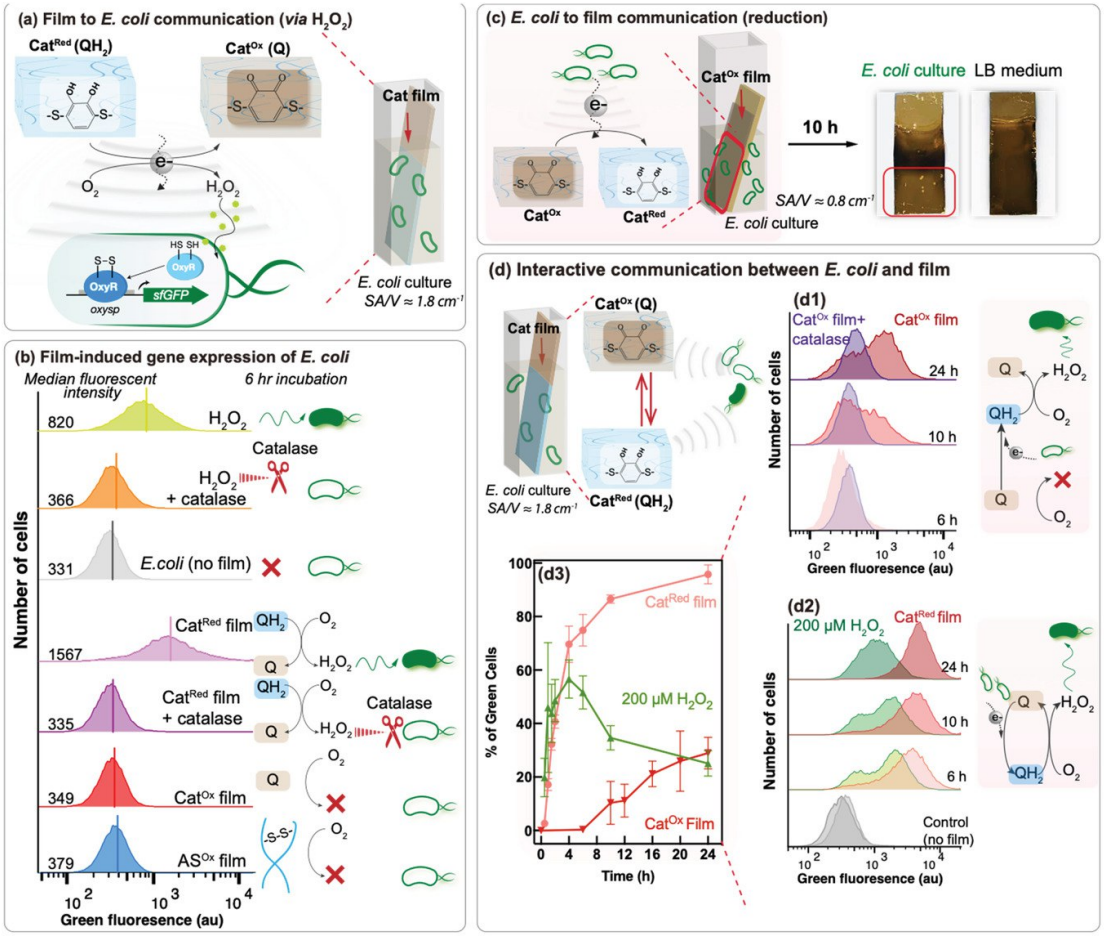

Figure 3.6 Interactive communication between redox-active film and engineered *E. coli* reporter cells.

(a) Schematic of communication from films to *E. coli*: Cat^{Red} films generate H_2O_2 to induce a response in *E. coli*. **(b)** FACS evidence that Cat^{Red} films induce H_2O_2-specific gene response (measured after 6 h). **(c)** Communication from *E. coli* to films: *E. coli* donate electrons to the Cat^{Ox} film which leads to a decrease in color of the exposed region. **(d)** Biological evidence for the interactive redox-based communication between films (Cat^{Ox} and Cat^{Red}) and *E. coli*.

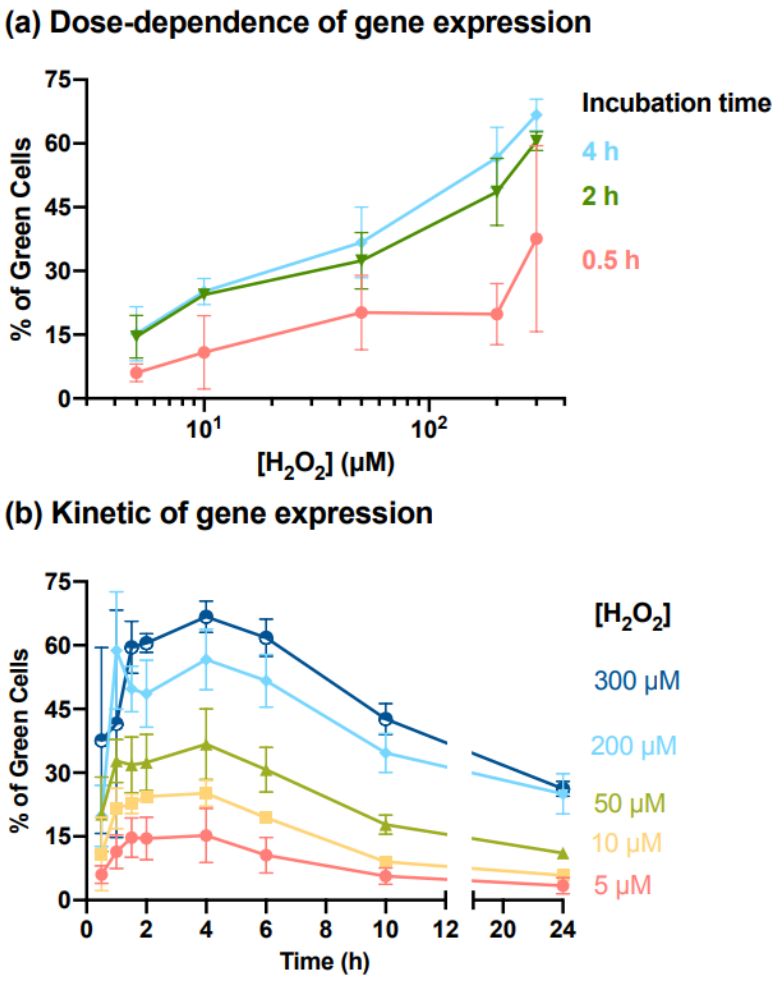

Figure 3.7 Dose-dependence and time-dependence of gene expression in response to H_2O_2.

Engineered H_2O_2 reporter cells were collected at pre-determined time points after exposure to exogenously-added H_2O_2. FACS was used to determine their fluorescence levels (% green cells).

3.3.5 Interactive communication between catechol-PEG-SH film and *E. coli*.

We then tested for communication in the opposite direction: the bacterial-mediated transfer of electrons to an oxidized Cat^{Ox} film. Bacterial extracellular electron transfer is well known for processes that include energy metabolism (226), biofilm development (227, 228), antioxidant protection (229), and virulence (230). The simplest illustration of electron transfer from bacteria to the film is to observe a change in the film's redox-state dependent optical properties upon contact with a bacterial culture. Experimentally, we prepared catechol-deposited film (10 mM PEG-SH, 30 mM catechol, +0.7 V, 5 min), poised the film's redox state to the oxidized state (by Ir^{4+} treatment) and transferred this film-coated electrode to 800 µL of a high-density *E. coli* culture (OD_{600} = 3) as illustrated in **Figure 3.6c**. The first photograph in **Figure 3.6c** showed the bottom portion of the initially brown Cat^{Ox} film lost color after 10 h contact with the *E. coli* culture, while the second photograph shows no such color change for the film that was exposed to cell-free LB media. These results are consistent with the redox-responsive color change of catechol-deposited film shown in **Figure 3.4**, indicating the oxidized Cat^{Ox} film can accept electrons from *E. coli* culture.

Next, the bidirectional interactive communication between the films and bacteria was demonstrated by a study of the biological response of the *E. coli* H_2O_2 reporters. Briefly, films were electrodeposited (10 mM PEG-SH, 30 mM catechol, +0.7 V, 20 min) and poised to specific redox state (by DTT or Ir^{4+} treatment), and these films were incubated with 1 mL *E. coli* culture (OD_{600} = 0.4) under shaking for 24 h. At predetermined intervals, the expression of sfGFP was analyzed and quantified by FACS as the percentages of the population responding (i.e., green cells). **Figure 3.6**

d(1) shows the representative FACS histogram of *E. coli* incubated with the Cat^{Ox} film: initially, the expression was negligible at 6 h; small fluorescent population was observed at 10 h; and a larger fluorescent population was observed at 24 h. When the H_2O_2-degrading catalase was included in the incubation mixture, expression of sfGFP was significantly suppressed over the full 24-h time course. As illustrated by the scheme in **Figure 3.6d**, these results provide biological evidence for interactive communication between the Cat^{Ox} film and *E. coli*: *E. coli* must provide the source of electrons that reduce the Cat^{Ox} film, which in turn enabling it to transfer these electrons for the generation the H_2O_2 and induction of the H_2O_2-specific response in the reporter cell culture.

The representative FACS histograms of *E. coli* reporter cells incubated with the Cat^{Red} film are shown in **Figure 3.6 d(2)** and compared with the response of a control culture exposed to 200 μM H_2O_2 (the concentration generated after 24 h from the Cat^{Red} film of **Figure 3.5**). These histograms show both cultures respond rapidly to H_2O_2 while the cultures exposed to the Cat^{Red} film show a stronger and more prolonged response (compared to the H_2O_2-control). As illustrated by the scheme in **Figure 3.6 d(2)**, this more prolonged response in the presence of the Cat^{Red} film suggested a redox cycling between the bacterial culture and the film which provides additional evidence for interactive communication. **Figure 3.6 d(3)** showed the time course FACS results which summarized the observations from this experiment. The culture exposed to the Cat^{Red} film showed a large and progressively increasing H_2O_2-induced response (compared to the H_2O_2-control), while the culture exposed to the Cat^{Ox} film shows a significant but delayed response.

3.4 Discussion and Conclusion

In this chapter, we first employed mediated electrochemistry to generate diffusible oxidants that enabled the generation and functionalization of polymeric hydrogels like PEG-SH. This approach mimics biology's oxidative matrix assembly in ways such as these reactions occur under physiologically relevant conditions which enable the incorporation of functional biological components (e.g., active enzymes and living cells). We then demonstrated a simple, controllable method for assembling live cells into 'artificial biofilms' directly on the electrode to ensure efficient information flow at the bio-electronic interface and eliminate transport-limited heterogeneous responses in suspended biological systems (231, 232). This approach does not require genetic engineering; thus, relieving the extra metabolic burden from the entrapped engineered cells for more effective use of resources on critical functions (233), or instead opening more possibilities for immobilizing any living organisms without the need for inserting non-native genetic circuitries. Moreover, cell/PEG-SH co-deposition is shown to be scalable and spatially programmable, inviting future opportunities for cell grafting on complex formats like three-dimensional, miniaturized, arrayed electrodes; or on soft, flexible, bio-compatible materials, for wearable, ingestible, or other portable system (234, 235).

We then reported a hydrogel film capable of interactively communicating with biology through a native redox modality. Specifically, a redox-active catechol conjugated/crosslinked PEG-SH film was formed by one-step electrodeposition. We demonstrated that this film could accept electrons from biological reductants and donate electrons to O_2 to generate the diffusible H_2O_2 signaling molecule. In the

presence of a culture of *E. coli* H_2O_2 reporters, this catechol-conjugated gel was shown to accept electrons from *E. coli* culture and autonomously synthesize H_2O_2 to induce redox-responsive gene expression. This demonstration that catecholic materials can communicate with biology through a native redox modality has relevance both for the development of interactive materials (236) and characterization of the participation of non-living components (e.g., melanin) in redox biology (237, 238).

3.5 Methods

3.5.1 Materials

Potassium chloride (KCl), H_2O_2 (30%), phosphate buffered saline (PBS), potassium phosphate monobasic (KH_2PO_4), potassium phosphate dibasic (K_2HPO_4), AS, and potassium hexachloroiridate(III) (K_3IrCl_6, Ir), and catalase were purchased from Sigma Aldrich. Lysogeny broth (LB) was from Fisher Scientific. PEG-SH (4 arm, MW 5000) was purchased from JenKem. Thiol-modified hyaluronic acid (Glycosil, GS222) was purchased from ESI-Bio. Fc was purchased from VWR. DMSO stock solutions of AS and Fc were prepared and diluted into desired concentration by PB (pH 7.4 0.1 M phosphate buffer) before use. All the other chemicals were dissolved in PB unless otherwise stated. MDA-MB-231 cells were purchased from American Type Culture Collection (ATCC). Pierce quantitative peroxide assay kits and LIVE/DEAD Viability/Cytotoxicity Kit (L3224) was purchased from ThermoFisher Scientific. Standard glassy carbon and gold electrodes were purchased from CH Instruments.

3.5.2 Electrode chip fabrication

Gold-coated wafer electrodes were purchased from LGA Thin Films. ITO-coated glass substrates were purchased from Sigma Aldrich. Gold patterned electrodes were purchased from Platypus Technologies and Pine Research. Steps for fabricating the custom patterned gold electrode on silicon wafers by Platypus Technologies were as follows: First, metal deposition was performed on standard 4-inch silicon wafers using a Denton thermal evaporator (Denton Vacuum), with metal deposition rates of 2–3 Å s^{-1}. Specifically, a 50 nm chromium adhesion layer was evaporated, followed by 100 nm gold. Next, photolithography utilized direct writing of photoresist via a DWL66fs laser writer (Heidelberg Instruments), guided by a laser exposure map designed in AutoCAD (Autodesk). Photoresist spin-coating and development steps were performed using an EVG120 automated resist processing system (EV Group). The patterned wafer was post-processed by etching, photoresist stripping and cutting individual electrodes with a DAD dicing saw (DISCO). The patterned gold electrode purchased from Pine research was made by screen-printing gold on a ceramic base, with a 2 mm^2 diameter gold working electrode, a printed Ag/AgCl reference electrode, and a printed gold reference electrode.

3.5.3 Instrumentation

For electrochemical measurement and deposition, a multichannel CHI1040C electrochemical analyzer was used. UV-Vis spectrometry measurements were performed on SpectraMax M2 from Molecular Devices. Mass Spectrometry was obtained by a Waters SQ Detector 2 single quadrupole mass spectrometer, combined with a Waters Alliance® e2695 HPLC system equipped 2 with a dual absorbance 2489

UV/Vis detector. Flow cytometry analysis were performed using a BD FACSCelesta flow cytometer (BD Bioscience).

3.5.4 Electrodeposition of PEG-SH

Electrodeposition was performed using a three-electrode system with Ag/AgCl as reference electrode, Pt wire as counter electrode, and the working electrode can be chosen from gold, glassy carbon, or ITO depending on the experiment. Solutions of PEG-SH (50 mg/mL) containing 5 mM mediator were deposited using constant voltage for 1–10 min, unless otherwise noted. For gold and glassy carbon working electrodes, voltages ranging from +0.4 – +0.7 V were applied to cue the Fc-mediated oxidation. For the ITO working electrode, a constant voltage of +0.8 V was applied to induce Fc oxidation.

3.5.5 Co-deposition of MDA-MB-231 Cells.

To demonstrate the oxidative mediators are benign enough to entrap viable cells, breast cancer cells (MDA-MB-231) were allowed to co-deposit with hydrogels. Prior to electrodeposition, ITO-electrode chips were cleaned with ethanol then sterilized via UV exposure for 30 min, and cells were resuspended at 3×10^5 cells/mL in PEG-SH (50 mg/mL, containing 5 mM Fc). (Note: 0.4% thiol-modified HA-SH were added to PEG-SH deposition solution to allow cell adhesion.) After 5 min electrodeposition, excess deposition solution was removed, and the cell-containing gels were rinsed with 37 °C PBS. Each chip was then placed into a well of a 6-well place, 2 mL of 37 °C medium was added, and the plate was placed in the incubator. After 48 h, the medium was removed from each well, the gels were rinsed with warm PBS, and 150 μL of PBS

solution containing 0.1% Calcein AM and 0.1% ethidium bromide was incubated with the sample for 25 min at 37 °C. Samples were then rinsed with 37 °C PBS and imaged on an Olympus IX83 inverted microscope using a live-cell imaging chamber maintained at 37 °C, 50% humidity, and 5% CO2:95% air. Z-stack images were collected every 20 μm using a 20× objective. Five Z-stack images were collected per sample and the fraction of live cells per imaging plane was calculated. The imaging plane was normalized as relative distance from the electrode for each gel to correct for slight variations in thickness.

3.5.6 Electrodeposition of *E. coli* and PEG-SH.

E. coli grown to mid-log phase were harvested via centrifugation at 3000 × g for 10 minutes, then resuspended in 1x PBS to 2x the desired OD. To prepare the 2x PEG-SH solution, 100 mg/mL of PEG-SH were dissolved in phosphate buffer (PB) containing 10 mM Fc. Prior to electrodeposition, the two solutions were mixed at a 1:1 ratio. We then performed chronoamperometry, poised at +0.8 V for 30 s, to initiate oxidation of the thiol group for crosslinking. The endpoint charge was recorded for each run. Excess cell/PEG-SH solution was then removed, and the generated film was carefully washed with PBS to remove any unbound *E. coli*/PEG-SH solution.

3.5.7 Mass Spectroscopy to characterize catechol-PEG-SH conjugation.

To investigate the reaction mechanism between thiols and catechol, the oxidation reaction product of cysteine/catechol was analyzed by Mass Spectrometry (MS). Experimentally, a Pt foil (2 cm × 2 cm) was used as working electrode, Ag/AgCl as reference electrode, and a Pt wire separated from the working electrode by a salt

bridge was used as counter electrode. The three electrodes were immersed in solution containing 5 mM cysteine and 5 mM catechol and constant voltage of +0.7 V was imposed. After 10 mins reaction, the product was collected and analyzed by ESI-MS immediately. Prior to the analysis, polarity-based separations were performed using an analytical reverse-phase C18 column (XBridge®, 2.1 × 50 mm, 3.5 μm) at a flow rate of 0.4 mL/min. The column was eluted using a linear gradient of 5- 90% MeCN in 8 min with both solvents containing 0.1% formic acid (FA).

3.5.8 Redox-responsive *E. coli* reporter cells and FACS measurements

Bacterial strains and plasmids used in this chapter are listed in **Table 3.1**. Plasmid pOxyRS-sfGFP was constructed with conventional PCR amplification and Gibson Assembly. The derived plasmid was confirmed by Sanger sequencing (Genewiz, NJ). To characterize the H_2O_2-responsive characteristics of the reporter cells, we performed studies in which the cultures were exposed to externally-added H_2O_2. Cells were grown overnight in LB media supplemented with ampicillin (50 μg/mL) at 37˚C in a shaker at 250 rpm, and the overnight cell culture was then diluted 100 times the next morning and grown in LB at 37°C to ensure exponential growth. As the cell density reached OD600 = 0.4, 1 ml of cell suspension were incubated with varying concentrations of exogenously-added H2O2 with shaking at 250 rpm at room temperature. 50 μL of cells were collected at pre-determined intervals and at once mixed with equal parts of sterile glycerol solution (50% v/v) and frozen at -80°C for subsequent flow cytometry experiments. On the day of analysis, 50 μl of samples were thawed and resuspended in 800 μl of ice-cold PBS. Flow cytometry analyses were

performed using a BD FACSCelesta flow cytometer (BD Bioscience) with which 20,000 events per sample were recorded and analyzed.

Table 3.1 *E. coli* strain and plasmid used in this chapter.

Strain	**Description**	**Reference**
NEB10β	Δ*(ara-leu) 7697 araD139 fhuA* Δ*lacX74 galK16 galE15 e14-* ϕ*80*d*lacZ*Δ*M15 recA1 relA1 endA1 nupG rpsL* (Str^R) *rph spoT1* Δ*(mrr-hsdRMS-mcrBC)*	New England Biolabs
Plasmid	**Description**	**Reference**
pOxyRS-sfGFP	pBR322, proD promoter, *oxyR*, *oxyS* promoter, *sfGFP*	This study

Chapter 4. Strategies to Facilitate Expression of 5xCys-Tagged Proteins for Electrobiofabrication

ⓘThis chapter is adapted, with permission, from the following publication: **Wang, S.**, Tsao, C.-Y., Motabar, D., Li, J., Payne, G. F., and Bentley, W.E. A Redox-Based Autoinduction Strategy to Facilitate Expression of 5xCys-Tagged Proteins for Electrobiofabrication *Front. Microbiol.* 2021, 12.

4.1 Chapter Overview

In this chapter, we introduced a polycysteine-tagged *Streptococcal* protein G for PEG-SH hydrogel surface decoration to enable recognition of cells and other biological molecules. We found, however, that its expression and purification from *E. coli* were difficult, owing to the extra cysteine residues. We developed a redox-based autoinduction methodology that greatly enhanced the yield, especially in the soluble fraction of *E. coli* extracts. The redox component involved the deletion of *oxyRS*, a global regulator of the oxidative stress response and the autoinduction component integrated a quorum sensing (QS) switch that keys the secreted QS autoinducer-2 to induction. Interestingly, both methods helped when independently employed and further, when used in combination (i.e., autodinduced *oxyRS* mutant) the results were best—we found the highest total yield and highest yield in the soluble fraction. We hypothesize that the production host was less prone to severe metabolic perturbations that might reduce yield or drive sequestration of the -tagged protein into inclusion bodies. We expect this methodology will be useful for the expression of many such Cys-tagged proteins, ultimately enabling a diverse array of functionalized devices.

4.2 Introduction

Affinity tags incorporated into the primary sequences of recombinant proteins were initially developed as a means to facilitate their purification and/or detection (239, 240). Because protein engineering is now fairly routine, the incorporation of "designer" tags has emerged enabling a variety of new functions including protein attachment onto both biotic and abiotic materials. For example, a pentatyrosine pro-tag was shown to allow tyrosinase-mediated covalent coupling of an IgG-binding protein G or a human glycoprotein, ApoH, with both polysaccharides (241) and silk fibroin from *Bombyx mori* (242); a polyglutamine tag facilitated the assembly of proteins onto both gelatin (243) and spider silk (185); and a polylysine tag was added to enzymes for covalent tethering onto engineered tobacco mosaic virus-derived virus like particles (244). Other peptide tags of varied amino acid composition enable binding onto solid materials such as gold (245), silver (246), and silicon (247) through non-covalent interactions. Methodologies that allow protein attachment to various substrates have created new possibilities to construct devices with diverse functions introduced by the assembled proteins. These "designer" proteins, however, can also present challenges in expression and purification, owing to the added tags (248, 249); yet their value is worth the challenge.

For example, we recently showed how a protein carrying a pentacysteine tag could be covalently tethered onto an electrode-assembled thiol-containing polyethylene glycol (PEG) hydrogel film. Film-associated thiol groups (250) served as substrates for covalent assembly of engineered proteins, especially when electrochemically converted to sulfenic acid groups so that the cysteine-tagged proteins could rapidly and

spontaneously form disulfide bonds. That is, the disulfide bonds were enabled by providing a redox mediator and an oxidizing voltage to the electrode so that the mediator abstracted electrons from the thiol, leaving the reactive sulfenic acid. In this way, the assembled proteins are restricted to the boundaries of the electrode, upon which the PEG is electroassembled. The same electrode surface can then serve as an electrochemical sensor with functionalized proteins to suit any purpose. Developing surfaces with functionalized PEG is attractive for many reasons, including detailed studies on a variety of biological interactions. For example, PEG is used as a mimic for extracellular matrix (ECM) (203) and mucins found in epithelial tissues (204); electrodeposited PEG could be functionalized with designer proteins and, because it is surface assembled, it also can be made accessible to various analytical measurements. As such, we showed how this film could be functionalized with a pentacysteine (5xCys)-tagged *Streptococcal* protein G to enable antibody-based immunoassays (251). In the present study, however, we further show how the same 5xCys-tagged protein G, oxidatively assembled onto a PEG hydrogel can serve to capture cells onto an electrode surface, via protein G-assembled IgG.

Despite their versatility, the expression of cysteine-rich proteins has long been considered tricky in *E. coli* due to inherent issues brought about by the extra cysteine residues. Aggregation of cysteine-rich proteins usually results in inclusion body formation as the reduced state in the cytoplasm makes forming the disulfide bonds difficult (which enables proper folding). A variety of methods have been reported to tackle these issues, for instance, optimizing culture and purification conditions (252), recovering and re-folding active proteins from inclusion bodies (253), expression in the

periplasm, and many others (254). In addition to this array of strategies, in this study we have coupled two, somewhat disjoint methodologies, but when combined lead to significantly increased yields of soluble protein.

First, we sought to reduce inclusion body formation with an autoinduction method mediated by rewired quorum sensing (QS). Overexpression of a recombinant protein is often accompanied by an imbalance of metabolism, often referred to as a "metabolic burden" (255). In addition, the induction process is typically initiated by the addition of a bolus of inducer, which, in turn, can bring about significant transients in precursors or energy levels (256-258). This imposed stress could exhaust the bacterium's innate protein folding and quality control machinery, leading to improperly folded proteins that aggregate and form inclusion bodies or get targeted for degradation. By rewiring the native quorum sensing system of *E. coli*, we had previously developed an autonomous induction system that used QS autoinducer signals (i.e., autoinducer 2, AI-2) to guide high level expression of recombinant proteins (109).

As shown in **Figure 4.1**, *E. coli* naturally secrete AI-2 that accumulates in the culture fluids as the cells grow in number. When the autoinducer reaches a certain level, as indicated by reaching a "quorum" of cells, it is transported back inside via an ATP-dependent transporter where it is phosphorylated and initiates transcription from a LuxS-dependent regulon (Lsr) (91, 93, 259, 260). In Tsao *et al*., the native *lsr* promoter was used to induce the T7 polymerase that, in turn, was used to activate T7-based expression from a common pET vector. In essence, the added T7 circuit serves to amplify the original *lsr*-mediated expression. Aside from being a signal for cell-cell communication, AI-2 is produced by the enzymes Pfs and LuxS which are key elements

in central metabolism (261), and because of this we reasoned that AI-2 might also serve as an indicator for the host's metabolic state (98). In fact, adding AI-2 by enhancing endogenous synthesis to cells overexpressing recombinant proteins served to increase yield (262). Owing to the nature of QS, which allows an individual bacterium's metabolic state to be probed and communicated to an entire population, we hypothesized that a QS-mediated autoinduction method would be "gentler" than the conventional, yet more "disruptive" IPTG induction method, and could cater to the expression and growth pace of the expression host.

Second, we sought to influence the ability of the cell to respond to oxidative/redox stresses, such as those that might accompany the rapid onset of protein synthesis where those proteins were potentially good substrates for sequestering reactive oxygen species (ROS). By deleting the oxidative stress regulon *oxyRS*, we not only attenuate the cell's ability to respond to oxidative stress but hope to alter the reduced state of *E. coli*'s cytoplasm enabling a more oxidized state that favors disulfide bond formation. Several strains with deficiency in enzymes related to reduction of antioxidants (e.g., thioredoxin and glutathione) have shown to produce higher yields of properly oxidized proteins (263, 264). As a global transcription regulator, OxyR regulates the expression of many of these enzymes such as glutathione oxidoreductase (*gor*) (265) and alkyl hydroperoxide reductase (*ahpC*) (266, 267). The non-coding RNA *oxyS*, too, is reported to regulate the oxidative state as in intracellular peroxide (H_2O_2) levels (268). Together, we aimed to investigate the effects of AI-2 mediated autoinduction and *oxyRS* deletion separately and in combination, to enable increased yield of 5xCys-tagged protein G.

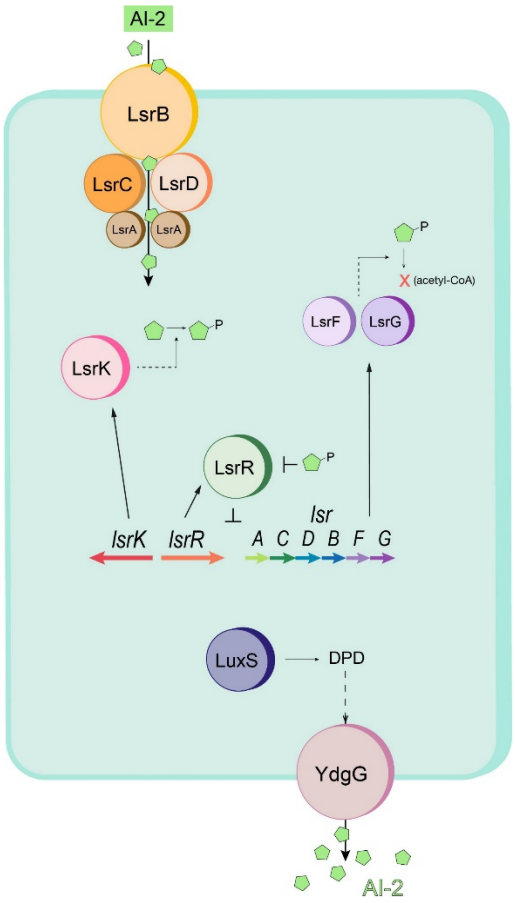

Figure 4.1 Schematic of the *E. coli* quorum sensing (Lsr) system.

AI-2 (green pentagons) is imported into the cell by the Lsr transporter (LsrACDB) and is then phosphorylated to AI-2P by LsrK. When AI-2P binds LsrR and releases LsrR from the promoter region (thus modulating Lsr gene expression), AI-2 uptake is increased. Intracellular AI-2P is processed and degraded by LsrF and LsrG. LuxS produces DPD, the precursor to AI-2. The autoinducer is exported by YdgG (TqsA).

4.3 Results

4.3.1 Polycysteine (5xCys) Tag Allows Protein Biofabrication on Thiolated Surfaces to Create Biohybrid Devices.

Though earlier biofabrication studies had focused on the gold-binding ability of cysteine residues (244, 269), in this study we sought to demonstrate its capability to form covalent bonds with thiol-containing biomaterials. To do so, we designed a polycysteine tag inserted at the C-terminus of the target protein and retained the N-terminus His-tag found in many commercial expression vectors (e.g., pET plasmids) for purification purposes (**Figure 4.2**). We had previously developed an electrodeposition method to build PEG-SH hydrogels and showed that 5xCys-tagged proteins can be oxidatively conjugated to electrodeposited hydrogels in a "targetable" manner (250). Here, we further show the possibility to build multifunctional, bio-hybrid devices with such fabrication methods and 5xCys-tagged biomaterials. First, an antibody-binding platform suitable for immunoassays was built (**Figure 4.3a**) by engineering the antibody-binding Streptococcal protein G Fc binding domain with the 5xCys tag. Both fluorescent (**Figures 4.3b-e**) and HRP-labeled (250) antibodies were shown to bind onto protein G-5xCys conjugated PEG hydrogels. Then, a cell-capture device was assembled using a similar setup (**Figures 4.3f-j**): the protein G bound to the PEG hydrogel was used to capture anti-*E. coli* antibodies. This assembly was proven to successfully capture *E. coli* from solutions of growth media over the course of an incubation period of 1–1.5 h at room temperature. Note that surfaces without the protein G-5xCys layer exposed identically to *E. coli* did not retain cells. While this is largely a result of the specificity of the anti-*E. coli* antibody, it also reflects the minimal

level of non-specific binding attributed to the PEG hydrogel, consistent with many reports regarding the properties of PEGylated surfaces. Note also that the spatial selectivity attributed to this electroassembly method, and the PEG surface is clearly visible at the electrode boundary in **Figure 4.3b**).

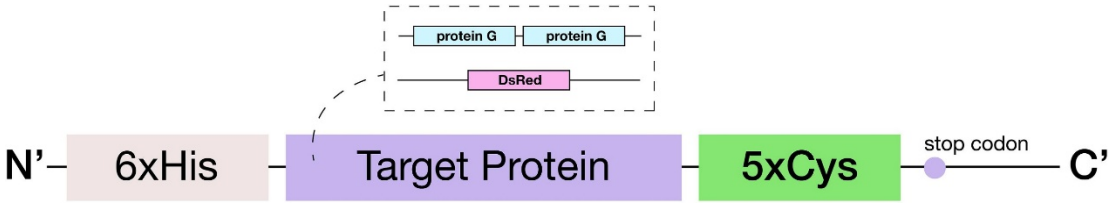

Figure 4.2 Schematic of the engineered 5xCys-tagged protein.

Two target proteins: (1) red fluorescent protein DsRed and (2) two copies of *Streptococcal* protein G Fc binding domain in tandem were engineered to consist of an N-terminus 6xHis tag and a C-terminus 5xCys tag.

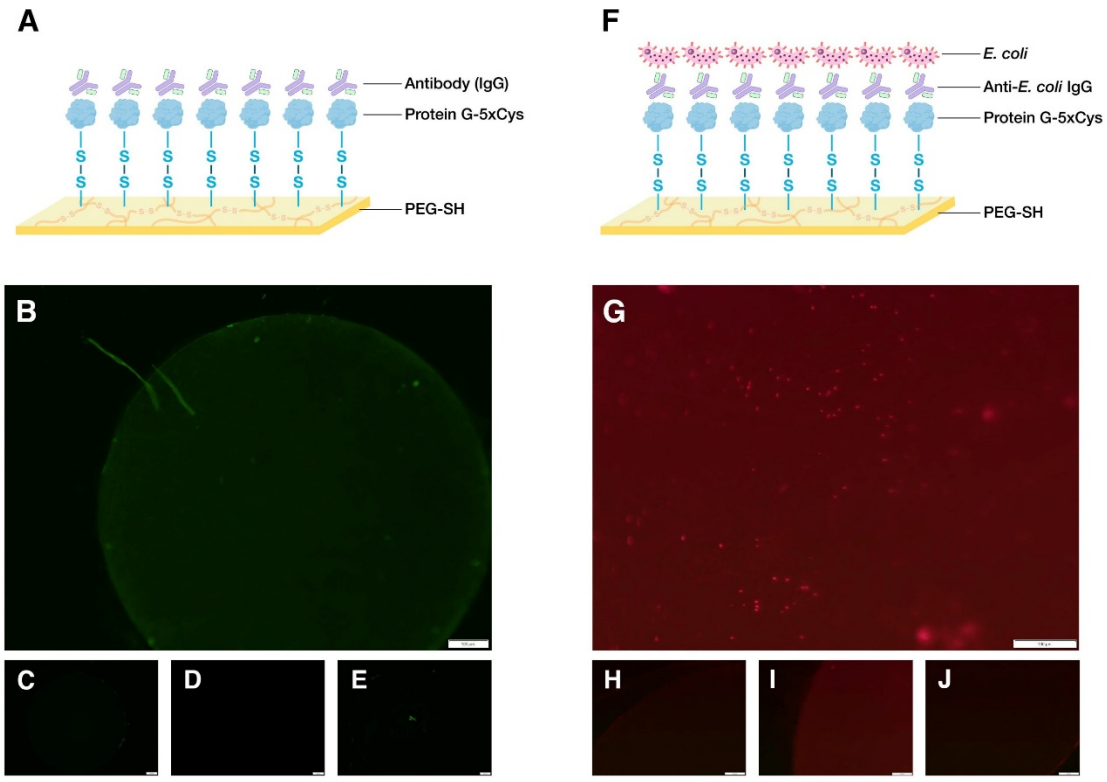

Figure 4.3 Demonstration of biodevice assemblies.

(a) Schematic of an antibody-binding platform, image created using assets from BioRender.com. Here, 5xCys-tagged protein G is covalently grafted onto sulfenic acid groups on the surface of electroassembled thiolated polyethylene glycol (PEG-SH). The protein G binds to the Fc region of IgG. **(b)** 1.6x microscope image of a working antibody-binding platform: PEG-SH coated standard gold electrode + protein G-5xCys + IgG:DyLight 488 **(c-e)** Control images: **(c)** standard gold electrode electrodeposited with PEG-SH hydrogel **(d)** PEG-SH coated electrode + protein G-5xCys. **(e)** PEG-SH coated electrode + IgG:DyLight 488 antibody. Exposure time = 200 ms. **(F)** Schematic of a cell-capture platform. Here, the IgG captured by the protein G in **(a)** presents anti-*E. coli* antigen binding domains to the solution containing *E. coli*,

enabling cell capture. **(g)** 12.6x microscope image of a working cell-capture platform: PEG-SH coated standard gold electrode + protein G-5xCys + Anti-*E. coli* IgG + *E. coli* BL21 (DE3) with constitutive DsRed expression. **(h-j)** Control Images: **(h)** standard gold electrode electrodeposited with PEG-SH hydrogel **(i)** PEG-SH coated electrode + protein G-5xCys **(j)** PEG-SH coated electrode + Anti-*E. coli* IgG + *E. coli* BL21 (DE3) with constitutive DsRed expression. Exposure time = 650 ms.

4.3.2 Cellular Induction Strategies to Improve 5xCys-Tag Recombinant Expression.

During the His-tag mediated purification processing of 5xCys-tagged proteins, we had observed their yields were significantly lower when compared to the identically expressed and purified non-Cys tagged counterparts. As shown in **Figure 4.4a**, overnight expression of both DsRed and DsRed-5xCys by 1 mM IPTG-induced BL21 (DE3) appeared to be roughly equal. That is, both the pellet size and the fluorescence intensity was similar whether or not the Cys-tag was present. After a standard cell lysis procedure, however, very little soluble DsRed-5xCys was found in the protein extraction reagent and instead, the insoluble cell debris remained bright red. This was the opposite for the DsRed counterpart with no tag (**Figure 4.4b**). Hence, we hypothesized that the inserted cysteine residues promoted aggregation and thus resulted in a more prominent insoluble fraction. Presumably, the protein had agglomerated into inclusion bodies. Though active proteins could be isolated and recovered from inclusion bodies, the process was laborious and the final yield remained very low. To overcome this issue, we have attempted two strategies that focus on the host as described below.

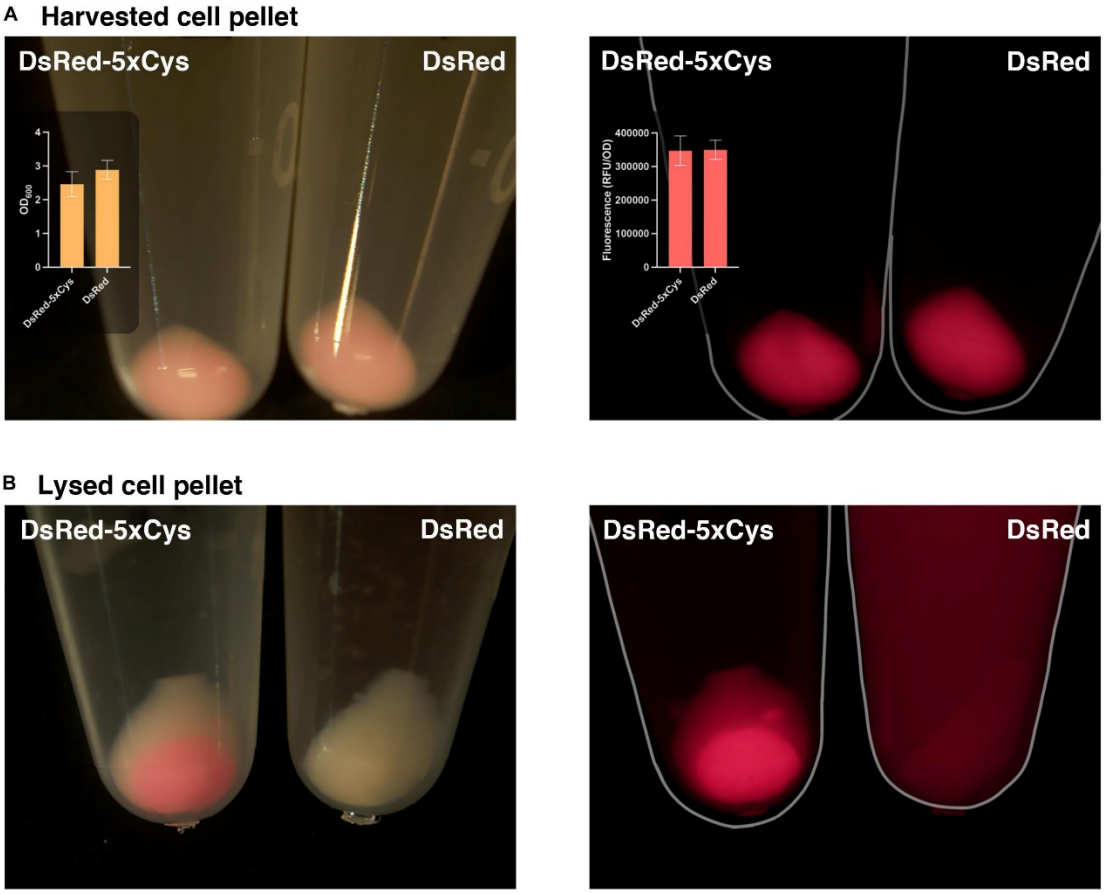

Figure 4.4 5xCys tag promotes inclusion body formation.

(a) Harvested BL21 (DE3) cells induced with 1 mM IPTG overnight for DsRed-5xCys or DsRed expression. Left: bright view; Left inset plot: Mean OD_{600} values (n = 3); Right: fluorescent microscope, CY3 filter; Right inset plot: Mean red fluorescence (RFU/OD_{600}) (n = 3). Error bars represent the standard deviation between replicates. **(b)** Cell pellets lysed with Bugbuster solution (shaking at 150 rpm for 1 h at room temperature) for soluble protein extraction. Left: bright view; Right: fluorescent microscope, CY3 filter.

4.3.3 QS-Mediated Autoinduction Reduces Inclusion Body Formation

First, we sought to lessen the metabolic burden brought about by overexpression with an alternative induction method. To enable QS-mediated autoinduction, the plasmid encoding the 5xCys-tagged protein G (pET-G2Cys5) along with a "switch" plasmid (pCT5) as described in (109), were transformed into wildtype (ZK126) and an *E. coli* W3110 *lsrFG* null mutant, which is an AI-2 hypersensitive strain (CT103). This strain, lacking AI-2 processing enzymes, LsrFG, accumulates phosphorylated AI-2 in the cell cytoplasm and is denoted "hypersensitive" because the level of *lsr*-mediated transcription can be much higher than would normally be expected for a given concentration of AI-2 outside of the cell (128, 270, 271). The gene deletions should not alter the promoter strength, nor transcription rate, but instead, should turn on the promoter at lower AI-2 levels. In **Figure 4.5**, we show Western blot results from the autonomously induced ZK126 strain, autonomously induced CT103, and control cultures of BL21 (DE3) where IPTG is added at mid-log phase to induce the *lac* promoter. The latter represents the standard method for IPTG induction. Note that in order for the autonomously induced cells to actuate gene expression, the level of AI-2 must accumulate and subsequently be transported back into the cells where it initiates transcription via the *lsr* promoter (**Figure 4.1**). Thus, the yield in the autonomously induced ZK126 was initially low (i.e., at 2 h), but this quickly increased and eventually surpassed the yield of BL21 (DE3), a control culture with inducer IPTG added at time zero. The autoinduced culture exhibited the highest total yield and the highest soluble fraction. Interestingly, upon IPTG induction of the *E. coli* BL21 (DE3) control, the target protein seemed to accumulate rapidly, resulting in the highest amount

of target protein at 2 h post-induction (**Figure 4.5**). Nonetheless, in agreement with our observations of the cell pellets, ~ 35% of the total target protein was found in the insoluble fraction (**Figure 4.5**).

Most noteworthy was that the amount of protein G-5xCys found in the insoluble fractions of both the two autonomously induced hosts CT103 and ZK126 was significantly lower than the IPTG-induced culture. We estimated that the protein G-5xCys in the insoluble fraction of the autonomously induced ZK126 cells constituted less than 10% of the total yield. To our surprise, the yield of autonomously induced CT103 was consistently low throughout, lower than both the ZK126 autoinduced culture and the traditional IPTG-induced BL21 (DE3) expression. These results demonstrate that even though the yield of IPTG-induced BL21 (DE3) was high, a substantial amount of the target protein was found to be insoluble and had gone to waste. With QS-mediated autoinduction, the insoluble fraction (presumably found in inclusion bodies) was shown to be drastically reduced. In the Discussion, we suggest why the CT103 results were so disappointing.

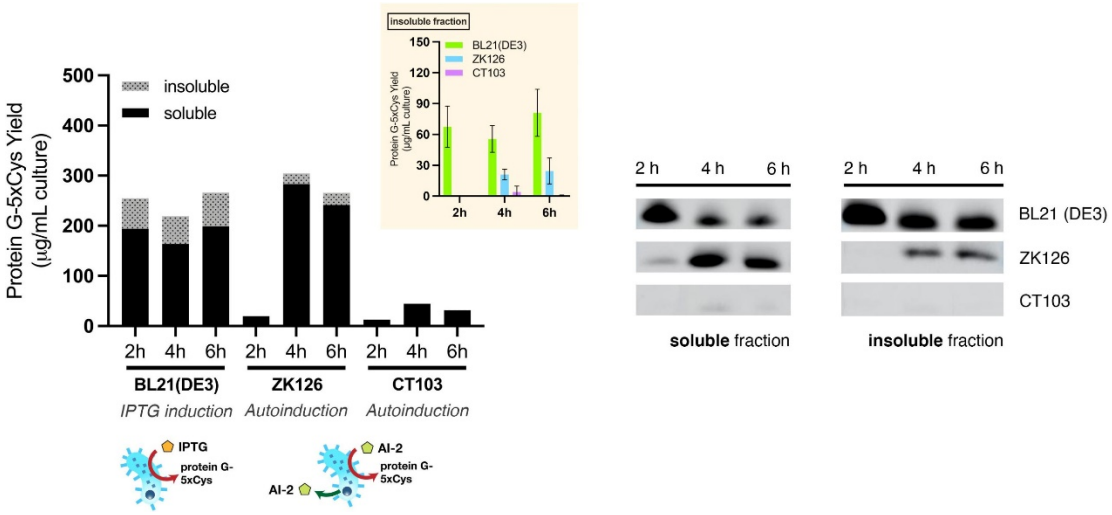

Figure 4.5 Protein G-5xCys production with conventional IPTG induction and QS-mediated autoinduction.

Total yield of protein G-5xCys (μg) per mL of BL21 (DE3), ZK126, and CT103 culture, analyzed by Western blotting. Black: soluble fraction; dotted: insoluble fraction. Plotted values represent the average of biological replicates (n = 3). Yields of protein G-5xCys in the insoluble fractions (μg/per mL culture) are also shown in the inset plot. Error bar represents the standard deviation between replicates.

4.3.4 Deletion of *oxyRS* Enhances 5xCys-Tagged Protein Production

Next, we had examined how deletion of the oxidative stress regulon, *oxyRS*, might affect the production of 5xCys-tagged proteins. Several genes that were reported to influence the cellular response to oxidative stress, such as *gor* and *ahpC*, are directly regulated by *oxyR*, and the global transcriptional activator *rpoS* is regulated by *oxyS*; while the actual disulfide-bond catalyzing *dsbB*, which is normally found in the periplasm, is not reported to be regulated by this regulon. Thus, by altering *oxyRS* functions we did not specifically target the ability or inability of cells to create disulfide bonds, rather our *oxyRS* approach deals more generally with oxidative stress, including that resulting from metabolic perturbations.

To evaluate the effect of *oxyRS* deletion toward expression of 5xCys-tagged proteins, we first transformed pET-G2Cys5 into BL21 (DE3) and its *oxyRS* null mutant (SW103). We observed no significant difference in the growth rate of the *oxyRS* mutant vs. its isogenic parent (**Figure 4.6**). Interestingly, however, the Δ*oxyRS* SW103 displayed significantly higher yields in both total and soluble protein at 4- and 6-h post-induction (**Figure 4.7a**). Moreover, SW103 produced less insoluble protein (**Figure 4.7a**). These results suggest that *oxyRS* deletion alone contributes to the expression of cysteine-tagged heterologous protein in *E. coli* by both enabling its partitioning away from the insoluble fraction to the soluble fraction and by enabling more total protein.

We then tried to combine both approaches, namely the QS-mediated autoinduction and the deletion of *oxyRS*, to see if the insoluble fraction could be reduced even further. Both plasmids pCT5 and pET-G2Cys5 were transformed into ZK126's isogenic *oxyRS* null mutant (SW102), which we created here to allow

autonomously inducible expression of protein G-5xCys. Similar to ZK126 and consistent with low initial AI-2 levels, the expression of protein G-5xCys started at low levels initially (see 2 h post-induction) but increased considerably thereafter (**Figure 4.7b**). By 4 and 6 h post-induction, the total and soluble yields in autonomously induced SW102 had become higher than autonomously induced ZK126. Also, the soluble quantity of protein G-5xCys was higher and the insoluble fraction was lower in SW102 (**Figure 4.7b**). Further, both autoinduced cultures yielded less insoluble fraction of the target protein than the IPTG-induced cultures, and the two *oxyRS*-null strains displayed higher total/soluble yield compared to their wildtype counterparts. These results supported our hypothesis that both methods independently facilitate the expression of 5xCys-tagged proteins and when employed in tandem, result in even better yields. We suggest that this works by altering the metabolic and oxidative state of the host strain which, in turn, helps to maintain solubility.

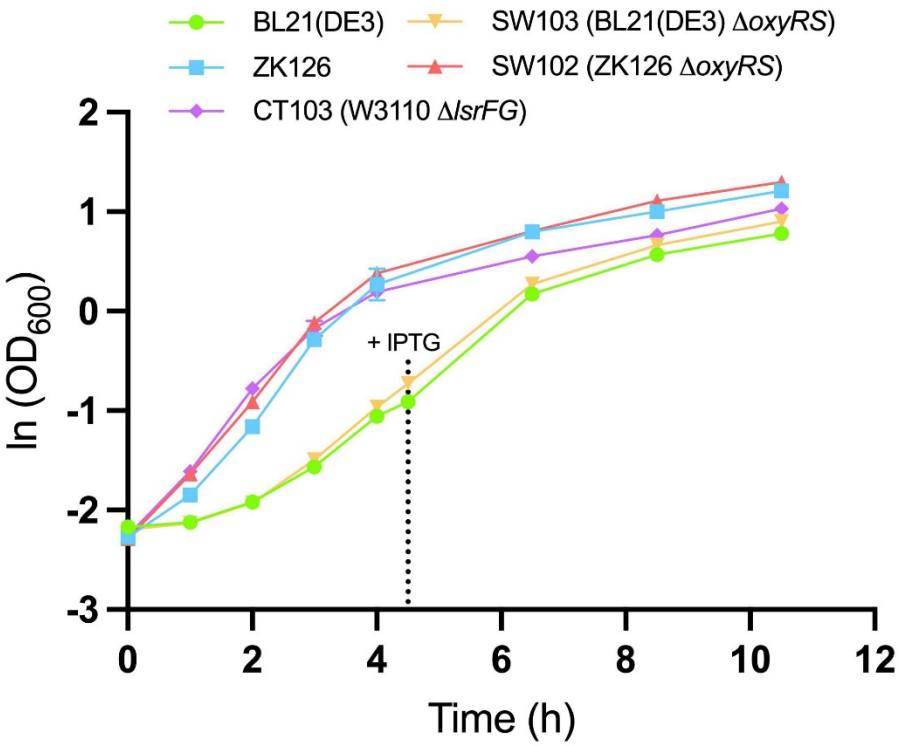

Figure 4.6 Growth of different cell cultures.

Mean OD_{600} values for IPTG-induced BL21 (DE3) (green, circle), IPTG-induced SW103 (yellow, downward triangle), autoinduced ZK126 (blue, square), autoinduced CT103 (purple, diamond), and autoinduced SW102 (red, upward triangle) cultures. Both BL21 (DE3) and SW103 cultures were induced with 1mM IPTG at OD_{600} = 0.4. Error bar represents the standard deviation between replicates (n = 3).

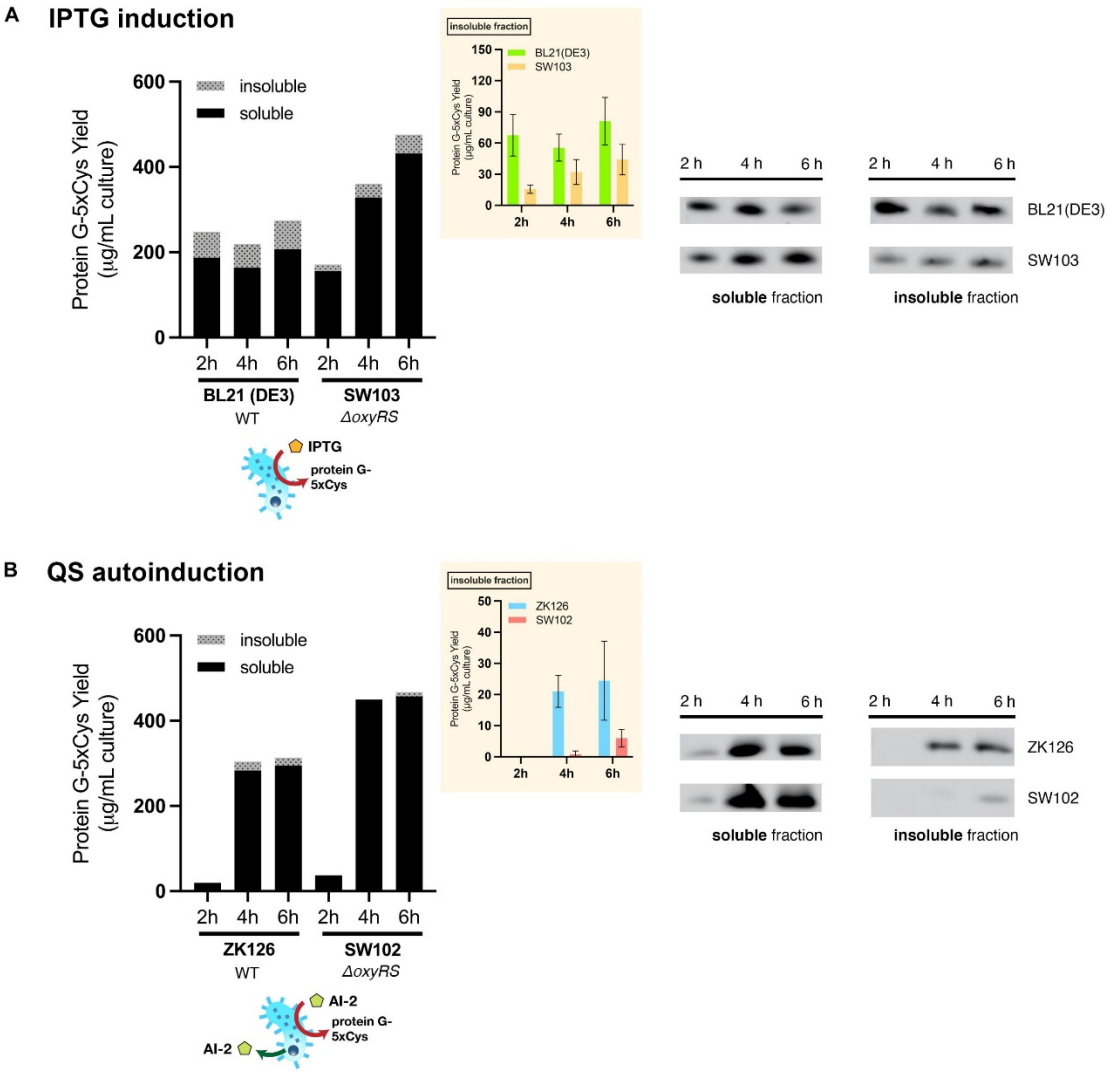

Figure 4.7 Effect of *oxyRS* deletion to protein G-5xCys expression.

(a) Total yield of protein G-5xCys (μg) per mL of IPTG-induced BL21 (DE3) and SW103 (Δ*oxyRS*) culture analyzed by Western blotting. **(b)** Total yield of protein G-5xCys (μg) per mL of QS-autoinduced ZK126 and SW102 (Δ*oxyRS*) culture analyzed by Western blotting. Black: soluble fraction; dotted: insoluble fraction. Plotted values are the average of biological replicates (n = 3). Yields of protein G-5xCys in the insoluble fraction (μg/per mL culture) are also shown in the inset plot. Error bar represents the standard deviation between replicates.

4.4 Discussion

As biohybrid devices have emerged, advances in developing tools that help to functionalize these devices will be all the more appreciated. That is, methodologies that enable integration of biological components with more traditional microdevice materials will enable significantly expanded diversity in the functions that are available. In this study, we show how a 5xCys tag that is incorporated onto the C-terminus of an IgG-binding protein G can easily and rapidly be assembled onto electrodes, preserving their function by the incorporation of simple device-born oxidation cues from the electrode. Rather than relying on electrostatic interactions (e.g., thiol-gold absorption; (272)), 5xCys tagged-proteins are capable of forming robust covalent disulfide bonds with a versatile PEG-SH hydrogel. Moreover, the PEG-SH coating, because it is in 3D, greatly increases binding sites for 5xCys tagged-protein conjugation when compared to a bare gold surface. Also, since our assembly methodology is demonstrated using a gold electrode, non-biochemical assays such as electroanalytical methods [e.g., cyclic voltammetry (CV), electrochemical impedance spectroscopy (EIS)] which allow fast and sensitive detection, can still be performed as the components are directly assembled onto the sensing electrode with the spatial resolution of the electrode (250, 251). We expect many devices with more sophisticated functions can be built based on our demonstrations.

Although the cloning processes for inserting a 5xCys tag into a target protein are fairly routine, we have observed that this affinity tag presents challenges in protein expression and purification, as it seems to promote the formation of troublesome inclusion bodies. While we explored two different cellular engineering methods to

overcome this problem, we made several interesting observations. First and foremost, the yield of soluble 5xCys was highest in the autoinduced host with *oxyRS* deletion. Although the conventional IPTG-induced BL21 (DE3) process delivered consistently high levels of expression upon induction, most of the protein was found in the insoluble fraction. That is, just by switching to the QS-mediated autoinduction method, we found the amount of insoluble protein had dropped significantly. This result further strengthened our previous hypothesis (109), that QS-mediated autoinduction enables the expression host to regulate protein expression based on its metabolic state and minimizes transient product-limiting perturbations. This in contrast to manual IPTG-induction, imposing "full-on" expression regardless of how much burden it brings (109, 256, 258). This would especially benefit the expression of problematic proteins, such as the 5xCys-tagged proteins in our study that are prone to aggregate. That said, QS-mediated autoinduction required a longer expression period, as our results showed low amounts of target protein at 2 h post-induction while at the same time the expression of IPTG-induced BL21 (DE3) was high. While we have demonstrated the benefits of QS-mediated expression for a cysteine-tagged protein, benefits for rewired QS circuitry have also appeared for non-Cys-tagged proteins including GFP (109, 110), β-galactosidase (109), chloramphenicol acetyltransferase (CAT) and an organophosphorus hydrolase (OPH) (109), bacterial AI-2 regulators LsrK and LsrACDB (110). It may well be that this methodology is generally beneficial, including for proteins with designer tags.

We were also surprised to find that CT103, while having very little difference in its growth rate compared to the wildtype ZK126 (**Figure 4.6**), produced very little

target protein throughout (including 2–6 h post-induction and even overnight, not shown). With the *lsrFG* deletion, we expected this strain would be extra sensitive to the autoinducer and result in higher expression since it lacks the machinery (LsrFG) to process and degrade AI-2 (128). There may be several factors for this observation, but more study would be required to pinpoint the main contributors: (i) the switch "on" was at a far lower OD and the transient may have resulted in the elicitation of product-degrading proteases, notably those that degrade the N-terminal His tag (we note that N-terminal degradation is common in *E. coli* (273) (ii) the initial synthesis rate of the target protein is dependent on the first observed signal concentration and this was likely lower in this strain in accordance with Δ*lsrFG* and a lower threshold level of AI-2 for activating *lsr* gene expression (110). Then this trajectory of low expression was subsequently maintained throughout the expression period despite increased levels of AI-2 in later stages; and/or (iii) we have also noted that CT103, derived from W3110, contains a genomic copy of the entire *lac* operon that is deleted in ZK126 and its derivative (SW102). Since complex media such as LB broth often contains residual lactose associated with the milk protein digest, tryptone (274), this could influence both the *lac* operator-governed pET-G2Cys plasmid and the *lsr* operon that is glucose-repressed (91). As noted, additional work would help to clarify our CT103 observations.

Beyond the induction method, we also investigated whether an altered oxidative stress response contributed to this agglomeration issue, noting that the cysteine-tagged protein is surely redox active. While the cytoplasm of wildtype bacteria is maintained in a reduced state, deletion of *oxyRS* will hinder its ability to eradicate H_2O_2, a major source of oxidative stress, and possibly shift the redox state of the cytoplasm to

becoming more oxidizing (268, 275). This, theoretically, will promote disulfide bond formation between two cysteine residues (276). Although it is unknown how the 5xCys tag would affect the folding of the fused protein, our results suggest that a more oxidized environment is preferred for the expression of 5xCys-tagged proteins, which helps to increase soluble target protein content and reduce inclusion body formation. Additional investigations would help us to understand the favored tertiary and quaternary structures of the 5xCys-tagged proteins, for example, how easily do they aggregate and form oligomers? Do they prefer to form inter- or intra-peptide disulfide bonds? Which conformation is more soluble while which is more likely to form inclusion bodies? This, we believe, can provide more insight to the phenomenon observed in this study. We note also that we have not explored varying the number of C-terminal cysteine residues, as this might be informative in developing an understanding of its role in contributing to the localization of the expressed products.

In summary, we have introduced a simple affinity tag to the C-terminus of a bacterial protein G, enabling its covalent tethering onto thiol-containing hydrogels. Moreover, to combat the challenging expression characteristics of this 5xCys-tagged protein, two cellular engineering methods were implemented and proved to successfully enhance its production and retain its presence in the soluble fraction. We envision these methods will benefit not only the production of the two 5xCys-tagged proteins studied here, but many other cysteine-rich proteins that are critical in biological systems.

4.5 Materials and Methods

4.5.1 Bacterial Strains and Growth Media

The bacteria strains and plasmids used in this study are listed in **Table 4.1**. Luria-Bertani broth (LB) contained 5 g of yeast extract liter^{-1}, 10 g of Bacto tryptone liter^{-1}, and 10 g of NaCl liter^{-1} (Fisher). When necessary, media were supplemented with antibiotics at the following concentrations: ampicillin, 100 μg mL^{-1}; kanamycin, 50 μg mL^{-1}.

Table 4.1 Bacteria strains and plasmids used in this chapter.

Strain	**Description**	**Reference**
NEB10β	Δ*(ara-leu) 7697 araD139 fhuA* Δ*lacX74 galK16 galE15 e14- ϕ80*d*lacZ*Δ*M15 recA1 relA1 endA1 nupG rpsL* (Str^R) *rph spoT1* Δ*(mrr-hsdRMS-mcrBC)*	New England Biolabs
BL21 (DE3)	B strain, F$^-$ *ompT hsdS$_B$* (r_B^- m_B^-) *gal dcm rne131*λ(DE3)	Invitrogen
ZK126	*E. coli* K-12 substr. W3110 Δ*lacU169 tna-2*	Laboratory Stock
CT103	W3110 Δ*lsrFG*	This study
SW102	ZK126 Δ*oxyRS*	This study
Plasmid	**Description**	**Reference**
pET200/D-TOPO	Cloning vector, containing *T7* promoter, Km^r	Invitrogen
pET-DsRed	pET200 derivative, containing *dsRed_Express_DR*	This study
pET-DsRedCys5	pET200 derivative, containing *dsRed_Express_DR* followed by 5xCys	(250)
pET-G2Cys5	pET200 derivative, containing two copies of *Streptococcal* protein G Fc binding domain followed by 5xCys	(250)
pCT5	pFZY1 derivative, containing *lsr* promoter fused with *T7RPol*, Ap^r	(109)
pET-E72G3	pET-32c derivative, containing three copies of *Streptococcal* protein G Fc binding domain	(277)

Table 4.2 Primers used in this chapter.

Primer Name	Sequence	Relevant Description
FWD_ProteinG	CACCATGGGAGTTAAGATCCGCATGAC	Upstream primer for cloning Protein G with a 5'-CACC sequence for directional cloning into pET200
REV_ProteinG-Cys	CTAGCAACAACAACAACACAAGATCTT CGGGTCCATTTCCG	Downstream primer for cloning Protein G with 5xCys tag from pET-E72G3
FWD_DsRed	CACCATGGCCTCCTCCGAGGAC	Upstream primer for cloning DsRed with a 5'-CACC sequence for directional cloning into pET200
REV_DsRed-Cys	CTAGCAACAGCAACAACAGCAGCACA CATTGATCCTAGCAGAAGCACAGG	Downstream primer for cloning DsRed with 5xCys tag from pET-DsRed
lsrFGHP3	ATCGGCAAATACGATTTCTGATGTGCA TTACTTAACCGGAGTAAGTTATGGTGT AGGCTGGAGCTGCTTC	Primer for deletion of gene *lsrF, lsrG*
lsrFGHP2	AGATTCCAGTTTCGCGACACAGGTTTT GTAGTGGGGCGTGCATATGAATATCCT CCTTAG	Primer for deletion of gene *lsrF, lsrG*
oxyHP1	CCTGTTTTAAAACTTTATCGAAATGGC CATCCATTCTTGCGCGGATGGCCGTGT AGGCTGGAGCTGCTTC	Primer for deletion of genes *oxyR, oxyS*, and the intergenic region
oxyHP2	GTATAAATTTGAGCCTGGCTTATCGCC GGGCTTTTTTATGGCAAAAAAAAGCAT ATGAATATCCTCCTTAG	Primer for deletion of genes *oxyR, oxyS*, and the intergenic region

4.5.2 Plasmid Construction

Escherichia coli strain NEB10β (New England Biolabs) was used for all subcloning. Proteins of interest (DsRed and *Streptococcus* protein G) were expressed with a C-terminal 5x cysteine tag (5x-Cys). Plasmid constructs are shown in **Figure 4.2**. The sequence for the protein of interest was both preceded by six His residues at the amino terminus and followed by five cysteine residues located at the carboxyl terminus. The coding sequence which comprised two copies of *Streptococcus* protein G's Fc-binding domain (G2) and five Cys residues inserted at the carboxyl terminus was prepared by PCR amplification from a protein G template (pET-E72G3) (241, 277) using primers listed in **Table 4.2**. All oligonucleotides were purchased from Integrated DNA Technologies (Coralville, IA). The DsRed-5xCys fragment was prepared with similar procedures except with a DsRed template (pET-DsRed) and its corresponding primers (**Table 4.2**). The PCR product was then purified through gel electrophoresis and inserted into a pET200 vector via the Champion™ pET200 Directional TOPO® Expression Kit (Invitrogen). The resultant plasmid that holds the protein of interest was confirmed by Sanger sequencing (Genewiz, NJ).

4.5.3 Chromosomal Deletion of *oxyRS, lsrFG*

The one-step replacement method (278) was used to construct deletions in *E. coli* ZK126 and W3110. The phage λ Red recombination system was used to replace *oxyR, oxyS,* and the intergenic region with an *oxyRS*::*kan* PCR fragment. PCR was performed using pKD4 as a template and the primers oxyHP1 and oxyHP2 (**Table 4.2**). The PCR products were treated with DpnI and introduced by electroporation into *E. coli* ZK126 containing plasmid pKD46, which expresses the λ Red recombinase,

and was cured later by growth at 37°C. Recombinants were selected on LB supplemented with kanamycin. Deletions of *lsrF and lsrG* in *E. coli* W3110 were constructed similarly by PCR amplification of pKD3 with primers lsrHP3 and lsrHP2 (**Table 4.2**). The deletion of genes in both cases was verified by PCR.

4.5.4 Recombinant 5xCys-Tagged Protein Expression and Purification

For traditional IPTG-induced expression, overnight cultures of BL21 (DE3) *E. coli* (Invitrogen) harboring plasmid pET-G2Cys5 in LB media were inoculated in 25 mL fresh media to OD_{600} = 0.10 in 250 mL flasks and incubated at 30 °C with shaking at 250 rpm. Upon reaching mid-log phase (OD_{600} ~ 0.4-0.6), the cultures were induced with a final concentration of 1 mM IPTG (Sigma). For QS-mediated autoinduction, plasmids pCT5 (109) and pET-G2Cys5 were electrically-transformed into host strains CT103, SW102, and ZK126. All strains are *luxS*$^{+}$ and synthesize AI-2 as a consequence of normal metabolism. Growth conditions were identical to that of BL21 (DE3) except no inducers were added. To purify 5xCys-tagged proteins, cells were harvested by centrifugation at 14000 x g under 4 °C for 20 min. After lysis by BugBuster solution (Novagen) at room temperature for 40 min followed by sonication, the soluble cell extracts were mixed with Co^{2+} affinity resin (BD TALON™, BD Biosciences), and the bound target proteins on the Co^{2+} were washed by phosphate buffer (pH = 7.4) (Sigma) three times to remove non-specifically bound proteins. The purified proteins were eluted with elution buffer (125 mM imidazole in phosphate buffer, pH = 7.4) for further experiments.

4.5.5 Western Blot

Culture volumes equivalent to 2 ml at an OD_{600} of 1.0 were withdrawn from experiments 2, 4, and 6 hours after IPTG induction of BL21 (DE3) cultures and centrifuged at 10,000 × g for 10 min. The cell pellets were resuspended and lysed in 300 µl BugBuster protein extraction reagent (Novagen) at room temperature for 40 min and centrifuged again at 10,000 × g for 10 min to separate soluble and insoluble cell fractions. A Bradford-based protein assay kit (Bio-Rad) was used to determine the protein concentration of the soluble fraction. Insoluble cell debris was resuspended with 0.1 ml resuspension buffer (0.1 M Phosphate Buffer [pH 6.8]). Both the soluble and insoluble fractions were mixed 1:1 (vol/vol) with sodium dodecyl sulfate (SDS) sample buffer (12.5% 0.5 M Tris-HCl [pH 6.8], 10% glycerol, 2% SDS, 5% β-mercaptoethanol, 0.0025% bromophenol blue), heated at 95°C for 10 min, and centrifuged at 4°C for 1 min. Samples with identical protein content, along with IMAC-purified protein G-Cys5x (0.13 µg) were loaded onto 10% Mini-PROTEAN TGX Gels (Bio-Rad) for electrophoresis and blotted onto nitrocellulose membranes (Bio-Rad) using a Mini Trans-Blot cell (Bio-Rad) and Bjerrum Schafer-Nielsen transfer buffer (48 mM Tris, 29 mM glycine, 20% methanol) for 20 min at 15 V and 20 min at 20 V. The primary antibody, monoclonal antipolyhistidine (Sigma), was diluted 1:5,000 in antibody buffer (0.1% Tween 20 [vol/vol], Tris-buffered saline with 1% [wt/vol] nonfat dry milk) to probe protein G-5xCys. The membranes were then introduced to a solution of 1:50,000-diluted rabbit anti-mouse IgG conjugated with horseradish peroxidase (HRP) (Abcam). Membranes were developed using the Clarity Western ECL Substrate (Bio-Rad) and visualized with the Amersham 600 Imager (GE Healthcare). Images

were analyzed using software ImageStudioLite (LI-COR Bioscience), and protein semi-quantitation was performed by correlating the band intensity of each sample to that of the loaded standard.

4.5.6 Electroassembly of PEG-SH, Protein G-5xCys, and Antibody Interfaces

A mixture of 5 mM 1,1′-Ferrocenedimethanol (Fc) (Santa Cruz Biotechnology) and 50 mg/mL 4-arm PEG-SH (JenKem) was first prepared in phosphate buffer (0.1 M, pH 7.0). The surface of a 2 mm diameter gold standard electrode (working electrode) was fully immersed in the solution along with a platinum wire (counter electrode) and an Ag/AgCl reference electrode. PEG electrodeposition occurred for 1 minute at a constant potential of 0.4 V. After PEG hydrogel formation, the surface was immersed in a solution of Fc (5 mM) and a constant voltage of 0.4 V was applied for 2 minutes to ensure maximal sulfenic acid group formation on the surface of the hydrogel. The protein G-5xCys functionalized surface was then generated by immersing the PEG-coated electrode in protein G-5xCys (250 µg/mL in 0.1 M PBS, pH 7.4) overnight at room temperature. After incubation, the surface was rinsed 3 times with wash buffer (0.1 M PBS, 0.05% Tween-20, pH 7.4). For the demonstration as an IgG-binding platform, the protein G-5xCys + PEG-coated electrode was incubated in 200 µL of sheep anti-rabbit IgG:DyLight®488 (Bio-Rad) diluted 1:1000 in antibody buffer for 1.5 hours at room temperature. To build a cell-capture platform, the protein G-5xCys+PEG-coated electrode was first incubated in 1:1000-diluted rabbit anti-*E. coli* antibody for 2 hours, followed by a 1.5-hour incubation with constitutively DsRed-expressing (to facilitate visualization of cell capture) BL21 (DE3) at a cell density of

OD_{600} = 1.5. Microscope images were captured with the MVX10 upright fluorescence microscope (Olympus).

Chapter 5. Genetically Focused, Feedback-Controlled Electrogenetic Guidance of Microbial Communities

ⓘThis chapter is adapted from an unpublished manuscript.

5.1 Introduction

The concept of communication, or the transmission of information, builds the basis of the interconnected modern world we live in today. While current electronic devices are capable of freely exchanging information through electron transfer and electromagnetic waves, building smart systems that can connect both biological processes and electronic systems remained a challenging task to overcome due to their disparate communication modalities. Recently, redox-active molecules, due to their dual nature, were introduced as a novel medium to connect biological systems and electronics (65, 66, 68, 279). No stranger to biology, redox-active molecules are present in the core of biological systems (e.g., NADH) serving as a bridge between electron transfer and molecular communication (51, 53). When electrons flow between them, causing their distinct redox state to change, the redox molecules can also freely move in and out of the cell initiating a molecular dialogue. In addition, these redox activities can be easily and precisely controlled through routine electrochemical instrumentation, thus realizing programmed, automated regulation, which is what we believe is one of the key functions in next generation biohybrid devices.

Employing peroxide (H_2O_2) as the electrochemical conduit, Terrell *et al.* first demonstrated an electrogenetic system that enables information exchange between a living cell-embedded bioelectronics interface and an engineered microbial network (68, 279). Similarly, an electrically controlled, CRISPR-mediated toolkit for transcriptional

regulation was built on the original “electrogenetics” archetype (65), adding an array of CRISPR functions to allow more genetically-focused intracellular control (66). In the following chapter, we built upon these two works and present a complete electrogenetic framework to achieve remote feedback control of eCRISPR activity and more importantly, multidirectional communication between living systems (**Figure 5.1**).

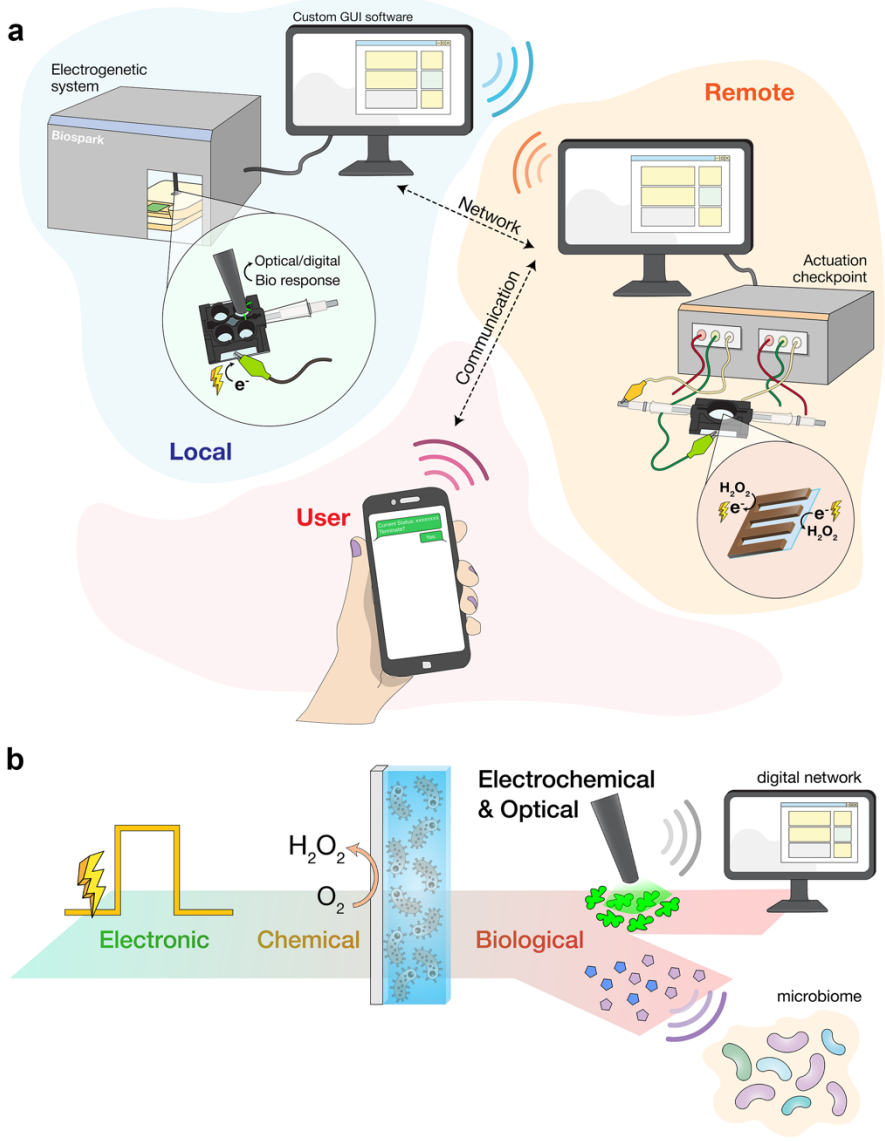

Figure 5.1 Information flow within the Bio-Nano Things Network.

(a) Electrogenetics allows direct electron flow to alter gene expression and generate digitizable optical signals for establishing connectivity with electronic systems. Information can thus be propagated within the network to other workstations and users through wireless connection enabled by the internet. The connected bio-electrochemical setup at a separate location demonstrates electronic-chemical-

electronic signal conversion, through encoding electronic input into a chemical signal (peroxide) followed by biochemically decoding the chemical signal back to an electronic output. **(b)** Transformation in signaling modality enables the connection of biology to electronics. An encoded electronic input is first transduced to a chemical signal interpretable by biological systems to generate two different biological outputs. On top illustrates the optical signal, serving as the conduit to electronic systems after digitization. The bottom depicts QS signaling molecules that provide information to other biological systems.

5.2 Results

5.2.1 ITO-based electrochemical biohybrid device

We created an ITO-based electronic device to serve as the experimental platform in our study (**Figure 5.2a**). Following a typical 3-electrode setup, we chose ITO-coated glass as our working electrode (WE) due to its transparency for optical observations and measurements. A 3D-printed housing was attached to the ITO electrode to generate separate wells with similar dimensions to a conventional 96-well plate. We then tested the device's ability to generate peroxide via electronic input. Although previous studies reported that peroxide can be generated by applying voltages ranging from -0.3 to -0.9 V (versus Ag/AgCl) to partially reduce oxygen (280) (according to reaction $O_2 + 2H^+ + 2e^- \leftrightarrow H_2O_2$), we found that biasing the ITO electrode to -0.8 V produced the highest level of peroxide (**Figure 5.2b**). Consistent with previous reports, oxygen reduction to peroxide was stoichiometrically proportional to the applied charge (**Figure 5.2c**). Altogether, we built a biohybrid device consisting of a living 'artificial biofilm' and an electronic platform capable of generating peroxide to provide as a transduction mechanism to enable electrogenetic regulation.

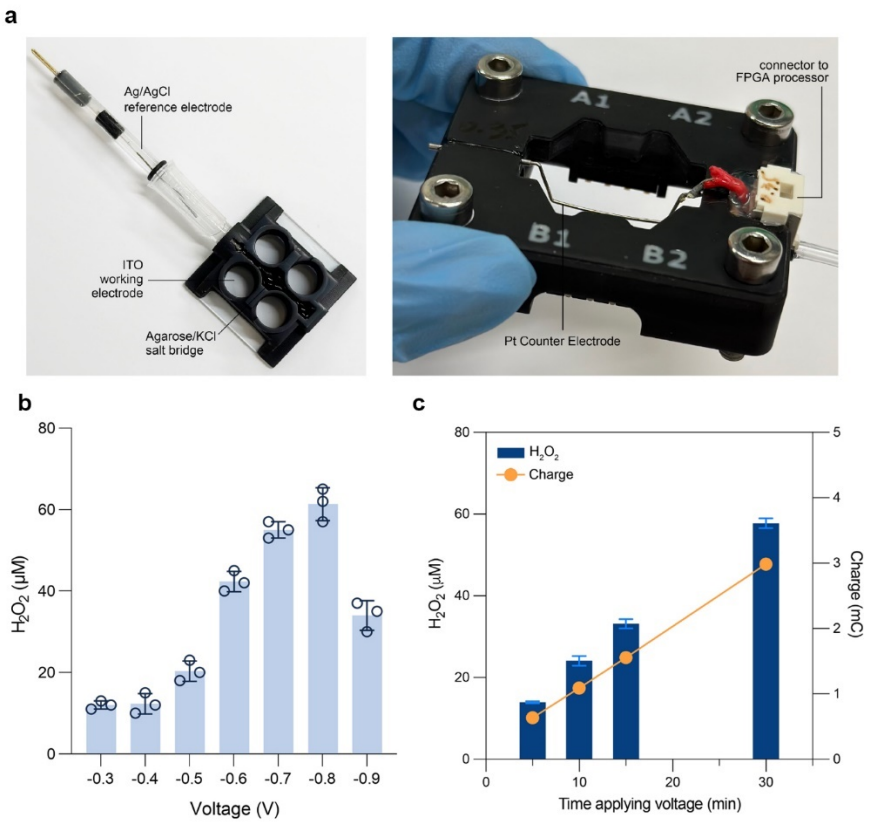

Figure 5.2 ITO-based electrochemical biohybrid device.

(a) The clear ITO glass serves as the working electrode and allows for optical observations. An Ag/AgCl electrode is used as the reference electrode, and a Pt wire (right, mounted on the connector) is the counter electrode. The three electrodes are connected through the salt bridge (1 M KCl in 1% agarose) casted in the central well of the device. **(b)** H_2O_2 generated in the device by poising the working electrode to various voltages for 30 min. Open circles denote technical replicates. **(c)** H_2O_2 generated (blue bar) in the ITO-based electrochemical platform as correlated to applied charge (orange circle). Error bars represent the standard deviation (n = 4).

5.2.2 *oxyRS*-based electrogenetics CRISPR activation

In hopes of expanding the *oxyRS*-based electrogenetics toolbox, we enlisted the versatile CRISPR transcriptional regulation system to allow activation, repression, and multiplexed regulation of genes at the transcription level. Here, a peroxide-mediated, electrically-inducible CRISPR transcriptional activation (CRISPRa) system was created by rewiring the previously developed *soxRS*-based electrogenetic CRISPR (eCRISPR) (66) and placing the single guide RNA (sgRNA) under the control of *oxyS* promoter (**Figure 5.3a**). To monitor CRISPRa performance, plasmid pMC-GFP was used in which the expression of reporter gene *gfpmut2* would be upregulated by the CRISPR components. First, we confirmed in liquid culture that both CRISPR activation of GFP and sgRNA's expression level were peroxide-inducible (**Figure 5.4**). Next, we sought to test the electroinduction of CRISPRa using our biohybrid device (**Figure 5.3b**). NB101 cells harboring the tunable CRISPRa plasmids (pSC-O108, pdCas9ω, and pMC-GFP) were grown to mid-log phase and assembled into an 'artificial biofilm' with an OD_{600} of 1/mL. In **Figures 5.3c and 5.3d**, we found the percentage of cells displaying CRISPRa-mediated fluorescence (ON%) increased as a function of the duration of voltage (-0.8 V) application and charge 4 hours after electroinduction. With 10 minutes of electroinduction, CRISPRa GFP levels (30%) were on par with a 200 μM peroxide exogenously- induced control (34%), while 30 minutes of electroinduction resulted in ~70% of cells exhibiting CRISPRa activity.

Having shown that we can electrically induce CRISPRa in the biohybrid device, we then sought to demonstrate information routing between electronic to biological signaling modalities by initiating a specific QS communication (i.e., *las* AI-1 QS

system from *Pseudomonas aeruginosa*) that is not natively found in *E. coli* through peroxide-mediated eCRISPR. A new reporter plasmid (pMC-lasI-LAA) was constructed by replacing *gfpmut2* with the AI-1 producer *lasI* (fused with a ssRA tag), allowing CRISPRa control of AI-1 production. This new reporter plasmid, along with the other CRISPRa components (dCas9ω and pSC-O108) were transformed into NB101 cells. We later referred to these populations as CRISPRa *lasI* cells. Prior to electro-induction tests, CRISPRa *lasI* cells were also confirmed to be peroxide-inducible in liquid culture (**Figure 5.5a**). For demonstrating on-device eCRISPRa, CRISPRa *lasI* cells (at OD_{600} = 3/mL) were electrically induced to activate AI-1 production following the assembly onto the biohybrid device. At 4 and 6 h post-induction, media submerging the 'artificial biofilm' (i.e., conditioned media, CM) were collected and incubated with AI-1 bioluminescent reporter cells for quantitation of AI-1 concentration (**Figure 5.5b**). Similar to the results of eCRISPRa GFP, we found that AI-1 levels were electrically inducible and were correlated to the duration of voltage application and charge (**Fig. 5.3e**). Finally, control of a second population through CRISPRa-mediated QS signal routing was demonstrated. To achieve this, CRISPRa *lasI* cells were assembled into an 'artificial biofilm' submerging in culture media inoculated with an AI-1 fluorescent reporter strain (NEB10β harboring plasmid pLasR_S129T-GFPmut3) (**Figure 5.5c**). After receiving electrogenetic induction, the AI-1 fluorescent reporters in the induced co-culture (ON) exhibited higher (~1.5-fold) GFP levels compared to those in the non-induced (OFF) co-culture (**Figure 5.3f**). In summary, we demonstrated on-device, peroxide-mediated eCRISPR that allows

propagation of the localized electrogenetic cue across different cell populations, and coordination of population-wide behavior with the help of QS communication.

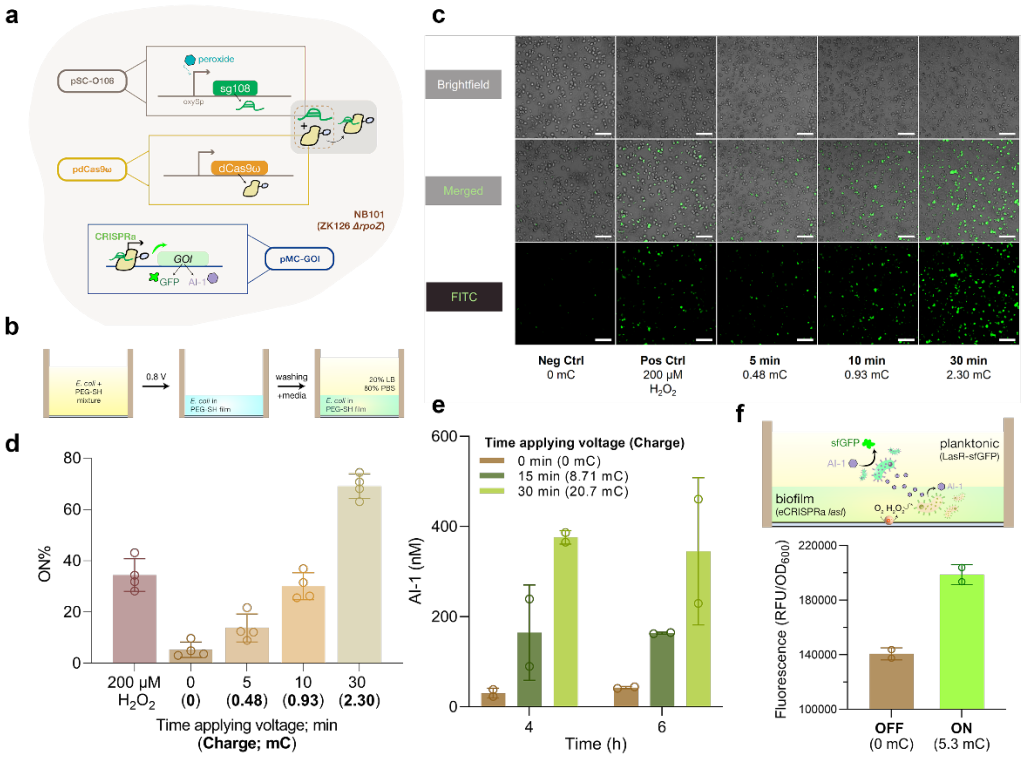

Figure 5.3 Demonstration of a tunable eCRISPRa on an "artificial biofilm."

(a) Schematic illustration of the electrogenetic CRISPRa system powered by the *oxyRS* regulon. Electro-induced gRNA sg108 (pSC-O108) forms a complex with constitutively-expressed dCas9ω to initiate transcription of the gene-of-interest (GOI) in plasmids pMC-GFPmut2 or pMC-LasI-LAA. **(b)** General workflow and setup for experiments on an 'artificial biofilm'. After electrodeposition, we thoroughly washed the film with PBS to remove excess cell/PEG-SH solution. 20% LB was then added into the well to submerge the film as culture media. **(c)** Confocal images of *E. coli* harboring the eCRISPRa-GFP genetic cassette that were embedded in the PEG-SH film. Varying times of electrical induction and the resulting charges (millicoulomb; mC) applied to the cells are indicated below. 200 μM of H_2O_2 was exogenously added to

culture media to activate the *oxyS* promoter as the positive control. Top: brightfield; Middle: Merged; Bottom: FITC filter. **(d)** Percentage of *E. coli* in the PEG-SH film that were activated through eCRISPRa. **(e)** AI-1 assay indicating the amounts of AI-1 generated via CRISPRa. **(f)** Measured fluorescence in coculture comprised of eCRISPRa *lasI* cells and AI-1 fluorescent reporters (NEB10β + LasR_S129T-GFPmut3). eCRISPRa *lasI* cells were confined in an 'artificial biofilm' submerged in the planktonic culture of AI-1 fluorescent reporters. For all figures, the height of the bar represents the mean, and error bars represent the standard deviation ($n \geq 2$). Individual replicates were indicated as open circles.

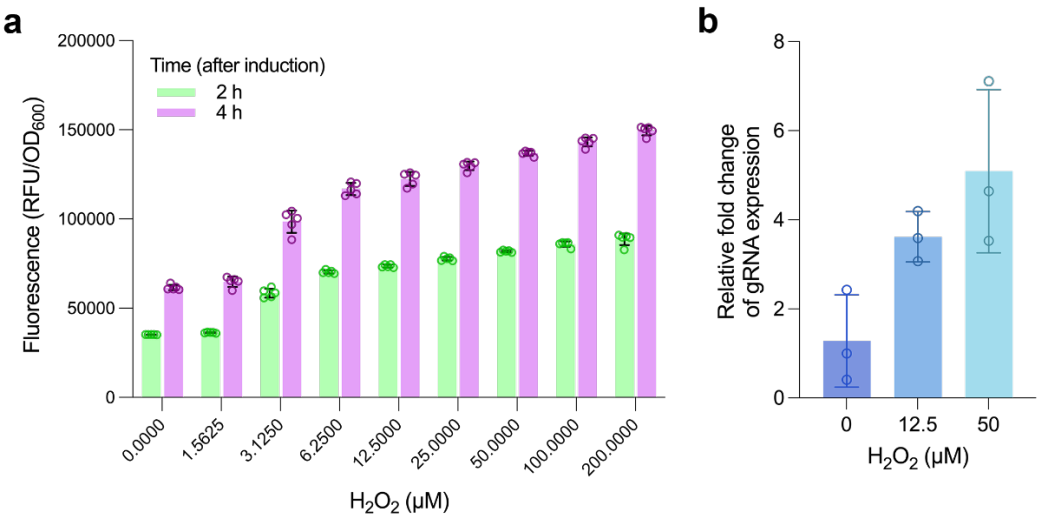

Figure 5.4 H_2O_2-inducible CRISPR activation of GFPmut2.

(a) Measured fluorescence from NB101 harboring pSC-O108, pdCas9ω, and pMC-GFP 2 hours (green) and 4 hours (purple) after H_2O_2 induction. Error bars represent the standard deviation. Open circles represent individual replicates (n = 5). **(b)** Relative fold change of gRNA (sg108) expression induced with various levels of H_2O_2. Error bars represent the standard deviation (n = 3). Open circles represent individual replicates.

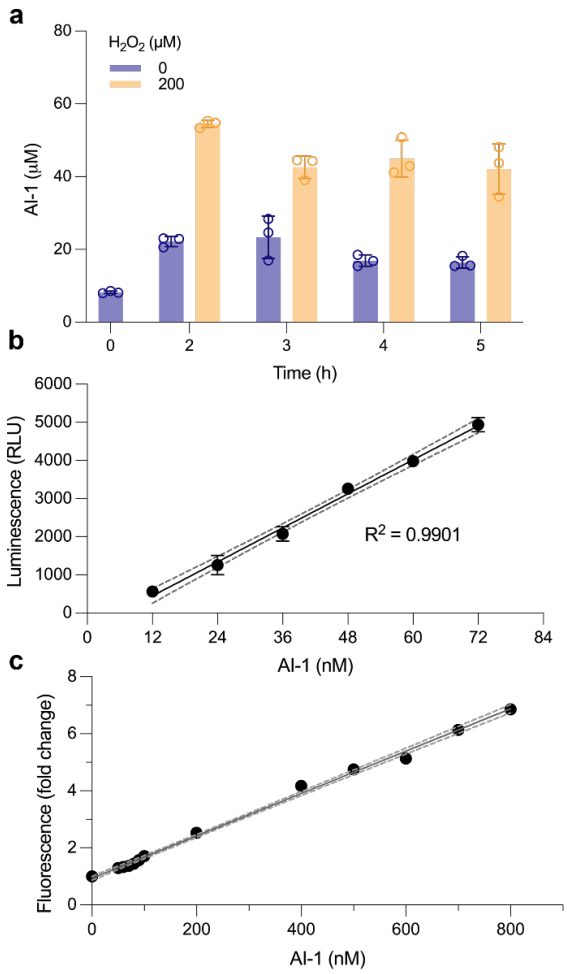

Figure 5.5 H_2O_2-inducible CRISPR activation of *lasI*.

(a) AI-1 produced by NB101 harboring pSC-O108, pdCas9ω, and pMC-lasI-LAA after being induced by 0 μM (blue) and 200 μM (yellow) of H_2O_2. Bar height represents the average value. Error bars represent the standard deviation (n = 3). Open circles represent individual replicates. **(b)** AI-1 bioassay standard curve. Error bars represent the standard deviation (n = 3). The calibration curve was generated via linear interpolation of experimental data, and dashed lines represent the 95% confidence interval. **(c)** Fluorescence response from AI-1 inducible strain (NEB10β + LasR_S129T-GFPmut3). Error bars represent the standard deviation (n = 3).

5.2.3 eCRISPR inhibition and multiplexed control of QS to enable 'multilingual' communication.

While we showed that by enabling peroxide-mediated eCRISPR activation of QS can open a new line of communication to other microbial or even mammalian populations (259, 281), CRISPR transcription regulation offers additional functions such as gene repression and multiplexed control for multi-locus transcription regulation. Here, we explored and applied these functions to enable electrically-controlled 'multilingual' QS communication. In particular, we aimed to create an engineered *E. coli* that switches its 'spoken language' (i.e., QS signaling) from its 'mother tongue' (*luxS*-based AI-2) to a 'foreign language' (*las* AI-1 from *P. aeruginosa*) upon receiving the electronic signal. Unlike the *las* system, *luxS*/AI-2 QS system is found natively in many bacteria, Gram positive and negative alike, including our experiment chassis *E. coli*. To prohibit *E. coli* from secreting AI-2, we designed a sgRNA LuxS1 that is homologous to the AI-2 producer gene *luxS* and repurposed dCas9ω for CRISPR inhibition (CRISPRi) (**Figure 5.6a**). We expressed the gRNA, along with a non-specific control, initially under a strong, constitutive promoter in suspension culture to examine the efficacy of LuxS1. Specifically, NB101 cells containing plasmids pLuxS1 or pControlgRNA along with pdCas9ω were grown from OD_{600} = 0.1 in LB media at 37°C. Cell-free conditioned media samples were collected every 2 hours followed by a bioassay using AI-2 reporters BB170 (282) to determine their AI-2 activity (**Figure 5.7a**). Compared to the control gRNA, we observed a ~400-fold decrease in AI-2 activity from the cultures that constitutively expressed LuxS1, demonstrating highly effective inhibition. Next, we verified whether our CRISPRi system could be inducibly

controlled via peroxide. For this, plasmid pSC-LuxS1 was constructed by replacing the constitutive promoter with the *oxyS* promoter to allow inducible expression of LuxS1. Suspension culture of NB101 cells harboring CRISPRi components (pSC-LuxS1 and pdCas9ω) were grown in 37°C and induced with 0 or 200 μM of peroxide at OD = 0.4. 0.8% (w/v) glucose was added to LB media to avoid the naturally occurring AI-2 self-uptake (91). Similarly, the collected conditioned media samples subsequently underwent BB170 bioassay for AI-2 quantification (**Figure 5.7b**). We found that AI-2 activity of the non-induced control was ~7-fold higher than that of the induced sample, confirming peroxide-inducible inhibition of AI-2 QS system by CRISPR inhibiting *luxS*. Prior to testing electrogenetic CRISPRi, we studied the AI-2 profile of entrapped cells in the 'artificial biofilm' (**Figure 5.7c**). Two films containing OD_{600} = 3/mL of empty chassis (no plasmid) or NB101 harboring the inducible CRISPRi components (pSC-LuxS1 and pdCas9ω) at early log phase (OD_{600} = 0.2 before harvesting) were assembled on the custom biohybrid device, and the submerging culture media (20% LB) was collected for BB170 assay. We observed substantial inhibition of *luxS* solely from leaky expression, judging from the fact that AI-2 activity of pSC-LuxS1 cultures was 3.4-fold lower than that of the empty chassis without any induction. However, this was also observed when cells were grown as liquid suspension cultures, and it's likely due to the intracellular peroxide generated from oxidative respiration. We too noted less significant AI-2 uptake of both cultures without the addition of glucose, especially the one haboring CRISPRi plasmids, within our observation window (2~8 h post-deposition). This was perhaps due to the altered growth when the cells were entrapped in film; also, since the intake of AI-2 creates a positive feedback loop from upregulating

the *lsr* operon (93, 94), the lower extracellular AI-2 levels of the CRISPRi cultures could impede its AI-2 uptake. Therefore, we decided to omit the addition of extra glucose into our system in later experiments. We then proceeded to test if CRISPRi of *luxS* could be regulated electronically. In **Figure 5.6b**, the film (containing CRISPRi cells) subjected to electroinduction 3 hours after deposition consistently exhibited lower AI-2 activity compared to the uninduced control, proving controllable quenching of AI-2 QS through electrogenetics.

Alternatively, we also utilized CRISPRi to inhibit *oxyS* for filtering biological noise which stemmed from the native oxdidative stress response. Previously, Bhokisham *et al.* (66) demonstrated by using CRISPRi to selectively silence genomic *soxS* and the ensuing oxidative defense responses, including superoxide dismutases (*sodA* and *sodB*), fumarate hydratase (*fumC*), this reduction in pleiotropic noise enabled a 4-fold increase in targeted electrogenetic *soxS* promoter activity in *E. coli*. Here, we aimed to employ the same method in hopes of increasing the *oxyRS* electrogenetic induction response. Unlike SoxS, *OxyS* is not a protein but a small regulatory RNA that governs cell division, global oxidative/osmotic response, motility, and enables more efficient recovery from oxidative stress (63) through the regulation of genes like *rpoS* (62), *fhlA* (283), and *fhlDC* (284). For *oxyS* CRISPRi, sgRNA O3 was designed to be homologous to *oxyS* and we tested its efficacy by placing it under a constitutive promoter to generate plasmid pO3. Specifically, NB101 cells containing plasmids pO3 or pControlgRNA (non-specific control) along with pdCas9ω were grown from OD_{600} = 0.1 in LB media at 37°C. When the cells reached mid-log phase, we induced the *oxyRS* response by exogenously adding 200 μM of peroxide. Both treated and untreated

cells were collected via centrifugation 10 minutes after being challenged with peroxide, followed by total RNA extraction and qRT-PCR to determine *OxyS* levels (**Figure 5.8a**). With O3 sgRNA constitutively expressed, the peroxide-treated cells displayed a ~10-fold increase of *OxyS* relative to the untreated cells, while we observed a ~120-fold increase of *OxyS* from the treated cells expressing non-specific gRNA. Next, we placed the O3 sgRNA under *oxyS* promoter to generate plasmid pSC-O3 for inducible *oxyS* silencing to enhance *oxyS* promoter activity. To test this, we co-transformed pdCas9ω and reporter plasmid pOxy-sfGFP along with pSC-O3 into NB101. We found the *oxyS* CRISPRi strain displayed higher green fluorescence levels than the no-plasmid NB101 and was comparable to the *oxyRS* mutant (**Figure 5.8b**). Despite the oxyS promoter activity being significantly higher than the wildtype, the GFP response from the *oxyS* CRISPRi strain displayed a mere ~1.2-fold increase that is a lot lower than the ~4-fold increase generated from *soxS* silencing. We hypothesized it is due to the more subsidiary role *OxyS* plays in regulation of the oxidative stress response when compared to SoxS, so that even when *oxyS* is inhibited the majority of the oxidative response will still be active and provide biological noises. Henceforth, we did not continue to utilize CRISPRi for enhancing *oxyS* promoter activity in this study.

Having shown successful eCRISPRi of *luxS*, we then sought to harness the multiplexed nature of CRISPR and combine CRISPRa of *lasI* and CRISPRi of *luxS* to create a 'bilingual' strain. Though many strategies for multiplexed gRNA expression have been previously explored (285), we chose a method derived from the native CRISPR–Cas system. By flanking an array of gRNAs with 'direct repeats' (DR), which are repetitive sequences required for crRNA processing, the tandem gRNAs can be

processed by RNase III in a tracrRNA-dependent manner, like how crRNAs are processed in Type II CRISPR systems (286-288). Based on this approach, we constructed plasmid pSC-sg108+LuxS1 that comprised two key parts for inducible expression of multiple gRNAs: (i) gRNAs sg108 and LuxS1 were flanked with DR sequences and together were placed downstream of the *oxyS* promoter for peroxide-inducible control. (ii) tracrRNA, required for gRNA processing, was individually expressed under a synthetic constitutive promoter. Next, pSC-sg108+LuxS1, with pdCas9ω and pMC-lasI-LAA were then transformed into NB101 cells to generate the 'bilingual' strain (**Figure 5.6c**). To verify peroxide-induced, multiplexed CRISPRa/CRISPRi activity, the 'bilingual' cultures were grown in LB media at 30°C and induced at OD_{600} = 0.4 with 200 μM of peroxide. We found elevated levels of AI-1 (**Figure 5.7d (i)**) and reduced levels of AI-2 (**Figure 5.7d (ii)**) in the induced samples compared to the uninduced control, confirming CRISPR-mediated activation and inhibition on both QS signal producers. We also noticed the difference in autoinducer level between the control and experimental group was smaller when compared to the singleplex experiments in which only one gRNA was expressed. This was possibly a result of the changes in the stoichiometry of CRISPR components from reforming the architecture of the gRNA plasmid, as our previous research had demonstrated that the balance between CRISPR components is crucial to achieve effective CRISPR transcription regulation (66). To overcome this, we tried inducing the 'bilingual cells' multiple times at a fixed interval. Surprisingly, we found that the cells that experienced more peroxide inductions displayed lower AI-2 activity (**Figure 5.7d (ii)**). A complimentary upward trend for the AI-1 levels was not observed (**Figure 5.7d (i)**),

yet it was the sample induced twice (at hours 3 and 4) exhibited the highest AI-1 level. We noted that unlike AI-2 inhibition which operates possibly on the timescale of gRNA transcription and processing, *lasI* upregulation required more time due to the need of translation and protein folding, contributing to the delay we observed in AI-1 levels. Nevertheless, these results demonstrated dynamic control of CRISPR transcription regulation, hinting that the peroxide-mediated CRISPR activity could be 'boosted' over time to reach the desired target response. Finally, to achieve electrogenetic multiplex CRISPR regulation, we assembled the 'bilingual' cells (final OD_{600} = 5/mL) on the biohybrid device, and electrically-induced the 'biofilm' once at hour 0 or twice at hours 0 and 3 post-deposition (1800 s per induction). As shown in **Figure 5.6d**, we observed elevated AI-1 levels and diminished AI-2 activity in both induced samples contrasted to the uninduced control. This also corroborated our 'bilingual' strain's capability of sending out different type of signals on cue, and thus driving certain populations to elicit a biological response (e.g., bioluminescence). Moreover, of the two induced samples, the twice-induced 'biofilm' displayed higher AI-1 levels and lower AI-2 levels. This confirmed electrogenetic multiplexed CRISPR can also be dynamically regulated, thus providing another tunable parameter for this system. Overall, we engineered a 'bilingual' *E. coli* strain capable of switching its QS signaling to reach different audiences on electronic cue by simultaneously exerting both CRISPR activation and inhibition control over crucial components in QS systems.

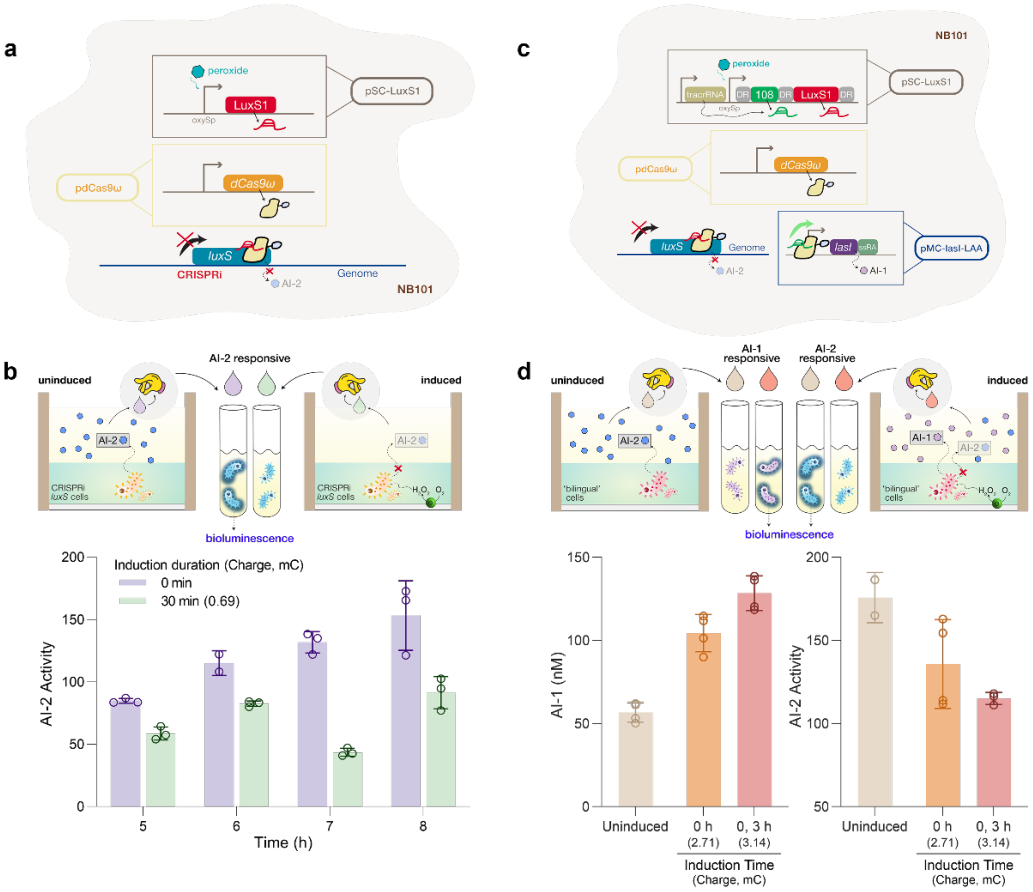

Figure 5.6 eCRISPR inhibition of a native QS signal and multiplexed control of QS communication.

(a) Schematic of *luxS* eCRISPRi to inhibit AI-2 QS signaling. *luxS* specific gRNA LuxS1 is expressed under *oxyS* promoter in pSC-LuxS1. Both pSC-LuxS1 and pdCas9ω were transformed into NB101 allowing gRNA expression. **(b)** Measured AI-2 activity of the CM samples collected at various times post-induction. In-film eCRISPRi cells were electro-induced for 0 or 30 minutes 3 h after deposition. **(c)** Schematic of multiplexed eCRISPR for engineering a 'bilingual' strain. gRNAs sg108 and LuxS1 were flanked with the DR sequence and placed downstream of the *oxyS* promoter in pSC-sg108+LuxS1. tracrRNA was individually expressed under a

synthetic constitutive promoter. Both pSC-LuxS1 and pdCas9ω were transformed into NB101 allowing gRNA expression. Plasmids pSC-sg108+Lux1, pdCas9ω, and pMC-lasI-LAA were all transformed into NB101 allowing multiplexed gRNA expression. **(d)** Measured AI-1 levels and AI-2 activity of the CM samples collected 7 h post-deposition. In-film 'bilingual' cells were electro-induced for 0 or 30 minutes at 0 or 0 and 3 h post-deposition. For all figures, the height of the bar represents the mean, and the error bars represent the standard deviation ($n \geq 3$). Individual replicates are indicated as open circles.

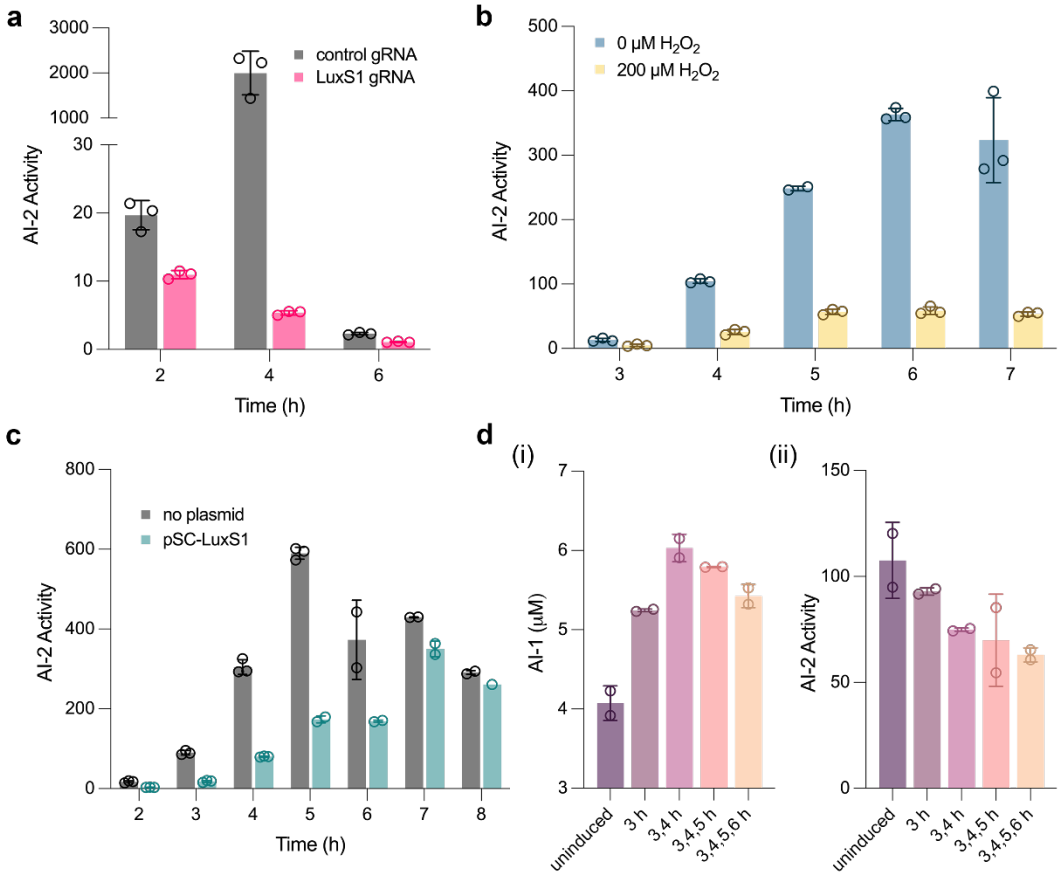

Figure 5.7 H_2O_2-inducible *luxS* CRISPRi and multiplexed control of QS signaling. **(a)** Extracellular AI-2 activity of NB101 cells constitutively expressing either a control gRNA (grey) or *luxS*-specific gRNA LuxS1 (pink) at various time points after reinoculation. Glucose was not added to LB media for inhibiting AI-2 uptake. **(b)** Extracellular AI-2 activity of NB101 cells carrying plasmids pSC-LuxS1 and pdCas9ω induced with 0 or 200 μM of peroxide at OD_{600} = 0.4. CM samples were collected at various time points after re-inoculation. A final concentration of 0.8% (w/v) glucose was added to LB media for inhibiting AI-2 uptake. **(c)** Extracellular AI-2 activity profile of NB101 cells harboring no plasmid (grey) or eCRISPRi components (pSC-

LuxS1 and pdCas9ω) when assembled as "artificial biofilms". **(d)** Measured AI-1 concentration (i) or AI-2 activity (ii) secreted from 'bilingual' cells 7 h post-reinoculation. Labels on the x-axis indicates when the cells received 200 μM H_2O_2 for inducing expression of both gRNAs. For all figures, bar height represents the mean and error bars represent the standard deviation (for (a) – (c) n = 3, for (d) n = 2). Open circle represents the individual replicates.

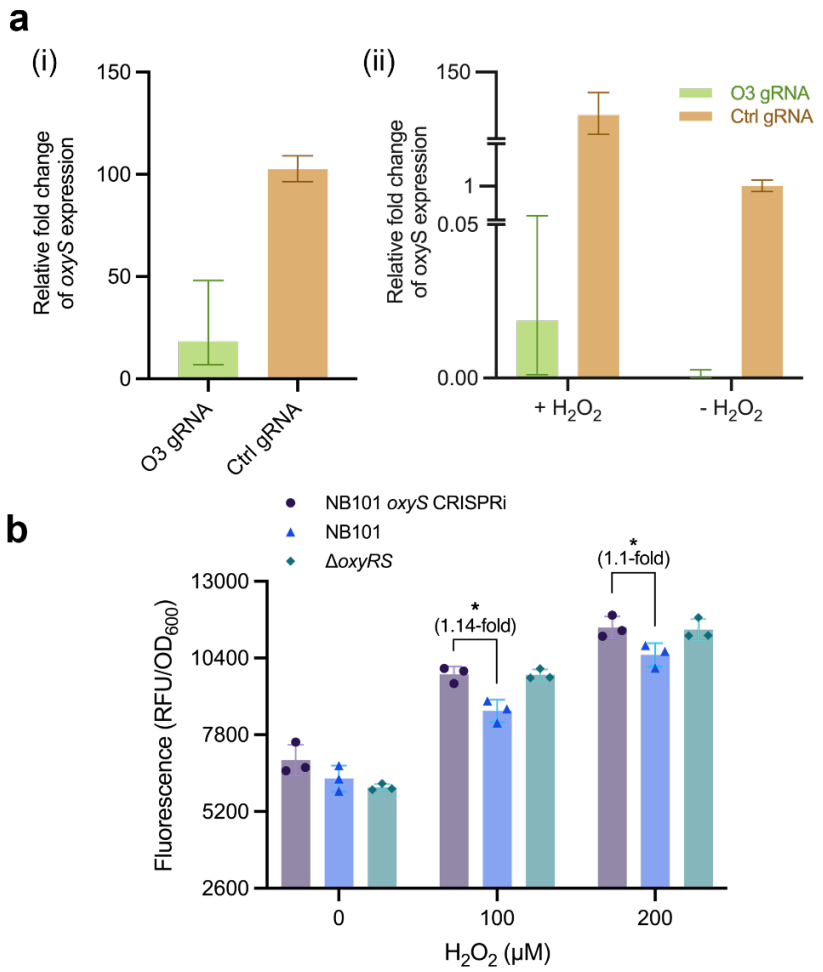

Figure 5.8 *oxyS* CRISPRi to selectively filter biological noise and enhance *oxyS* promoter activity.

(a) Relative fold change of *oxyS* expression when challenged with 0 or 200 μM of peroxide. (i) *oxyS* expression level normalized to the untreated (0 μM H_2O_2) sample. (ii) *oxyS* expression level normalized to the untreated control gRNA sample. **(b)** GFP fluorescence levels from NB101 + pOxyRS-sfGFP (blue triangle), NB101 + pSC-O3 + pdCas9ω + pOxyRS-sfGFP (NB101 *oxyS* CRISPRi, violet circle), and SW102 + pOxyRS-sfGFP (ZK126 Δ*oxyRS*, green diamond) when challenged with 0, 100, and 200 μM of peroxide.

5.2.4 Automated dynamic control of eCRISPRa activity

Inspired by our discovery of which the *oxyRS*-based eCRISPR transcription regulation toolbox could be dynamically controlled, we aimed to investigate and employ the temporal nature of this system to build a fully automated bioelectronic platform for electrogenetics control. First, we created a simpler construct (pOxy-sfGFP-AAV) that was stripped of the CRISPR components but retained its ability to respond to peroxide, for studying the dynamics of the *oxyRS* induction system in suspension culture (**Figure 5.9**). We began by inducing these peroxide reporters with 0, 50, and 100 μM of peroxide and saw a sustained, upregulated response in both induced samples. We then added another dose of peroxide (50 or 100 μM) to the previously induced sample. Consistent with the last cycle, both induced samples exhibited response above basal level in 15 minutes. An inducible behavior was observed in the first 30 minutes post-induction, however the difference in fluorescence response between all three samples quickly rendered indiscernible within 45 minutes. Similar behavior was seen when we applied a third dose of peroxide, proving peroxide induction is transient and can be administered repeatedly. Additionally, we noticed the response attenuated over time when the same amount of peroxide was added. We hypothesized this temporal behavior resulted mostly from the consumption of peroxide, and with a growing number of cells, a higher concentration of peroxide is required to maintain the molar ratio per cell to achieve a similar level of response.

While electrogenetics provides us an approach to seamlessly integrate signal transmission from electronic devices to biological systems, a pathway allowing communication from bio to electronics is also needed to form a closed network for fully

automated control. We chose optical signaling (in our case, fluorescence) to bridge this gap since (i) fluorescence proteins have long been serving as proxy for gene expression (289, 290), (ii) fluorescence output allows for real-time measurements, and (iii) optical signals are easily translated into electronic signal. Therefore, we constructed a bioelectronic system named "Biospark" that consists of a fluorescence detection module for gene expression measurements, a built-in potentiostat for sending electronic commands, and a custom environmental chamber for cell culture (**Figure 5.10a** and **Section 5.4**). Metrics such as linearity, detection limit, and robustness of the fluorescence detection module in Biospark were all characterized and was on par with a commercial microplate reader (**Figure 5.11**). Next, multiple studies were carried out to study the expression dynamics driven by on-film, *in situ* electroinduction. First, we deposited cells that constitutively expressed GFP to track its growth curve (**Figure 5.12a**). A "lag-phase" of approximately 1.25 hours was observed in which there was no increase in fluorescence detected, suggesting that there was no growth during this period. Henceforth, we have chosen to initiate electroinduction at 1.25 h after film deposition. Next, films containing peroxide reporters (pOxy-sGFP) were electrically induced for different durations. Similar characteristics were observed to that of suspension cultures: (i) regarding the dynamics, we saw an initial surge in electro-induced gene expression followed by quick deceleration to a plateau (**Figure 5.12b**); (ii) this system retained its inducibility, as shown by the increasing GFP levels when more charge was applied (**Figure 5.12c**). Based on these findings, we built an algorithm for monitoring gene expression (**Figure 5.12d** and **Section 5.4**). In **Figure 5.10b**, we illustrated the automation workflow: gene expression, as represented by GFP levels,

was measured via the fluorescence detection module and transformed into a digital data to be fed into the custom algorithm. Two user-defined parameters in the algorithm, including the ratio threshold and expression level target, dictated when to 'boost' expression by electroinduction and when to terminate the experiment upon reaching the desired level of expression. We then assembled both peroxide reporters (**Figure 5.13**) and the cells carrying CRISPRa components (specifically, with pMC-GFP as the reporter plasmid) (**Figure 5.10c**) into 'artificial biofilms' and controlled their expression with the automated bioelectronic system. In both cases, our algorithm effectively identified every 'plateaus' in the GFP expression profile and at each time signaled the potentiostat to apply charge (2 mC) for extra electroinduction. Cells were able to reach our target expression level after several inductions. We noted that although a fixed charge was applied for every electroduction, this parameter could also serve as an orthogonal input to enable a more precise control. To summarize, the bioelectronic Biospark system endowed with the expression-tracking algorithm enabled autonomous, self-regulated control of electroinduced gene expression, including eCRISPR activity.

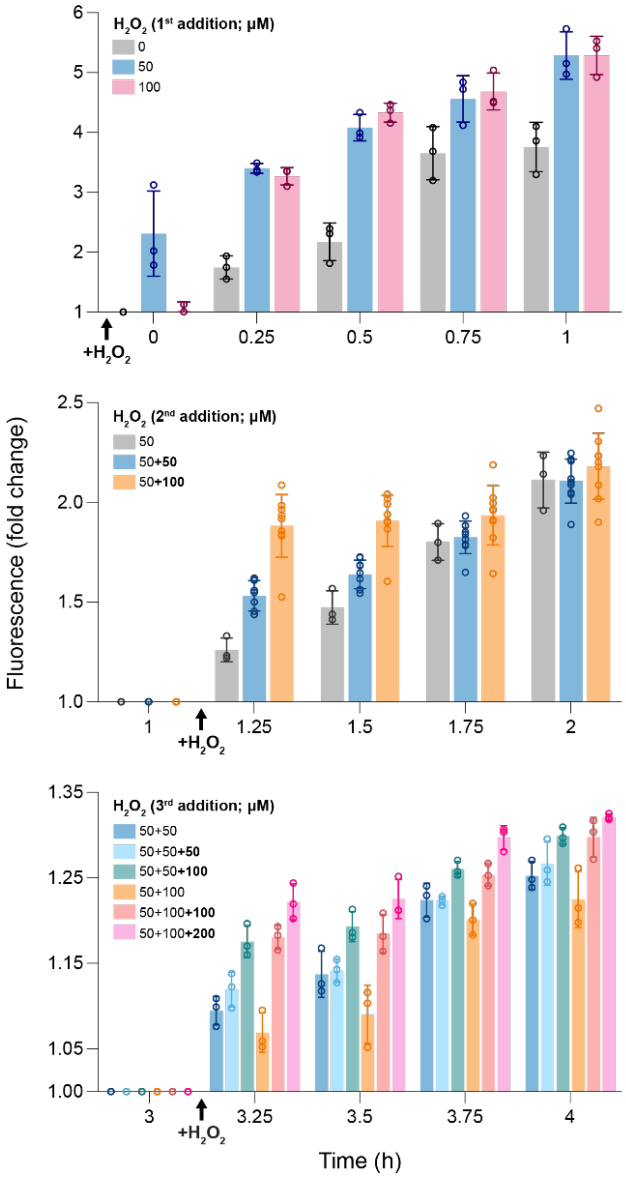

Figure 5.9 H_2O_2-induced gene expression is temporal and can be dynamically controlled.

Measured Fluorescence from peroxide-reporter cells (NEB10β + pOxyRS-sfGFP-AAV). Cells were harvested at OD = 0.4 via centrifugation and re-inoculated the same OD in 20% LB. Peroxide was added to each sample at indicated times. For the data in time points 0-1 h, fluorescence was normalized to the fluorescence of the uninduced

control at time 0. For data in time points 1-4 h, fluorescence was normalized each sample's fluorescence at the beginning of each cycle (i.e., 1 or 3 h). Bar Height represents the mean, and error bars represent the standard deviation ($n \geq 3$). Individual replicates were indicated by the open circles.

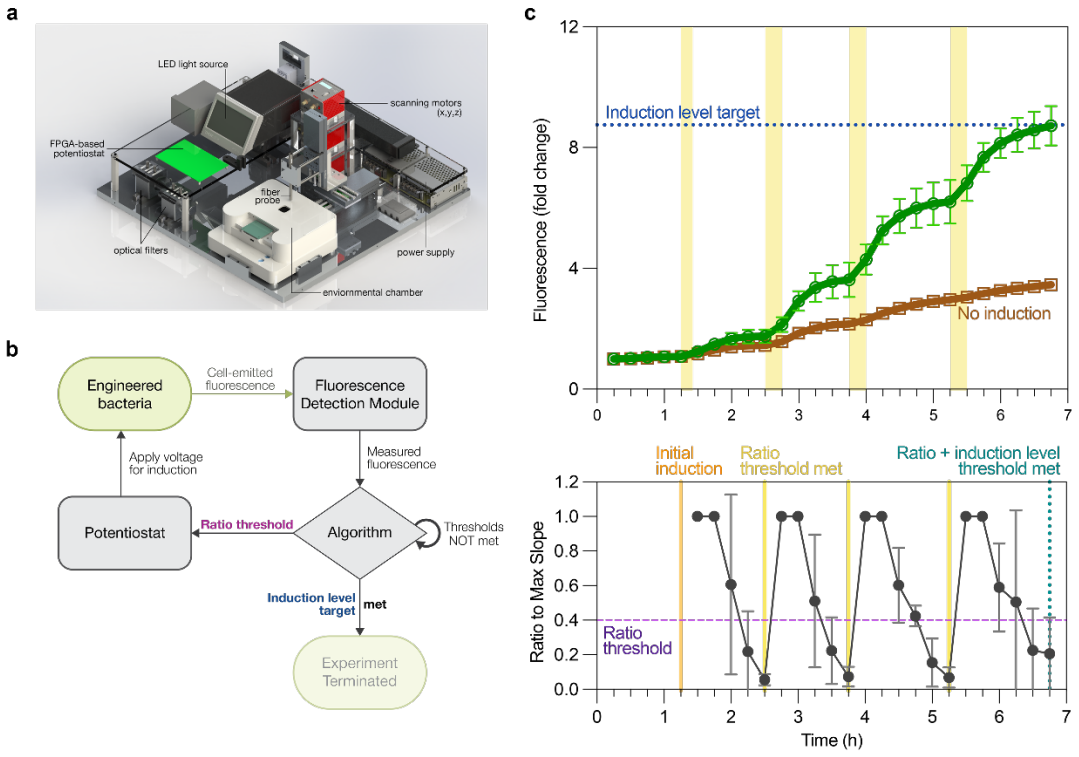

Figure 5.10 Autonomous dynamic control of gene expression via electrogenetic CRISPR.

(a) Schematic illustration of the Biospark system allowing real-time fluorescence measurements and electrochemical induction. **(b)** Automation experiment workflow. Artificial biofilm containing engineered bacteria are assembled onto the ITO electrode of the biohybrid device. Its level of gene expression, represented by the emitted fluorescence, is constantly monitored by the Biospark system and sent to the PC (diamond) for processing. Our custom algorithm (**Figure 5.11**) then determines the status of expression via calculating the ratio of the slopes. When the user-customizable ratio threshold is met, the potentiostat is triggered to apply an induction voltage for a set time or charge. The experiment is automatically terminated when the fluorescence

level is over the user-set induction level threshold. **(c)** Autonomous dynamic control of eCRISPRa-regulated gene expression. *Top*: fluorescence level of the artificial biofilm containing the engineered eCRISPRa bacteria (NB101 harboring pSC-O108, pdCas9ω, and pMC-GFP). Fluorescence measurement was taken every 15 minutes (0.25 h). Experiment ended automatically when fluorescence is over the induction level threshold (blue dotted line). Brown line indicates the fluorescence level of the negative control to which no induction voltage is applied. Yellow zones indicate the periods when the induction voltage (-0.8 V) is applied. A total charge of 2 mC were applied to the cells in each zone. *Bottom*: Ratio to S_{max} computed by our custom algorithm. Ratio threshold (purple dotted line) was set at 0.4. The orange line indicates when the algorithm applied the initial induction voltage. Yellow lines indicate when two consecutive ratios were below set threshold, thus meeting the ratio threshold and triggering the potentiostat to apply induction voltage. The teal dotted line indicates when both the ratio threshold and the induction level threshold were met, hence no voltage was applied, and the experiment was terminated. Open circle, open square, and filled circle represent the mean and error bars represent the standard deviation of individual replicates (n = 2).

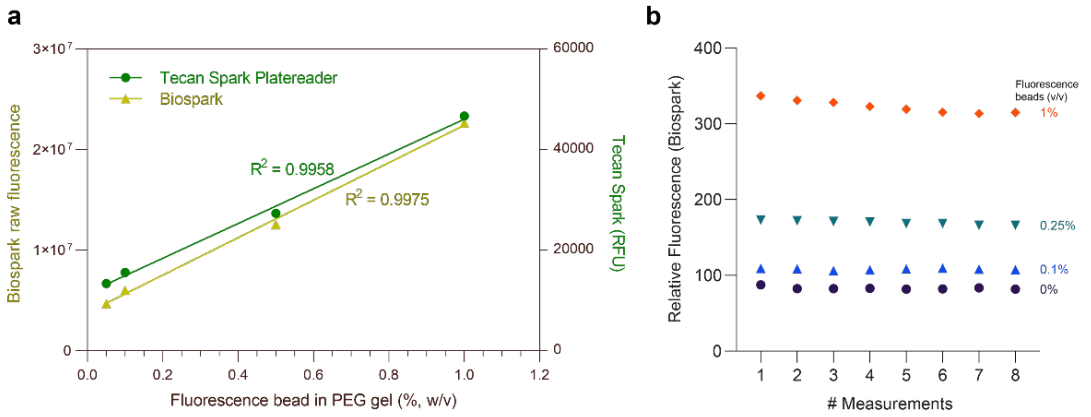

Figure 5.11 Performance in fluorescence measurements of the optical module from our custom Biospark System.

(a) Green fluorescence particles were co-deposited with PEG-SH to various concentrations for simulating fluorescence emitted from engineered bacteria in the 'artificial biofilm'. The resulted hydrogel was submerged in 150 µL of 20% LB, which is identical to the cell experiments. Fluorescence was read using Biospark and the Tecan Spark® microplate reader. **(b)** Relative measured fluorescence from fluorescence particles/PEG-SH hydrogel. The four samples were read in the sequence of 0% → 0.1% → 0.25% → 1% consecutively for 8 cycles.

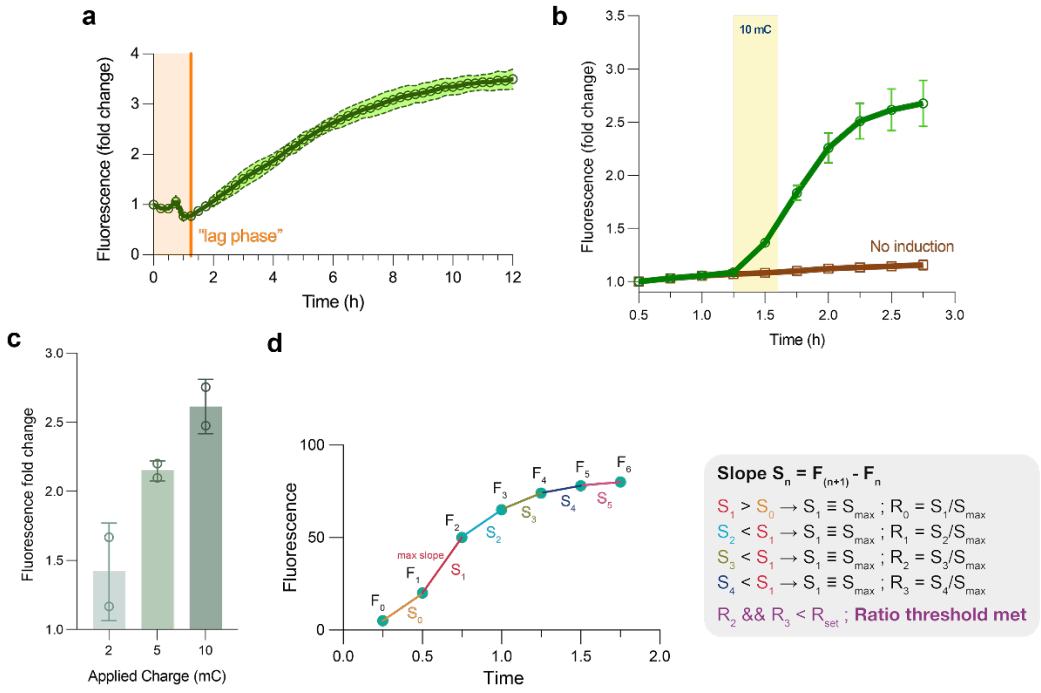

Figure 5.12 Development of a custom algorithm to achieve dynamic control of gene expression.

(a) "Growth curve" of engineered *E. coli* entrapped in artificial biofilm from measured fluorescence of DH5α-sfGFP cells co-deposited with PEG-SH. A "lag-phase" of approximately 1.25 hours was observed in which there was no increase in fluorescence detected, suggesting that there was no growth during this period. Open circles represent the mean fluorescence, and the dashed curves represented the error from individual replicates (n = 4). **(b)** Selected representation of the gene expression dynamic of in-film peroxide reporters (NEB10β + pOxy-sfGFP). Yellow zone indicates when voltage was applied for electroinduction. The uninduced negative control is plotted in brown. Open circles and squares represent the mean and error bars represent the standard deviation of individual replicates (n = 2). **(c)** Fold change in fluorescence before and

after electroinduction. Bar height represents the mean and error bars represent the standard deviation (n = 2). Individual replicates are indicated by the open circles. **(d)** Custom algorithm to monitor gene expression. Since the fluorescence were taken at a fixed time interval, we defined the slope as the difference between two neighboring fluorescence measurements. The algorithm will store and update the value of the maximum slope. It will also compute the ratio between the current slope and the maximum slope (S_{max}). If two consecutive ratios fall below the user-set ratio limit, the algorithm considers the ratio threshold met and will initiate electro-induction via the potentiostat. The S_{max} will in turn return to 0 and start a new cycle.

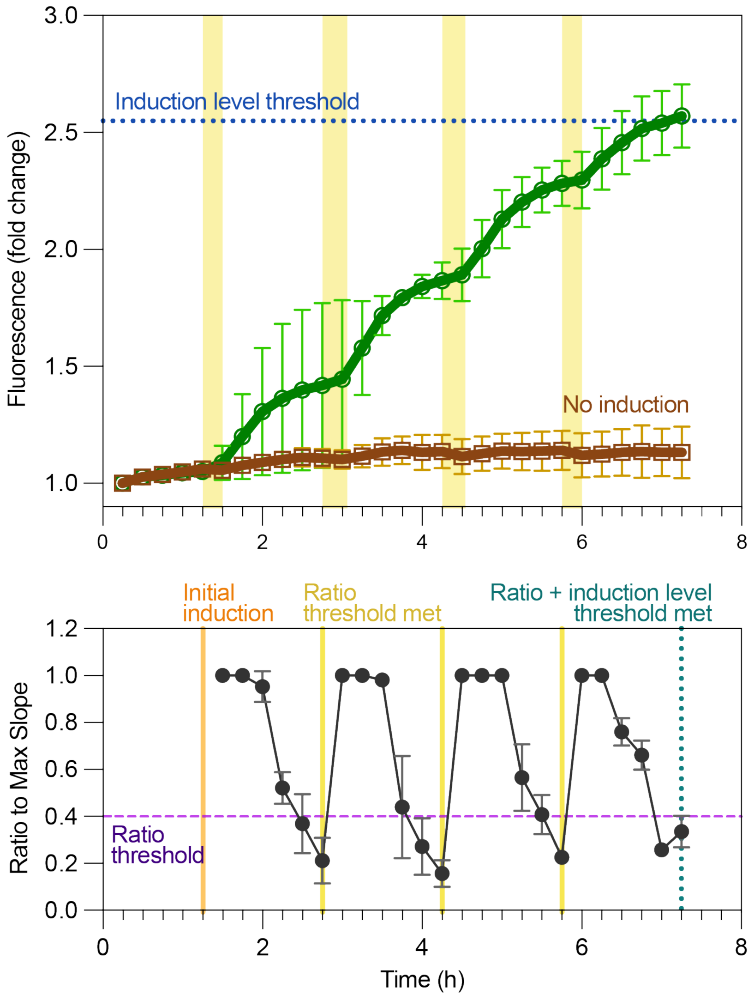

Figure 5.13 Automated control of electro-induced gene expression.

Autonomous dynamic control of gene expression via H_2O_2-inducible electro-induction. *Top*: fluorescence level of the artificial biofilm containing NB101 harboring plasmid pOxy-sfGFP. The experiment was automatically terminated when the fluorescence is over the induction level threshold (blue dotted line). Brown line indicates the fluorescence level of the negative control to which no induction voltage is applied. Yellow zones indicate the periods when the induction voltage (-0.8 V) is applied. A total charge of 2 mC were applied to the cells in each zone. *Bottom*: Ratio to S_{max} computed by our custom algorithm. Ratio threshold (purple dotted line) was set at 0.4.

The orange line indicates when the algorithm applied the initial induction voltage. Yellow lines indicate when two consecutive ratios were below set threshold, thus meeting the ratio threshold and triggering the potentiostat to apply induction voltage. The teal dotted line indicates when both the ratio threshold and the induction level threshold were met, hence no voltage was applied, and the experiment ended. Error bars represent the standard deviation of individual replicates (n = 2).

5.2.5 Network integration for remote, feedback control

By connecting everyday electronic devices to the internet and forming a collective network like the Internet of Things (IoT) (1), each member within can collect data and respond intelligently to users, benefitting our daily lives. We, too, aimed to integrate our local bioelectronic device into a network allowing multidirectional communication between 'living' systems, and realize remote or even remote feedback control of a dynamic biological system. **Fig. 5.14a** illustrates the full network, which is built upon the communication between (i) the local bioelectronic device, (ii) the remote 'actuation checkpoint' enabled by a bio-electrochemical platform, and (iii) human users through the web and SMS (short message service). Instead of immediately sending a command to 'boost' expression when the local algorithm deemed a slump in GFP levels, this status is then wirelessly routed to the remote 'actuation checkpoint' to verify if additional electroinduction is needed. The 'actuation checkpoint' station is an algorithm-controlled, bio-electrochemical platform with the ability to 'write' and 'store' the generated information for documenting the number of times that electroinduction was administered. The platform consists of a patterned ITO electrode that is divided into two working electrodes and attached to a custom 3D-printed housing (**Figure 5.15a** and **Section 5.4**). Working electrode 1 (WE1) is tasked with generating peroxide as 'writing data' when receiving the signal from the local system, while working electrode 2 (WE2) is responsible for sensing the generated peroxide and record this information in the form of electric current. Specifically, a gelatin-based hydrogel containing horseradish peroxidase (HRP) was deposited on WE2 for peroxide measurements (**Figure 5.15c**), as facilitated by the HRP-catalyzed enzymatic reaction

and the following redox cycling with mediator Fc (250, 251). We found the endpoint current from WE2 increased each time we applied charge on WE1 (**Figure 5.15d**), even with long periods in between (**Figure 5.15e**), confirming its ability to write, output, and store data. Controlled by a simple algorithm, the 'actuation checkpoint' then makes decisions based on the user-defined current threshold to either actuate the local potentiostat for electroinduction (via internet) or alert the user in real-time (via SMS) to terminate the experiment. To demonstrate a closed-loop feedback control, user-initiated termination will trigger photobleaching of the select samples, as a representation of "destroying" the product expressed by the engineered bacteria. In **Figure 5.14b**, we showed successful network integration of a dynamic and complex biological system, a robust bio-electrochemical platform, and user intervention allowing real-time communication to jointly regulate eCRISPR-mediated GFP expression.

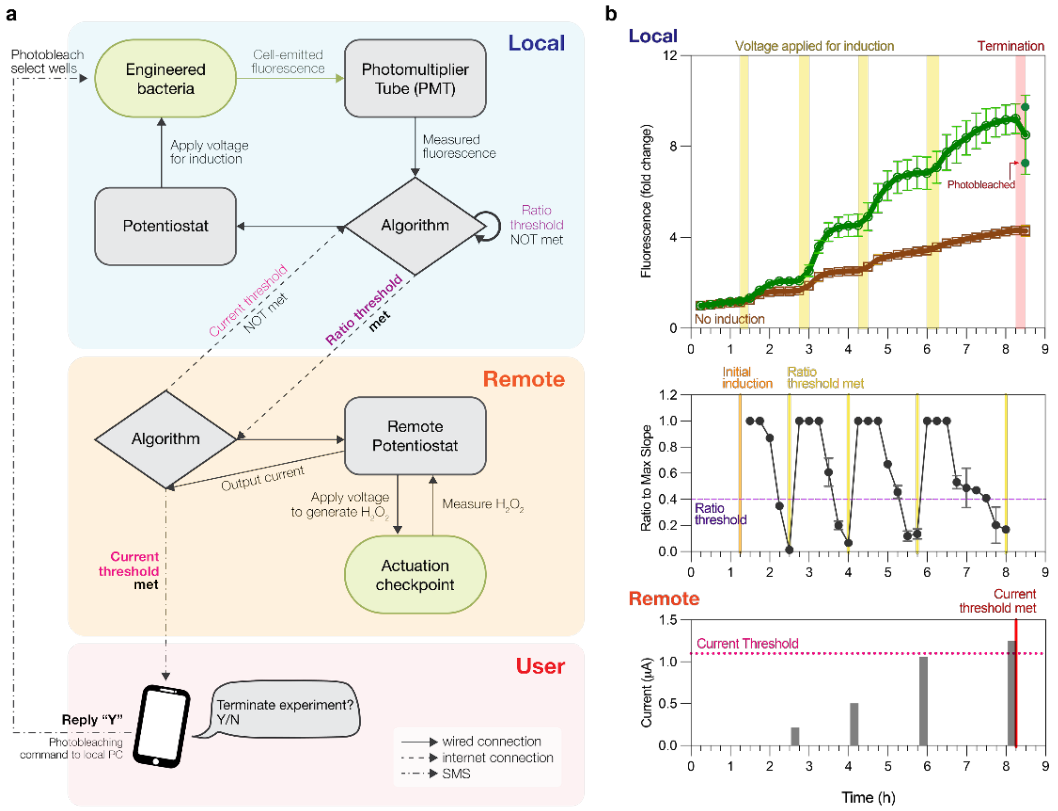

Figure 5.14 Network integration for establishing a Bio-Nano Things framework to enable remote feedback control of eCRISPR activity.

(a) System diagram of the complete Bio-Nano Things network. **(b)** Automated feedback control of eCRISPRa-regulated gene expression. *Local (top)*: fluorescence level of the artificial biofilm containing the engineered eCRISPRa bacteria (NB101 harboring pSC-O108, pdCas9ω, and pMC-GFP). Fluorescence measurement was taken every 15 minutes (0.25 h). Brown open squares and line indicates the mean in fluorescence level of the negative control to which no induction voltage was applied. Yellow zones indicate the periods when the induction voltage (-0.8 V) is applied. A total charge of 2 mC were applied to the cells in each zone. The red zone indicates when the selected sample was being photobleached. *Local (bottom)*: Ratio to S_{max}

computed by our custom algorithm. Ratio threshold (purple dotted line) was set at 0.4. The orange line indicates when the algorithm applied the initial induction voltage. Yellow lines indicate when two consecutive ratios were below set threshold, thus meeting the ratio threshold and proceeded to trigger the remote 'actuation checkpoint'. *Remote*: Current threshold (pink dotted line) was set at 1.1 μA. The red line indicates when the current threshold was met, which prompted the PC at the remote location to send a text message to users. Error bars represent the standard deviation of individual replicates (n = 2).

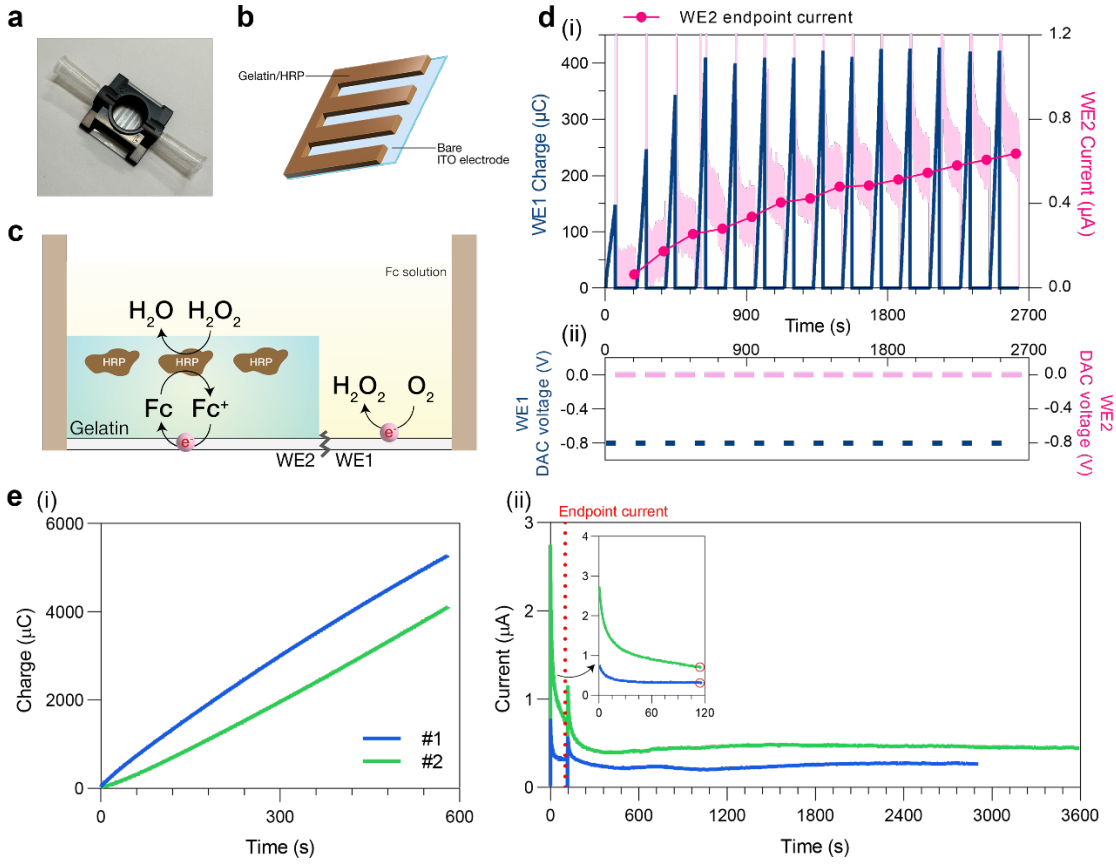

Figure 5.15 Bio-electrochemical platform serving as an actuation checkpoint in the smart feedback-control system.

(a) Custom electrochemical platform with a patterned ITO glass slide attached to a 3D-printed housing. **(b)** A patterned electrode is generated through laser-cutting the ITO-coated glass into a zig-zag pattern to ensure the generated H_2O_2 is at the vicinity of the HRP/gelatin hydrogel for detection. **(c)** Working mechanism of the electrochemical "actuation checkpoint" platform. A gelatin hydrogel containing horseradish peroxidase (HRP) is deposited initially on working electrode 2 (WE2). Working electrode 1 (WE1), consists of just the bare ITO electrode, is tasked to generate H_2O_2 when we apply a reducing voltage. HRP in the gelatin gel on WE2 then catalyzes the generated H_2O_2, and the resulting electron cycles with the electrochemical mediator ferrocene that is

present in the solution. A current (from the cycling of ferrocene) can be read when an oxidizing voltage is applied (0 V vs Ag/AgCl). **(d)** Demonstration of data writing and storage. Generated charge on WE1 and current obtained from WE2 were plotted over the time. **(e)** Demonstration of "long-term" data storage. Total charge from applying -0.8 V on WE1 for 600 s is plotted in (i). The following currents obtained for up to an hour on WE2 are plotted in (ii) (inset: 0 – 120s). Red line and open circles indicate when the endpoint current was recorded (at 120 s).

5.3 Discussion and Conclusion

In this chapter, we expanded the repertoire of *oxyRS*-based electrogenetics by engineering peroxide-mediated eCRISPR, enabling not only upregulation, but inhibition, and multiplexed control of a variety of genetic targets. These include two crucial QS-related genes that allowed the relay of electrochemical signal to a broader yet selective audience of microbial populations through QS communication. Prevalent in nature, QS signaling is an ideal candidate for dispatching the highly-localized electrochemical cue to other *ex situ* biological populations with none or minimal genetic rewiring (54, 259), and achieving coordination within a natural or synthetic consortium (279, 291).

Next, we studied the transient nature of *oxyRS*-based electrogenetics and harnessed this feature for dynamic control of eCRISPR activity. We presented the first integrated electrogenetic system, including both custom-made hardware and software, for fully automated control of eCRISPR-mediated expression. Here, biological responses were coupled with light to facilitate their transition into electronic signals in real time. Though we noted that optogenetics, the use of light-sensitive proteins for regulation of various biological functions, has been a blooming field for interfacing biology and cybernetics (39, 42), our multimodal approach that incorporated electrogenetics induction eliminated the need of an optical input in situations where light is not penetrable, such as commercial bioreactors with high-densities of cells. Furthermore, eCRISPR also provides us an adaptable platform for simultaneous control of genes other than fluorescent proteins via multiplexed transcriptional regulation. We also envisioned the addition of artificial intelligence such as machine learning

techniques for combining the data obtained in our study, for example, correlative dose response relationships between charge inputs and outputs with gene expression, to generate an optimized model allowing smarter precision control.

Finally, we demonstrated the integration of bioelectronic systems with the internet to form a complete electrogenetic framework. By establishing this network of Bio-Nano Things, we were able to realize real-time, feedback control of eCRISPR activity regardless of the constraint in physical distances. An immediate application of this framework would be for online monitoring and feedback control of cells inside bioreactors for smart biomanufacturing (292). Nevertheless, since all electrogenetics components in this study (that is, peroxide signaling, CRISPR techniques, and QS communication) are either native to or can be easily ported to most biological systems, we foresee our Bio-Nano Things network could be employed as the foundation of a plethora of intelligent systems or devices (293). These include self-regulated, real-time reporting drug delivery biomedical devices for *in situ* production of a therapeutic (294, 295), smart agriculture systems for monitored rhizosphere microbiome manipulation (296), or "sense-and-clean" strategies for battling environmental pollution to actively sense and remove contaminants (32), together serving as the blueprint for a more connected world in the future.

5.4 Methods

5.4.1 Chemicals

Potassium chloride (KCl), H_2O_2 (30%), phosphate buffered saline (PBS), potassium phosphate monobasic (KH_2PO_4), potassium phosphate dibasic (K_2HPO_4),

potassium hexachloroiridate(III) (K_3IrCl_6, Ir), and gelatin from porcine skin (gel strength ≈175 g Bloom, Type A, G2625) were purchased from Millipore-Sigma. All antibiotics (ampicillin, kanamycin and chloramphenicol) were purchased form Millipore-Sigma. Lysogeny broth (LB) and agarose were from Fisher Scientific. Fluorescent beads and Pierce® horseradish peroxidase (HRP) were purchased from Thermo Fisher Scientific. 4-arm PEG-SH (MW 5000) were from JenKem USA. 1,1'-Ferrocene dimenthanol (Fc) was from Santa Cruz Biology. AI-1 (N-3-oxo-dodecanoyl-L-Homoserine lactone) was from Cayman Chemicals. Ir, Fc, and AI-1 were initially prepared as 20 mM, 1 M, and 10 mM DMSO stocks, respectively.

5.4.2 Culture media and conditions

Unless otherwise indicated, cells were grown overnight in LB at 37 °C, 250 r.p.m. shaking, inoculated at OD_{600} = 0.1 in LB media the following day, and grown until the indicated cell density (optical density at 600 nm, OD_{600}). Optical density was measured using an UV-Vis Spectrophotometer (Beckman Coulter).

5.4.3 Plasmid construction

All bacterial strains and constructs used in this study were listed in **Table 5.1**. All enzymes, competent cells and reagents were from New England Biolabs and used according to provided protocols. Q5 polymerase and primers in **Table 5.3** (gene sequences in **Table 5.2**) were used for PCR reactions. DpnI digestion, polynucleotide kinase phosphorylation, T4 ligations, Gibson assembly and *E. coli* chemical transformation were performed using New England Biolabs product protocols. DNA clean-up (Zymo Research), gel extraction (Zymo Research) and plasmid preparation kits (Qiagen) were performed using provided protocols. Synthetic gene fragment

containing the multiplex crRNAs was purchased from Thermofisher Scientific. Synthetic gene fragment containing the 108 spacer and gRNA scaffold was purchased from Integrated DNA Technologies (IDT). Synthetic gene fragment containing tracrRNA was purchased from Integrated DNA Technologies (IDT).

Plasmid pSC-O108 (**Table 5.1**) for peroxide-inducible expression of sgRNA sg108 was made via PCR amplification and Gibson assembly. First, pSC-108gRNA (66) was removed of *soxR*, *soxRS* promoter region, and sgRNA sg108 by restriction digestion with ClaI and BamHI. Gene fragment containing *oxyR* and *oxyS* promoter (**Table 5.2**) was amplified from plasmid pOxy-LacZlaa (68) with primers SW01 and SW02 (**Table 5.3**). After DpnI treatment, fragments were ligated by Gibson Assembly. Next, gene fragment containing spacer 108 and gRNA scaffold was then PCR amplified with primers SW03 and SW04 and inserted into the linearized intermediate product via primers SW05 and SW06 to generate the construct pSC-O108.

Plasmid pSC-LuxS1 for peroxide-inducible expression of sgRNA LuxS1 was made via site-directed mutagenesis. Spacer 108 (**Table 5.2**) in plasmid pSC-O108 was swapped with LuxS1 (**Table 5.2**) using primers SW07 and SW08.

Plasmid pSC-sg108+LuxS1 for peroxide-inducible expression of crRNAs spacer 108 and LuxS1 was made vis PCR linearization, restriction digestion, and T4 ligation. pSC-O108 was initially PCR linearized using primers SW09 and SW10 to remove the spacer 108 and the gRNA scaffold, as well as adding restriction sites BamHI and XhoI. Gene fragment containing crRNAs spacer 108 and LuxS1 (**Table 5.2**) was inserted into linearized pSC-O108 backbone via restriction digestion and T4 ligation. After this, the gene fragment containing the tracrRNA (**Table 5.2**) was

inserted into the product generated from the previous step via restriction digestion and T4 ligation to generate the final construct.

Plasmid pLuxS1 for constitutive expression of sgRNA LuxS1 was constructed via site-directed mutagenesis using primers SW11 and SW12 to swap the spacer 108 in plasmid pS108gRNA (66) to LuxS1.

Plasmid pMC-lasI-LAA was constructed via PCR amplification and Gibson assembly. pMC-GFP (66) was linearized and removed of GFPmut2 by primers SW13 and SW14. Primers SW15 and SW16 were used to amplify and add the LAA ssRA tag to *lasI*. *lasI* with the added LAA tag was then inserted to the linearized backbone via Gibson assembly.

Plasmid pOxy-sfGFP-AAV was constructed via site-directed mutagenesis using primers SW17 and SW18 to add the AAV ssRA tag to pOxy-sfGFP (232).

Table 5.1 Strains and plasmids used in this chapter.

Strains		
Name	Genotype	Reference
NEB10β	*E. coli Δ(ara-leu) 7697 araD139 fhuA ΔlacX74 galK16 galE15 e14- ϕ80dlacZΔM15 recA1 relA1 endA1 nupG rpsL* (Str^R) *rph spoT1 Δ(mrr-hsdRMS-mcrBC)*	New England Biolabs
DH5α-sfGFP	*E. coli* DH5α *attTn7::mTn7ΦsfGFP*	This study
NB101	*E. coli* ZK126 Δ*rpoZ*	Bhokisham *et al.*(66)
JLD271	*E. coli* K-12 *ΔlacX74 sdiA271::Cam*	Lindsay *et al.*(297)
BB170	*V. harveyi luxN*::Tn5	Surrette *et al*.(282)
Plasmids		
Name	Description	Reference
pSC-S108gRNA	pSC101 ori, Kan^r, *soxR*, *soxRSp*, spacer 108, gRNA scaffold	Bhokisham *et al.* (66)
pOxy-LacZ-laa	pBR322 ori, Amp^r, *oxyR*, *oxyRSp*, *lacZ* fused with the LAA ssRA tag	Terrell *et al*. (68)
pSC-O108	pSC101 ori, Kan^r, proD promoter, RBS31, *oxyR*, *oxySp*, spacer 108, gRNA scaffold	This study
pdCas9ω	ω was inserted into C termini of dCas9 in pdCas9-bacteria (Addgene plasmid # 44249), p15A ori, pLtetO-1, Cm^r	Bhokisham *et al.* (66)
pMC-GFP	pWJ89 with pBR322 and Amp^r instead of pSC101 ori and Kan^r	Bhokisham *et al.* (66)
pMC-lasI-LAA	pMC-GFP *lasI* with the LAA ssRA tag instead of *gfpmut2*	This study
pLasR_S129T-GFPmut3	pBR322, *lasR*S129T, GFPmut3	This study
pS1gRNA	*soxS* specific gRNA spacers S1 inserted into pgRNAbacteria (Addgene plasmid # 44251) with pBR322 ori, Amp^r, BBa_J23119 promoter	Bhokisham *et al.* (66)
pControlgRNA	Control spacer (from Bikard *et al*.(298)) in pgRNA-bacteria (Addgene plasmid # 44251) with pBR322 origin, Amp^r, J23119 promoter	Bhokisham *et al.* (66)
pLuxS1	pS1gRNA with *luxS* specific gRNA spacer LuxS1 instead of S1	This study
pSC-LuxS1	pSC-O108 with *luxS* specific gRNA spacer LuxS1 instead of 108	This study
pSC-sg108+LuxS1	pSC101 ori, Kan^r, BBa_J23100 promoter, tracrRNA, b1002 terminator, proD promoter, RBS 31, *oxyR*, *oxyRS* promoter, DR, spacer 108, DR, spacer LuxS1, DR, b1006 terminator	This study
pOxy-sGFP	pBR322 ori, Amp^r, proD pomoter, RBS 31, *oxyR*, *oxyRS* promoter, RBS 33, *sfGFP*	Li, Wang *et al*. (232)
pOxy-sfGFP-AAV	AAV ssRA tag inserted to *sfGFP* in pOxy-sfGFP	This study

Table 5.2 Sequences of relevant genetic parts.

Name	Sequence (5'-3')
proD promoter	AAAGTTAAACAAAATTATTTGTAGAGGGAAACCGTTGTGGTCTCCCT GAATATATTATACGAGCCTTATGCATGCCCGTAAAGTTATCCAGCAA CCACTCATAGACCTAGGGCAGCAGATAGGGACGACGTGGTGTTAGCT GTG
oxyR	ATGAATATTCGTGATCTTGAGTACCTGGTGGCATTGGCTGAACACCG CCATTTTCGGCGTGCGGCAGATTCCTGCCACGTTAGCCAGCCGACGC TTAGCGGGCAAATTCGTAAGCTGGAAGATGAGCTGGGCGTGATGTTG CTGGAGCGGACCAGCCGTAAAGTGTTGTTCACCCAGGCGGGAATGCT GCTGGTGGATCAGGCGCGTACCGTGCTGCGTGAGGTGAAAGTCCTTA AAGAGATGGCAAGCCAGCAGGGCGAGACGATGTCCGGACCGCTGCA CATTGGTTTGATTCCCACAGTTGGACCGTACCTGCTACCGCATATTAT CCCTATGCTGCACCAGACCTTTCCAAAGCTGGAAATGTATCTGCATG AAGCACAGACCCACCAGTTACTGGCGCAACTGGACAGCGGCAAACT CGATTGCGTGATCCTCGCGCTGGTGAAAGAGAGCGAAGCATTCATTG AAGTGCCGTTGTTTGATGAGCCAATGTTGCTGGCTATCTATGAAGAT CACCCGTGGGCGAACCGCGAATGCGTACCGATGGCCGATCTGGCAG GGGAAAAACTGCTGATGCTGGAAGATGGTCACTGTTTGCGCGATCAG GCAATGGGTTTCTGTTTTGAAGCCGGGGCGGATGAAGATACACACTT CCGCGCGACCAGCCTGGAAACTCTGCGCAACATGGTGGCGGCAGGT AGCGGGATCACTTTACTGCCAGCGCTGGCTGTGCCGCCGGAGCGCAA ACGCGATGGGGTTGTTTATCTGCCGTGCATTAAGCCGGAACCACGCC GCACTATTGGCCTGGTTTATCGTCCTGGCTCACCGCTGCGCAGCCGCT ATGAGCAGCTGGCAGAGGCCATCCGCGCAAGAATGGATGGCCATTTC GATAAAGTTTTAAAACAGGCGGTTTAA
RBS BBa_B0031	TCACACAGGAAACC
oxyS promoter	TATCCATCCTCCATCGCCACGATAGTTCATGGCGATAGGTAGAATAG CAATGAACGATTATCCCTATCAAGCATTCTGACTGATAATTGCTCAC A
Spacer 108	GCGTGTTGTGGAAGATCCGGCCTGCAGCCA
gRNA scaffold	GTTTTAGAGCTAGAAATAGCAAGTTAAAATAAGGCTAGTCCGTTATC AACTTGAAAAAGTGGCACCGAGTCGGTGC
GFPmut2	ATGAGTAAAGGAGAAGAACTTTTCACTGGAGTTGTCCCAATTCTTGT TGAATTAGATGGTGATGTTAATGGGCACAAATTTTCTGTCAGTGGAG AGGGTGAAGGTGATGCAACATACGGAAAACTTACCCTTAAATTTATT TGCACTACTGGAAAACTACCTGTTCCATGGCCAACACTTGTCACTACT TTCGCGTATGGTCTTCAATGCTTTGCGAGATACCCAGATCATATGAA ACAGCATGACTTTTTCAAGAGTGCCATGCCCGAAGGTTATGTACAGG AAAGAACTATATTTTTCAAAGATGACGGGAACTACAAGACACGTGCT GAAGTCAAGTTTGAAGGTGATACCCTTGTTAATAGAATCGAGTTAAA AGGTATTGATTTTAAAGAAGATGGAAACATTCTTGGACACAAATTGG AATACAACTATAACTCACACAATGTATACATCATGGCAGACAAACAA AAGAATGGAATCAAAGTTAACTTCAAAATTAGACACAACATTGAAG ATGGAAGCGTTCAACTAGCAGACCATTATCAACAAAATACTCCAATT GGCGATGGCCCTGTCCTTTTACCAGACAACCATTACCTGTCCACACA ATCTGCCCTTTCGAAAGATCCCAACGAAAAGAGAGACCACATGATCC TTCTTGAGTTTGTAACAGCTGCTGGGATTACACATGGCATGGATGAA CTATACAAA

lasI-LAA	ATGATCGTACAAATTGGTCGGCGCGAAGAGTTCGATAAAAAACTGCT GGGCGAGATGCACAAGTTGCGTGCTCAAGTGTTCAAGGAGCGCAAA GGCTGGGACGTTAGTGTCATCGACGAGATGGAAATCGATGGTTATGA CGCACTCAGTCCTTATTACATGTTGATCCAGGAAGATACTCCTGAAG CCCAGGTTTTCGGTTGCTGGCGAATTCTCGATACCACTGGCCCCTACA TGCTGAAGAACACCTTCCCGGAGCTTCTGCACGGCAAGGAAGCGCCT TGCTCGCCGCACATCTGGGAACTCAGCCGTTTCGCCATCAACTCTGG ACAGAAAGGCTCGCTGGGCTTTTCCGACTGTACGCTGGAGGCGATGC GCGCGCTGGCCCGCTACAGCCTGCAGAACGACATCCAGACGCTGGTG ACGGTAACCACCGTAGGCGTGGAGAAGATGATGATCCGTGCCGGCCT GGACGTATCGCGCTTCGGTCCGCACCTGAAGATCGGCATCGAGCGCG CGGTGGCCTTGCGCATCGAACTCAATGCCAAGACCCAGATCGCGCTT TACGGGGGAGTGCTGGTGGAACAGCGACTGGCGGTTTCAGCAGCGA ACGACGAAAATTACGCCCTTGCAGCGTGATAATAA
Spacer LuxS1	GGTATGATCGACTGTGAAGCTATCTAACAA
Spacer Control	TGAGACCAGTCTCGGAAGCTCAAAGGTCTC
crRNAs 108, LuxS1, and terminator BBa_b0016	CTCGAGGTTTTAGAGCTATGCTGTTTTGAATGGTCCCAAAACGCGTGT TGTGGAAGATCCGGCCTGCAGCCAGTTTTAGAGCTATGCTGTTTTGA ATGGTCCCAAAACGGTATGATCGACTGTGAAGCTATCTAACAAGTTT TAGAGCTATGCTGTTTTGAATGGTCCCAAAACAAAAAAAAACCCCGC CCCTGACAGGGCGGGGTTTTTTTTGGATCC
Promoter BBa_J23100, tracrRNA, and terminator BBa_b1002	AAGCTTTTGACGGCTAGCTCAGTCCTAGGTACAGTGCTAGCGGAACC ATTCAAAACAGCATAGCAAGTTAAAATAAGGCTAGTCCGTTATCAAC TTGAAAAAGTGGCACCGAGTCGGTGCTTTTTTTCGCAAAAAACCCCG CTTCGGCGGGGTTTTTTCGCGACGTC
sfGFP-AAV	ATGAGCAAAGGAGAAGAACTTTTCACTGGAGTTGTCCCAATTCTTGT TGAATTAGATGGTGATGTTAATGGGCACAAATTTTCTGTCCGTGGAG AGGGTGAAGGTGATGCTACAAACGGAAAACTCACCCTTAAATTTATT TGCACTACTGGAAAACTACCTGTTCCGTGGCCAACACTTGTCACTACT CTGACCTATGGTGTTCAATGCTTTTCCCGTTATCCGGATCACATGAAA CGGCATGACTTTTTCAAGAGTGCCATGCCCGAAGGTTATGTACAGGA ACGCACTATATCTTTCAAAGATGACGGGACCTACAAGACGCGTGCTG AAGTCAAGTTTGAAGGTGATACCCTTGTTAATCGTATCGAGTTAAAG GGTATTGATTTTAAAGAAGATGGAAACATTCTTGGACACAAACTCGA GTACAACTTTAACTCACACAATGTATACATCACGGCAGACAAACAAA AGAATGGAATCAAAGCTAACTTCAAAATTCGCCACAACGTTGAAGAT GGTTCCGTTCAACTAGCAGACCATTATCAACAAAATACTCCAATTGG CGATGGCCCTGTCCTTTTACCAGACAACCATTACCTGTCGACACAATC TGTCCTTTCGAAAGATCCCAACGAAAAGCGTGACCACATGGTCCTTC TTGAGTTTGTAACTGCTGCTGGGATTACACATGGCATGGATGAGCTC TACAAAGCAGCAAACGACGAAAACTACGCTGCTGCTGTT

Table 5.3 Primers used in this chapter.

Name	Sequence (5'-3')
SW01	TGTTTGACAGCTTATCATC
SW02	GCGTCCGGCGTAGAGTCGTGTGAGCAATTATCAG
SW03	CACACGAGCGTGTTGTGG
SW04	GTAGAGAAAAAAGCACCGACTCGG
SW05	GTCGGTGCTTTTTTCTCTACCTCTACGCCGGACGCATC
SW06	TTCCACAACACGCTCGTGTGTCGTGTGAGCAATTATCAGTCAG
SW07	GAAGCTATCTAACAAGTTTTAGAGCTAGAAATAGCAAGTTAAAATAAG
SW08	ACAGTCGATCATACCTCGTGTGTCGTGTGAGCA
SW09	CTAACGGATCCGCTTTTTTCTCTACCTCTACGCC
SW10	CTAAGCTCGAGTGTGAGCAATTATCAGTCAGAATG
SW11	GAAGCTATCTAACAAGTTTTAGAGCTAGAAATAGC
SW12	ACAGTCGATCATACCACTAGTATTATACCTAGGAC
SW13	GGATCCCATGGTACGCGTG
SW14	CTAGATTTCTCCTCTTTAAAGGAATTCGC
SW15	TTTAAAGAGGAGAAATCTAGATGATCGTACAAATTGGTCGG
SW16	GCACGCGTACCATGGGATCCTTATTATCACGCTGCAAGGG
SW17	TGATGCGGTAGTTTATCAC
SW18	AACAGCAGCAGCGTAGTTTTCGTCGTTTGCTGCTTTGTAGAGCTCATCCAT

5.4.4 Fabrication of the biohybrid electronic device

The custom-designed housing was 3D-printed with Mars 3 MSLA 3D printer (ELEGOO) and attached to the ITO-coated glass slide (Sigma) as the working electrode using the same resin and UV-curing (Creative CADWorks). The Ag/AgCl reference electrode (Pine Research) can be inserted from the side well into the central trough in which the salt bridge is casted. To cast the agarose salt bridge, 0.1% agarose in 1M KCl was heated and added into the central well. After the agarose solidified, 1M KCl was added to submerge the salt bridge. A separate custom connector was also printed (with this 3D printer), and a Pt wire was attached as the counter electrode. With the device fully assembled, the counter electrode was immersed in the 1M KCl solution present in the central salt bridge trough.

5.4.5 Peroxide Generation and Quantification

Electrochemical peroxide generation was performed in the biohybrid electronic device with its setup as described above. 150 μL of culture media containing LB and PBS mixed in a 1:4 ratio (referred as 20% LB) was added into each well. The working electrode solution was undisturbed (or, where indicated, stirred via blowing O_2 into the wells). The electrodes were connected to a potentiostat (either 700-series CH Instruments or a custom FPGA-based potentiostat). Chronoamperometry, poised at −0.8 V for the indicated duration, was performed to generate hydrogen peroxide. The endpoint charge was recorded for each run.

To quantify the generated peroxide, we used the Pierce® quantitative peroxide assay kit (aqueous) (Thermo Fisher Scientific) according to the manufacturer's instructions. Briefly, the working reagent was prepared by mixing one volume of

Reagent A with 100 volumes of Reagent B, with at least 200 µl prepared for each sample to be assayed. Ten volumes of the working reagent were added to one volume of sample (typically 200 µl working reagent to 20 µl sample) in a well of a clear-bottomed 96-well plate. The reaction was mixed and incubated for 15–20 min, after which a Spark® microplate reader (Tecan) was used to measure the absorbance at 595 nm. Sample peroxide concentration was calculated by comparison with a standard curve (dilutions of 30% peroxide) performed the same day.

5.4.6 General and coculture electroinduction set-up

Electroinduction experiments were performed in the custom biohybrid electronic device. Deposition of the cell/PEG-SH film was performed as described in previous sections. After thorough washing to remove excess cell/PEG-SH solution, 150 µL of 20% LB was added to each well as the culture media. Peroxide was generated via chronoamperometry as described in sections above, with voltage application for a specified duration (e.g., 1800 s). The biohybrid device was then moved to an incubator (30 or 37°C, as indicated) for incubation. For all automated experiments, the biohybrid device remained in a custom-made environmental chamber inside the Biospark system with temperature (34°C) and humidity (≥ 80%) control. 0.4 ft^3/h (scfh) of oxygen was supplied during electroinduction for media perturbation and oxygen supply to generate sufficient peroxide for induction.

Samples (i.e., the media immersing the film) were removed at indicated time intervals and sterile filtered for downstream bioassays. For coculture experiments, the AI-1 responsive strain (NEB10β + pLasR_S129T-GFPmut3) that were grown to mid-

log phase were inoculated to an OD_{600} of 0.025 in 20% LB, then added into the wells containing the generated 'artificial biofilm' for electroinduction.

5.4.7 AI-1 quantification

AI-1 quantification was performed by bioluminescence assay. AI-1 reporter cells JLD271 pAL105 were grown overnight in LB at 37 °C and 250 r.p.m. shaking with the appropriate antibiotics. The following day, AI-1 solutions (0 – 84 nM) for the standard calibration curve were prepared in 20% LB. The reporter cells were diluted 500-fold in LB with the appropriate antibiotics. For every experimental replicate, 90 µl of diluted reporter cells and 10 µl of the standard AI-1 solutions were added into the wells of a white-bottom 96-well plate (Corning). Experimental conditioned media samples were prepared similarly after sterile filtering and diluting between two- and thousand-fold to maintain a linear assay range. Microplate with reporter cells and conditioned media samples were incubated at 30 °C and 250 r.p.m. shaking in a Tecan® microplate reader, and its luminescence was measured by the plate reader every 30 minutes for 3-5 hours. The AHL concentration of each sample was calculated using the standard curve.

5.4.8 RT-qPCR

NB101 harboring the plasmids that allow CRISPR activation of GFP (pSC-O108 + pdCas9ω + pMC-GFP) were grown at 37°C and 250 r.p.m in LB overnight. The following day, overnight cultures were diluted to OD600 = 0.1 and grown at 37°C and 250 r.p.m until reaching mid-log phase. Peroxide stock solution (10 mM) was then spiked into the cultures to induce the expression of sgRNA. After 3 hours of incubation,

samples were collected via centrifugation. Total and microRNA were extracted using the miRNeasy Kit (Qiagen) and quantified using a Nanodrop (Thermo Scientific). RT-qPCR was then carried out using the Power SYBR™ Green RNA-to-CT™ 1-Step Kit (Applied Biosystems) and a Quantstudio 7 Flex Real-time PCR system (Applied Biosystems).

Similar steps were carried out for the quantitation of *oxyS* expression. NB101 harboring plasmid pO3 or pControlgRNA were grown at 37°C and 250 r.p.m in LB overnight. The following day, overnight cultures were diluted to OD600 = 0.1 and grown at 37°C and 250 r.p.m until reaching mid-log phase. Peroxide stock solution (10 mM) was then spiked into the cultures to induce the expression of sgRNA. After 10 minutes of incubation, samples were collected via centrifugation. Total RNA was extracted using the TRIzol™ Max™ Bacterial RNA Isolation Kit (Invitrogen). RNA quantification and RT-qPCR methods were the same as described above.

5.4.9 AI-2 activity assay

Relative AI-2 levels were determined using the *V. harveyi* reporter BB170 bioluminescence assay (282) with slight modifications. AI-2 reporter cells BB170 were grown overnight in AB media at 30°C and 250 r.p.m shaking with appropriate antibiotics. The following day, overnight BB170 culture was diluted 5000-fold in AB media. For every experimental replicate,180 µl of diluted BB170 culture and 20 µl of conditioned media were added into the wells of a white-bottom 96-well plate (Corning). The microplate was then incubated at 30 °C and 250 r.p.m. shaking in a Tecan® microplate reader, and its luminescence was monitored by the plate reader every 30 minutes after 3-hour incubation. AI-2 activity was calculated by dividing the RLU

produced by the reporter after addition of conditioned media by the RLU of the reporter when growth medium alone was added.

5.4.10 Custom-built bioelectronic system (Biospark) setup

The Biospark system consists of a custom two-channel arbitrary waveform potentiostat with simultaneous sampling of up to two PMT sensors, a motorized fiber-coupled fluorescence reader, and a custom environmental chamber.

Fluorescence measurement module

The fluorescence reader consists of a 470nm excitation light source and driver (Thorlabs #M470F4 and #DC2200) that sends light to a fiber-coupled filter mount (Thorlabs #FOFMS) via a 1000µm diameter core multimode fiber (Thorlabs #FT1000EMT-CUSTOM). An OD6 fluorescence filter (Edmund Optics #67-027) was used to set the excitation band. This light was then directed onto the test target via a fiber coupled reflection probe (Thorlabs #RP22). The emission from the target was collected by the other fibers in this bundle and directed to a second fiber coupled filter mount (Thorlabs #FOFMS) which contained two OD6 emission filters (Edmund Optics #67-030). The filtered light in turn passed through another fiber (Thorlabs #FT1000EMT-CUSTOM) to a fluorescence enhanced PMT (Thorlabs #PMT2101) where it was converted to an electrical signal that travelled to the Analogue to Digital Converter (ADC) on the FPGA potentiostat board. A 3-axis motion platform consisting of three stepper motor kits (Thorlabs #KMTS50E) that were assembled with a base plate (Thorlabs #MTS50A-Z8), XY plate (Thorlabs #MTS50B-Z8) and right-angle plate (Thorlabs #MTS50C-Z8) was used to allow x, y, and z-axis movement of the probe.

Custom FPGA-potentiostat

We built a custom potentiostat through fabrication and assembly of a FPGA board. The core component is a Spartan-7 module (Opal Kelly #XEM7305) and breakout board (Opal Kelly #BRK7305). Power was supplied via an ultralow-noise linear power supply (Acopian #DB5-50). While many components were used on the custom potentiostat board, the three primary components of interest included the (a) femtoampere input bias current op-amps (Analog Devices #ADA4530), (b) the 16-bit multichannel Digital-to-analog converter (DAC) (Analog Devices #AD5765), and the 18-bit multichannel ADC (Texas Instruments #ADS8698).

Power source, connection to PC, and custom control software

General power for the Biospark system was provided from four power supplies: a 5VDC (CUI # VGS-75C-5), a 12VDC (CUI # VGS-75W-12), a 15VDC (CUI #VGS-75C-15), and a 48VDC (CUI #VGS-75W-48). The system is connected to an PC via USB (Latorice #B07GLP8SD, purchased from Amazon). A custom Windows GUI program written in C# was used to control the system. Functions included adjusting metrics related to the (i) various potentiostat modes (e.g., chronoamperometry mode, cyclic voltammetry mode, manual, algorithm-controlled), (ii) potentiostat settings (e.g., voltage, pulse period, slew rate, max charge, etc...), (iii) fluorescence reading (e.g., pulse width, pulse count, measurement interval), and (iv) Algorithm control (e.g., algorithm/manual control mode, ratio thresholds, expression level target, SMS settings, etc...). Data were saved in a custom binary format but could be exported into an Excel spreadsheet (.xlsx). Four real-time diagrams on the main screen of the program

displayed the fluorescence values, potentiostat currents and charges, applied counter voltages, and the CV curve or fluorescence slope ratios.

5.4.11 Algorithm for "smart" control of gene expression

We built a custom algorithm to monitor gene expression as represented by the emitted fluorescence. Since the fluorescence were taken at a fixed time interval (15 min), we defined the slope as the difference between two neighboring fluorescence measurements as described by **Equation 5.1**.

$$\boldsymbol{Slope\ S_n = F_{(n+1)} - F_n} \qquad \text{(Equation 5.1)}$$

The algorithm stores and updates the value of the maximum slope (S_{max}) to serve as a reference point for the progression of the fluorescence level. To determine the rate of change in fluorescence levels, we took the ratio between the current slope and S_{max} as described by **Equation 5.2**.

$$\boldsymbol{Slope\ Ratio\ R_{(n-1)} = S_n \div S_{max}} \qquad \text{(Equation 5.2)}$$

If two consecutive ratios fall below the user-defined ratio limit, the algorithm considers the ratio threshold met and will initiate electro-induction by sending a command to the potentiostat. Variables such as the duration of voltage application or the total charge applied can be set in the GUI program. The S_{max} will return to 0 and a new cycle will start subsequently.

5.4.12 Electrodeposition of HRP/gelatin hydrogel and electrochemical detection of H_2O_2.

We followed the protocol for HRP/gelatin deposition and electrochemical detection of peroxide as described by Li *et al.* with slight modifications (250).

Deposition of HRP/gelatin was performed on a custom patterned electrode generated through laser-cutting the ITO-coated glass slide into two separate interweaving working electrode. This zig-zag pattern was chosen to ensure the generated peroxide be at the vicinity of the deposited HRP/gelatin hydrogel for detection. A custom 3D-printed housing with one central well exposing the working electrodes and two side openings for the insertion of Ag/AgCl reference electrodes was then attached to the patterned ITO electrode (**Figure 5.14 a-c**). A custom connector attached with two Pt wires provided the 3-electrode system with counter electrodes. Upon deposition, a solution containing HRP (1 mg/mL), gelatin (25 mg/mL), and 5 mM Ir) was pipetted into the central well of the device followed by applying an oxidative voltage (+1.2 V) for 2 minutes on working electrode 2 (WE2). After removing the excess HRP/gelatin, a solution of 0.25 mM Fc in 0.1 M phosphate buffer was added into the well submerging both working electrodes. Electrochemical peroxide generation was performed on working electrode 1 (WE1) by applying -0.8 V for the desired duration. To detect the peroxide generated from WE1, a constant voltage (0 V vs Ag/AgCl) was imposed on WE2 for 120 s, and the current output was recorded (**Figure 5.14e**).

5.4.13 Custom algorithm for controlling the remote 'actuation checkpoint'.

A simple algorithm was built to control the 'actuation checkpoint' bio-electrochemical platform. After receiving the initiation message from the local bioelectronic system, the algorithm then commands a custom-built potentiostat at the remote location to run a pre-set program (specifically, apply -0.8 V on WE1 for 600 s, followed by 0 V on WE2 for 120s). It then compares the value of the output current to that of the user-defined current threshold: if the output current does not exceed the

threshold, a message is sent to the local system to administer electroinduction right after the upcoming fluorescence measurement (for a user-defined duration or charge); otherwise, the algorithm sends a SMS message to alert the users. If 'Y' is received from the users for termination, a termination message will be sent to the local system to initiate photobleaching right after the upcoming fluorescence measurement. If 'N' is received form the users, the 'actuation checkpoint' proceeds to run the potentiostat program once more.

Chapter 6. Conclusion and Future Outlooks

Since the launch of the first iPhone in 2007, the introduction of a small, portable, and multifunctional device has transformed our lives immensely. Nowadays, the advent of inexpensive computer chips and high bandwidth telecommunication together allowed billions of devices to connect to the internet. Running out of toilet paper? With a simple push of Amazon Dash buttons and the toilet paper will be delivered on your doorstep (in less than two days if you are a Prime member). Wondering if you should buy more eggs during your grocery run? Smart fridges can help you keep track of what is in your refrigerator at all times. Accidentally burnt your dinner so you are incredibly "hangry"? McDonald's McDelivery sensor picks up your frustration and orders a meal to sooth your hunger. These somewhat futuristic scenarios are all powered by IoT, or Internet of Things, which consists of many interconnected sensor/actuator-integrated devices that are capable of collecting data and responding intelligently to users. While we are currently installing more and more everyday, "mundane" objects with sensors and connecting them to the internet for constant monitoring, our body or any other complex biological systems remain untapped territories to IoT due to the communication difficulties between electronics and biology.

In my dissertation, we started by reviewing current methodologies developed for overcoming such disparity in communication. Lately, redox reactions have garnered interest as another molecular communication modality and bioelectronic signaling medium thanks to its dual nature. In **Chapter 1**, we discussed two redox-based electrogenetic archetypes in which rewired oxidative stress regulon can serve as a conduit for electronic signal (i.e., freely-diffusible electrons) to enter and be recognized

by biological components; and in turn, initiate gene expression to alter cellular behavior. These endeavors have inspired the works in the following chapters, in which we aimed to engineer information transfer with abiotic materials or electrodes through redox communication (specifically H_2O_2 signaling). Next, **Chapter 2** introduced us to the vast universe of quorum sensing communication, which we presented as a paradigm for native molecular communication in biological systems. This remarkable phenomenon found in most microbes allows them to propagate information and organize population-wide behavior despite being single cell organisms. We showed that by minimally rewiring these native QS circuits, one may be able to endow cells with smart functions, like biosensing, living therapeutics, and precise biosynthesis. More importantly, QS systems can be manipulated to initiate communication between other microbial communities, enabling intentional engineering of synthetic consortia. We also showcased several examples that utilized rewired QS systems to connect with abiotic materials and create biohybrid, microelectronic devices. Although the communication gap between biology and electronics remains the major bottleneck for the connection of the two realms, we argued that it is equally important to generate more techniques to facilitate information transfer within biologically systems for the "translated" electronic signal to disseminate.

Since the transformation of electronic to biological signal are usually the most efficient at the biotic/abiotic interface, in **Chapter 3** we chose to focus on engineering the interface in hope of improving information transfer between these domains. Due to the diffusion nature of molecular communication, it is the most reasonable to place signal receptors in close proximity to where the signal is being generated. For this

reason, we developed a simple, yet controllable method for assembling live cells with PEG-SH to form a hydrogel on the surface of an electrode which resembled the microbial biofilms found in nature. Despite many existing methods exploited peptide-metal interactions and cell surface engineering to prompt cell adsorption on electrodes, our approach does not require genetic engineering; thus, opening more possibility for immobilizing any living organisms without the need for inserting non-native genetic circuitries. Easily scalable (from ~3 – 100 mm^2) and spatially programmable, we believe PEG-SH co-deposition can invite future opportunities for cell grafting on complex formats wearable and implantable soft bioelectronics (299). Then, instead of embedding cells in PEG-SH to facilitate cell-electrode communication, we sought the possibility of engineering molecular communication between this abiotic material and its nearby biological system. By covalently conjugating a common biological redox moieties catechol to PEG-SH, this new material was shown to interactively communicating with neighboring *E. coli* cultures through H_2O_2 signaling. We note that this process is completely autonomous and self-sufficient (so long as the cells keep providing reductants), so it does not require extra input of energy to trigger the molecular communication. These characteristics make this interactive material highly energy efficient, and we believe is also suitable for application in wearable/implantable technologies.

In **Chapter 4**, we continued to focus on the cell-electrode interface (facilitated by PEG-SH hydrogel) and demonstrated other biomolecular tools to decorate such platform. We showed by incorporating a 5xCys tag to the C-terminus of an IgG-binding protein G allows it (along with PEG-SH) to be easily assembled onto electrodes and

still be able to preserve their function, enabling novel functions like biomolecule recognition and cell capture. However, the added 5xCys tag makes any protein notoriously hard to express, as cysteines tend to aggregate due to their redox nature. We implemented two orthogonal cellular engineering methods to lessen the cells' metabolic burden (via QS rewiring) and alter their redox state (via deletion of H_2O_2 signaling pathways); collectively, they proved to successfully enhance production and retain 5xCys-tagged proteins' presence in the soluble fraction. As one major form of the "electron shuttles" in biological systems, more and more studies have unveiled that cysteines play such a critical role in redox biology (300). We envision these methods will benefit the expression and investigation of other cysteine-rich proteins.

Finally, we demonstrated a complete network of Bio-Nano Things and achieved multidirectional communication of living systems in **Chapter 5**. First, to broaden the bandwidth of electrochemical signaling, we developed *oxyRS*-based eCRISPR to expand the current repertoire of electrogenetic molecular tools. Owing to the versatility of eCRISPR, we achieved multiplexed electrogenetic control on various genetic targets, including two crucial QS signal producers *lasI* and *luxS*. We hope by electronically controlling QS communication, we will be able to regulate the relay of electrochemical signal to neighboring microbial or even mammalian cell communities. Next, we integrated the engineered biotic/abiotic interface developed in **Chapter 3** with eCRISPR to present "Biospark", a full electrogenetic system for algorithm-governed automated control of gene expression. While we employed optical approaches to achieve real-time bio-to-electronic signal transition, our multimodal approach that incorporated electrogenetics induction can ultimately eliminate the need of an optical

input in places where light is hard to penetrate. Our current fluorescence-based system still bears many limitations and in turn faces several challenges, including the need for oxygen and an excitation light. Bioluminescence, however, does not require the exogenous optical input and we believe it is a suitable candidate for advancing our system. The multiplexed nature of eCRISPR also provides us an adaptable platform for simultaneous control of genes other than fluorescent proteins. Furthermore, although the model implemented in the Biospark system is simple and robust, we believe additional support from artificial intelligence will be able to process more information (e.g., applied charge, current…etc.) and create a more holistic and optimized model for smarter, precise control. Lastly, we connected the Biospark system with another custom bio-electrochemical device to the internet, establishing a complete electrogenetic framework and a network of Bio-Nano Things. As a demonstration, we employed this network for remote feedback control of eCRISPR activity in near real-time. We again would like to emphasis the fact that all electrogenetics components in this study, including peroxide signaling, CRISPR techniques, and QS communication, are either native to or can be easily ported to most biological systems. Therefore, we foresee that the framework developed in this study could be employed as the foundation of future intelligent systems or devices, benefitting humankind in fields such as biomedicine, agriculture, environment, and manufacturing.

The recent revolution in mobile devices and IoT in many ways have connected and brought all of us closer to another. One TED Talk lecture, titled “We Are All Cyborgs Now,” even argues that smart phones have become more than just a device in our pockets but something closer to a digital extension of ourselves. Therefore, it is my

hope that in this world where people are now inseparable from our electronic devices, the power of biology can be accessed and harnessed to spawn new ways to improve health and sustainability.

Bibliography

1. Kumar S, Tiwari P, Zymbler M. 2019. Internet of Things is a revolutionary approach for future technology enhancement: a review. Journal of Big Data 6:111.
2. Das D, Maity S, Chatterjee B, Sen S. 2019. Enabling Covert Body Area Network using Electro-Quasistatic Human Body Communication. Sci Rep 9:4160.
3. Jensen MA, Rahmat-Samii Y. 1995. EM interaction of handset antennas and a human in personal communications. Proceedings of the IEEE 83:7-17.
4. Muramatsu D, Sasaki K. 2021. Transmission Analysis in Human Body Communication for Head-Mounted Wearable Devices. Electronics 10:1213.
5. Kuscu M, Unluturk BD. 2021. Internet of bio-nano things: A review of applications, enabling technologies and key challenges. arXiv preprint arXiv:211209249.
6. Logan BE, Regan JM. 2006. Electricity-producing bacterial communities in microbial fuel cells. Trends Microbiol 14:512-8.
7. Kim HJ, Park HS, Hyun MS, Chang IS, Kim M, Kim BH. 2002. A mediator-less microbial fuel cell using a metal reducing bacterium, Shewanella putrefaciens. Enzyme and Microbial Technology 30:145-152.
8. Bond DR, Lovley DR. 2003. Electricity production by Geobacter sulfurreducens attached to electrodes. Appl Environ Microbiol 69:1548-55.
9. Chaudhuri SK, Lovley DR. 2003. Electricity generation by direct oxidation of glucose in mediatorless microbial fuel cells. Nat Biotechnol 21:1229-32.
10. Rabaey K, Boon N, Siciliano SD, Verhaege M, Verstraete W. 2004. Biofuel cells select for microbial consortia that self-mediate electron transfer. Appl Environ Microbiol 70:5373-82.
11. Shi L, Squier TC, Zachara JM, Fredrickson JK. 2007. Respiration of metal (hydr)oxides by Shewanella and Geobacter: a key role for multihaem c-type cytochromes. Mol Microbiol 65:12-20.
12. Gralnick JA, Newman DK. 2007. Extracellular respiration. Mol Microbiol 65:1-11.
13. Shi L, Richardson DJ, Wang Z, Kerisit SN, Rosso KM, Zachara JM, Fredrickson JK. 2009. The roles of outer membrane cytochromes of Shewanella and Geobacter in extracellular electron transfer. Environ Microbiol Rep 1:220-7.
14. Myers CR, Myers JM. 2004. The outer membrane cytochromes of Shewanella oneidensis MR-1 are lipoproteins. Lett Appl Microbiol 39:466-70.
15. Hartshorne RS, Jepson BN, Clarke TA, Field SJ, Fredrickson J, Zachara J, Shi L, Butt JN, Richardson DJ. 2007. Characterization of Shewanella oneidensis MtrC: a cell-surface decaheme cytochrome involved in respiratory electron transport to extracellular electron acceptors. J Biol Inorg Chem 12:1083-94.
16. Ross DE, Ruebush SS, Brantley SL, Hartshorne RS, Clarke TA, Richardson DJ, Tien M. 2007. Characterization of protein-protein interactions involved in

iron reduction by Shewanella oneidensis MR-1. Appl Environ Microbiol 73:5797-808.
17. Reardon CL, Dohnalkova AC, Nachimuthu P, Kennedy DW, Saffarini DA, Arey BW, Shi L, Wang Z, Moore D, McLean JS, Moyles D, Marshall MJ, Zachara JM, Fredrickson JK, Beliaev AS. 2010. Role of outer-membrane cytochromes MtrC and OmcA in the biomineralization of ferrihydrite by Shewanella oneidensis MR-1. Geobiology 8:56-68.
18. Slate AJ, Whitehead KA, Brownson DAC, Banks CE. 2019. Microbial fuel cells: An overview of current technology. Renewable and Sustainable Energy Reviews 101:60-81.
19. Meylani V, Surahman E, Fudholi A, Almalki WH, Ilyas N, Sayyed RZ. 2023. Biodiversity in microbial fuel cells: Review of a promising technology for wastewater treatment. Journal of Environmental Chemical Engineering 11:109503.
20. Webster DP, TerAvest MA, Doud DF, Chakravorty A, Holmes EC, Radens CM, Sureka S, Gralnick JA, Angenent LT. 2014. An arsenic-specific biosensor with genetically engineered Shewanella oneidensis in a bioelectrochemical system. Biosens Bioelectron 62:320-4.
21. Golitsch F, Bucking C, Gescher J. 2013. Proof of principle for an engineered microbial biosensor based on Shewanella oneidensis outer membrane protein complexes. Biosens Bioelectron 47:285-91.
22. West EA, Jain A, Gralnick JA. 2017. Engineering a Native Inducible Expression System in Shewanella oneidensis to Control Extracellular Electron Transfer. ACS Synth Biol 6:1627-1634.
23. Kracke F, Vassilev I, Kromer JO. 2015. Microbial electron transport and energy conservation - the foundation for optimizing bioelectrochemical systems. Front Microbiol 6:575.
24. Jensen HM, Albers AE, Malley KR, Londer YY, Cohen BE, Helms BA, Weigele P, Groves JT, Ajo-Franklin CM. 2010. Engineering of a synthetic electron conduit in living cells. Proc Natl Acad Sci U S A 107:19213-8.
25. Bird LJ, Onderko EL, Phillips DA, Mickol RL, Malanoski AP, Yates MD, Eddie BJ, Glaven SM. 2019. Engineered living conductive biofilms as functional materials. MRS Communications 9:505-517.
26. Nolfi-Donegan D, Braganza A, Shiva S. 2020. Mitochondrial electron transport chain: Oxidative phosphorylation, oxidant production, and methods of measurement. Redox Biol 37:101674.
27. Weber S. 2005. Light-driven enzymatic catalysis of DNA repair: a review of recent biophysical studies on photolyase. Biochim Biophys Acta 1707:1-23.
28. Aukauloo A. 2012. Proton-Coupled Electron Transfer. A Carrefour of Chemical Reactivity Traditions. RSC Catalysis Series. Edited by Sebastião Formosinho and Mónica Barroso. Angewandte Chemie International Edition 51:9217-9217.
29. Shomar H, Gontier S, van den Broek NJF, Tejeda Mora H, Noga MJ, Hagedoorn PL, Bokinsky G. 2018. Metabolic engineering of a carbapenem antibiotic synthesis pathway in Escherichia coli. Nat Chem Biol 14:794-800.

30. Kallio P, Pasztor A, Thiel K, Akhtar MK, Jones PR. 2014. An engineered pathway for the biosynthesis of renewable propane. Nat Commun 5:4731.
31. Atkinson JT, Campbell IJ, Thomas EE, Bonitatibus SC, Elliott SJ, Bennett GN, Silberg JJ. 2019. Metalloprotein switches that display chemical-dependent electron transfer in cells. Nat Chem Biol 15:189-195.
32. Atkinson JT, Su L, Zhang X, Bennett GN, Silberg JJ, Ajo-Franklin CM. 2022. Real-time bioelectronic sensing of environmental contaminants. Nature 611:548-553.
33. Endo M, Ozawa T. 2017. Strategies for development of optogenetic systems and their applications. Journal of Photochemistry and Photobiology C: Photochemistry Reviews 30:10-23.
34. Guglielmi G, Falk HJ, De Renzis S. 2016. Optogenetic Control of Protein Function: From Intracellular Processes to Tissue Morphogenesis. Trends Cell Biol 26:864-874.
35. de Mena L, Rizk P, Rincon-Limas DE. 2018. Bringing Light to Transcription: The Optogenetics Repertoire. Front Genet 9:518.
36. Baumschlager A, Khammash M. 2021. Synthetic Biological Approaches for Optogenetics and Tools for Transcriptional Light-Control in Bacteria. Adv Biol (Weinh) 5:e2000256.
37. Gerhardt KP, Olson EJ, Castillo-Hair SM, Hartsough LA, Landry BP, Ekness F, Yokoo R, Gomez EJ, Ramakrishnan P, Suh J, Savage DF, Tabor JJ. 2016. An open-hardware platform for optogenetics and photobiology. Sci Rep 6:35363.
38. Shao J, Xue S, Yu G, Yu Y, Yang X, Bai Y, Zhu S, Yang L, Yin J, Wang Y, Liao S, Guo S, Xie M, Fussenegger M, Ye H. 2017. Smartphone-controlled optogenetically engineered cells enable semiautomatic glucose homeostasis in diabetic mice. Sci Transl Med 9.
39. Mansouri M, Hussherr MD, Strittmatter T, Buchmann P, Xue S, Camenisch G, Fussenegger M. 2021. Smart-watch-programmed green-light-operated percutaneous control of therapeutic transgenes. Nat Commun 12:3388.
40. Lindner F, Diepold A. 2022. Optogenetics in bacteria - applications and opportunities. FEMS Microbiol Rev 46.
41. Liu Z, Zhang J, Jin J, Geng Z, Qi Q, Liang Q. 2018. Programming Bacteria With Light-Sensors and Applications in Synthetic Biology. Front Microbiol 9:2692.
42. Milias-Argeitis A, Rullan M, Aoki SK, Buchmann P, Khammash M. 2016. Automated optogenetic feedback control for precise and robust regulation of gene expression and cell growth. Nat Commun 7:12546.
43. Aoki SK, Lillacci G, Gupta A, Baumschlager A, Schweingruber D, Khammash M. 2019. A universal biomolecular integral feedback controller for robust perfect adaptation. Nature 570:533-537.
44. Gutierrez Mena J, Kumar S, Khammash M. 2022. Dynamic cybergenetic control of bacterial co-culture composition via optogenetic feedback. Nat Commun 13:4808.

45. Benisch M, Benzinger D, Kumar S, Hu H, Khammash M. 2023. Optogenetic closed-loop feedback control of the unfolded protein response optimizes protein production. Metab Eng 77:32-40.
46. Frei T, Chang CH, Filo M, Arampatzis A, Khammash M. 2022. A genetic mammalian proportional-integral feedback control circuit for robust and precise gene regulation. Proc Natl Acad Sci U S A 119:e2122132119.
47. Misteli T, Spector DL. 1997. Applications of the green fluorescent protein in cell biology and biotechnology. Nat Biotechnol 15:961-4.
48. Winson MK, Swift S, Hill PJ, Sims CM, Griesmayr G, Bycroft BW, Williams P, Stewart GS. 1998. Engineering the luxCDABE genes from Photorhabdus luminescens to provide a bioluminescent reporter for constitutive and promoter probe plasmids and mini-Tn5 constructs. FEMS Microbiol Lett 163:193-202.
49. Mimee M, Nadeau P, Hayward A, Carim S, Flanagan S, Jerger L, Collins J, McDonnell S, Swartwout R, Citorik RJ, Bulovic V, Langer R, Traverso G, Chandrakasan AP, Lu TK. 2018. An ingestible bacterial-electronic system to monitor gastrointestinal health. Science 360:915-918.
50. Moser CC, Page CC, Farid R, Dutton PL. 1995. Biological electron transfer. Journal of Bioenergetics and Biomembranes 27:263-274.
51. Kim E, Li J, Kang M, Kelly DL, Chen S, Napolitano A, Panzella L, Shi X, Yan K, Wu S, Shen J, Bentley WE, Payne GF. 2019. Redox Is a Global Biodevice Information Processing Modality. Proceedings of the IEEE 107:1402-1424.
52. Green J, Paget MS. 2004. Bacterial redox sensors. Nat Rev Microbiol 2:954-66.
53. VanArsdale E, Pitzer J, Payne GF, Bentley WE. 2020. Redox Electrochemistry to Interrogate and Control Biomolecular Communication. iScience 23:101545.
54. Wang S, Payne GF, Bentley WE. 2018. Repurposing *E. coli* by Engineering Quorum Sensing and Redox Genetic Circuits, p Ch. 9. *In* Fumiaki U (ed), Gene Expression and Control doi:10.5772/intechopen.81245. IntechOpen, Rijeka.
55. Demple B. 1996. Redox signaling and gene control in the Escherichia coli soxRS oxidative stress regulon--a review. Gene 179:53-7.
56. Imlay JA. 2015. Transcription Factors That Defend Bacteria Against Reactive Oxygen Species. Annu Rev Microbiol 69:93-108.
57. Choi H, Kim S, Mukhopadhyay P, Cho S, Woo J, Storz G, Ryu SE. 2001. Structural basis of the redox switch in the OxyR transcription factor. Cell 105:103-13.
58. Lee C, Lee SM, Mukhopadhyay P, Kim SJ, Lee SC, Ahn WS, Yu MH, Storz G, Ryu SE. 2004. Redox regulation of OxyR requires specific disulfide bond formation involving a rapid kinetic reaction path. Nat Struct Mol Biol 11:1179-85.
59. Toledano MB, Kullik I, Trinh F, Baird PT, Schneider TD, Storz G. 1994. Redox-dependent shift of OxyR-DNA contacts along an extended DNA-

binding site: a mechanism for differential promoter selection. Cell 78:897-909.
60. Jo I, Chung IY, Bae HW, Kim JS, Song S, Cho YH, Ha NC. 2015. Structural details of the OxyR peroxide-sensing mechanism. Proc Natl Acad Sci U S A 112:6443-8.
61. Salim NN, Feig AL. 2010. An upstream Hfq binding site in the fhlA mRNA leader region facilitates the OxyS-fhlA interaction. PLoS One 5.
62. Zhang A, Altuvia S, Tiwari A, Argaman L, Hengge-Aronis R, Storz G. 1998. The OxyS regulatory RNA represses rpoS translation and binds the Hfq (HF-I) protein. EMBO J 17:6061-8.
63. Barshishat S, Elgrably-Weiss M, Edelstein J, Georg J, Govindarajan S, Haviv M, Wright PR, Hess WR, Altuvia S. 2018. OxyS small RNA induces cell cycle arrest to allow DNA damage repair. EMBO J 37:413-426.
64. Weber W, Luzi S, Karlsson M, Sanchez-Bustamante CD, Frey U, Hierlemann A, Fussenegger M. 2009. A synthetic mammalian electro-genetic transcription circuit. Nucleic Acids Res 37:e33.
65. Tschirhart T, Kim E, McKay R, Ueda H, Wu HC, Pottash AE, Zargar A, Negrete A, Shiloach J, Payne GF, Bentley WE. 2017. Electronic control of gene expression and cell behaviour in Escherichia coli through redox signalling. Nat Commun 8:14030.
66. Bhokisham N, VanArsdale E, Stephens KT, Hauk P, Payne GF, Bentley WE. 2020. A redox-based electrogenetic CRISPR system to connect with and control biological information networks. Nat Commun 11:2427.
67. Lawrence JM, Yin Y, Bombelli P, Scarampi A, Storch M, Wey LT, Climent-Catala A, PixCell i GEMT, Baldwin GS, O'Hare D, Howe CJ, Zhang JZ, Ouldridge TE, Ledesma-Amaro R. 2022. Synthetic biology and bioelectrochemical tools for electrogenetic system engineering. Sci Adv 8:eabm5091.
68. Terrell JL, Tschirhart T, Jahnke JP, Stephens K, Liu Y, Dong H, Hurley MM, Pozo M, McKay R, Tsao CY, Wu HC, Vora G, Payne GF, Stratis-Cullum DN, Bentley WE. 2021. Bioelectronic control of a microbial community using surface-assembled electrogenetic cells to route signals. Nat Nanotechnol 16:688-697.
69. Kuscu M, Akan OB. 2016. On the Physical Design of Molecular Communication Receiver Based on Nanoscale Biosensors. IEEE Sensors Journal 16:2228-2243.
70. Zhao JF, Chen XM, Liang BD, Chen QX. 2017. A Review on Human Body Communication: Signal Propagation Model, Communication Performance, and Experimental Issues. Wireless Communications and Mobile Computing 2017:5842310.
71. Wen E, Sievenpiper DF, Mercier PP. 2022. Channel Characterization of Magnetic Human Body Communication. IEEE Transactions on Biomedical Engineering 69:569-579.
72. Nealson KH, Platt T, Hastings JW. 1970. Cellular control of the synthesis and activity of the bacterial luminescent system. J Bacteriol 104:313-22.

73. Whiteley M, Diggle SP, Greenberg EP. 2017. Progress in and promise of bacterial quorum sensing research. Nature 551:313-320.
74. Tomasz A. 1965. Control of the competent state in Pneumococcus by a hormone-like cell product: an example for a new type of regulatory mechanism in bacteria. Nature 208:155-9.
75. Engebrecht J, Nealson K, Silverman M. 1983. Bacterial bioluminescence: isolation and genetic analysis of functions from Vibrio fischeri. Cell 32:773-81.
76. Engebrecht J, Silverman M. 1984. Identification of genes and gene products necessary for bacterial bioluminescence. Proc Natl Acad Sci U S A 81:4154-8.
77. Eberhard A, Burlingame AL, Eberhard C, Kenyon GL, Nealson KH, Oppenheimer NJ. 1981. Structural identification of autoinducer of Photobacterium fischeri luciferase. Biochemistry 20:2444-9.
78. Waters CM, Bassler BL. 2005. Quorum sensing: cell-to-cell communication in bacteria. Annu Rev Cell Dev Biol 21:319-46.
79. DeLisa MP, Wu CF, Wang L, Valdes JJ, Bentley WE. 2001. DNA microarray-based identification of genes controlled by autoinducer 2-stimulated quorum sensing in Escherichia coli. J Bacteriol 183:5239-47.
80. Manefield M, Turner SL. 2002. Quorum sensing in context: out of molecular biology and into microbial ecology. Microbiology 148:3762-4.
81. Miller MB, Bassler BL. 2001. Quorum sensing in bacteria. Annu Rev Microbiol 55:165-99.
82. Davis RM, Muller RY, Haynes KA. 2015. Can the natural diversity of quorum-sensing advance synthetic biology? Front Bioeng Biotechnol 3:30.
83. Greenberg EP, Hastings JW, Ulitzur S. 1979. Induction of luciferase synthesis in Beneckea harveyi by other marine bacteria. Archives of Microbiology 120:87-91.
84. Chen X, Schauder S, Potier N, Van Dorsselaer A, Pelczer I, Bassler BL, Hughson FM. 2002. Structural identification of a bacterial quorum-sensing signal containing boron. Nature 415:545-9.
85. Winans SC. 2002. Bacterial esperanto. Nat Struct Biol 9:83-4.
86. Miller ST, Xavier KB, Campagna SR, Taga ME, Semmelhack MF, Bassler BL, Hughson FM. 2004. Salmonella typhimurium recognizes a chemically distinct form of the bacterial quorum-sensing signal AI-2. Mol Cell 15:677-87.
87. Schauder S, Shokat K, Surette MG, Bassler BL. 2001. The LuxS family of bacterial autoinducers: biosynthesis of a novel quorum-sensing signal molecule. Mol Microbiol 41:463-76.
88. Rezzonico F, Smits TH, Duffy B. 2012. Detection of AI-2 receptors in genomes of Enterobacteriaceae suggests a role of type-2 quorum sensing in closed ecosystems. Sensors (Basel) 12:6645-65.
89. Quan DN, Bentley WE. 2012. Gene network homology in prokaryotes using a similarity search approach: queries of quorum sensing signal transduction. PLoS Comput Biol 8:e1002637.

90. Li J, Wang L, Hashimoto Y, Tsao CY, Wood TK, Valdes JJ, Zafiriou E, Bentley WE. 2006. A stochastic model of Escherichia coli AI-2 quorum signal circuit reveals alternative synthesis pathways. Mol Syst Biol 2:67.
91. Wang L, Hashimoto Y, Tsao CY, Valdes JJ, Bentley WE. 2005. Cyclic AMP (cAMP) and cAMP receptor protein influence both synthesis and uptake of extracellular autoinducer 2 in Escherichia coli. J Bacteriol 187:2066-76.
92. Wang L, Li J, March JC, Valdes JJ, Bentley WE. 2005. luxS-dependent gene regulation in Escherichia coli K-12 revealed by genomic expression profiling. J Bacteriol 187:8350-60.
93. Xavier KB, Bassler BL. 2005. Regulation of uptake and processing of the quorum-sensing autoinducer AI-2 in Escherichia coli. J Bacteriol 187:238-48.
94. Quan DN, Tsao CY, Wu HC, Bentley WE. 2016. Quorum Sensing Desynchronization Leads to Bimodality and Patterned Behaviors. PLoS Comput Biol 12:e1004781.
95. Rezzonico F, Duffy B. 2008. Lack of genomic evidence of AI-2 receptors suggests a non-quorum sensing role for luxS in most bacteria. BMC Microbiol 8:154.
96. Li J, Attila C, Wang L, Wood TK, Valdes JJ, Bentley WE. 2007. Quorum sensing in Escherichia coli is signaled by AI-2/LsrR: effects on small RNA and biofilm architecture. J Bacteriol 189:6011-20.
97. Gonzalez Barrios AF, Zuo R, Hashimoto Y, Yang L, Bentley WE, Wood TK. 2006. Autoinducer 2 controls biofilm formation in Escherichia coli through a novel motility quorum-sensing regulator (MqsR, B3022). J Bacteriol 188:305-16.
98. DeLisa MP, Valdes JJ, Bentley WE. 2001. Quorum signaling via AI-2 communicates the "Metabolic Burden" associated with heterologous protein production in Escherichia coli. Biotechnol Bioeng 75:439-50.
99. Bansal T, Jesudhasan P, Pillai S, Wood TK, Jayaraman A. 2008. Temporal regulation of enterohemorrhagic Escherichia coli virulence mediated by autoinducer-2. Appl Microbiol Biotechnol 78:811-9.
100. Englert DL, Jayaraman A, Manson MD. 2009. Microfluidic techniques for the analysis of bacterial chemotaxis. Methods Mol Biol 571:1-23.
101. Hegde M, Englert DL, Schrock S, Cohn WB, Vogt C, Wood TK, Manson MD, Jayaraman A. 2011. Chemotaxis to the quorum-sensing signal AI-2 requires the Tsr chemoreceptor and the periplasmic LsrB AI-2-binding protein. J Bacteriol 193:768-73.
102. Neumann S, Hansen CH, Wingreen NS, Sourjik V. 2010. Differences in signalling by directly and indirectly binding ligands in bacterial chemotaxis. EMBO J 29:3484-95.
103. Laganenka L, Colin R, Sourjik V. 2016. Chemotaxis towards autoinducer 2 mediates autoaggregation in Escherichia coli. Nat Commun 7:12984.
104. Bailey JE. 1991. Toward a science of metabolic engineering. Science 252:1668-75.
105. Yokobayashi Y, Weiss R, Arnold FH. 2002. Directed evolution of a genetic circuit. Proc Natl Acad Sci U S A 99:16587-91.

106. Chen W, Kallio PT, Bailey JE. 1993. Construction and characterization of a novel cross-regulation system for regulating cloned gene expression in Escherichia coli. Gene 130:15-22.
107. You L, Cox RS, 3rd, Weiss R, Arnold FH. 2004. Programmed population control by cell-cell communication and regulated killing. Nature 428:868-71.
108. Danino T, Mondragon-Palomino O, Tsimring L, Hasty J. 2010. A synchronized quorum of genetic clocks. Nature 463:326-30.
109. Tsao CY, Hooshangi S, Wu HC, Valdes JJ, Bentley WE. 2010. Autonomous induction of recombinant proteins by minimally rewiring native quorum sensing regulon of E. coli. Metab Eng 12:291-7.
110. Zargar A, Quan DN, Bentley WE. 2016. Enhancing Intercellular Coordination: Rewiring Quorum Sensing Networks for Increased Protein Expression through Autonomous Induction. ACS Synth Biol 5:923-8.
111. Wan X, Ho TYH, Wang B. 2019. Engineering Prokaryote Synthetic Biology Biosensors. Conference Proceedings.
112. van der Meer JR, Belkin S. 2010. Where microbiology meets microengineering: design and applications of reporter bacteria. Nat Rev Microbiol 8:511-22.
113. Steindler L, Venturi V. 2007. Detection of quorum-sensing N-acyl homoserine lactone signal molecules by bacterial biosensors. FEMS Microbiol Lett 266:1-9.
114. Bassler BL, Wright M, Silverman MR. 1994. Multiple signalling systems controlling expression of luminescence in Vibrio harveyi: sequence and function of genes encoding a second sensory pathway. Mol Microbiol 13:273-86.
115. Saurav K, Costantino V, Venturi V, Steindler L. 2017. Quorum Sensing Inhibitors from the Sea Discovered Using Bacterial N-acyl-homoserine Lactone-Based Biosensors. Mar Drugs 15.
116. Gamby S, Roy V, Guo M, Smith JA, Wang J, Stewart JE, Wang X, Bentley WE, Sintim HO. 2012. Altering the communication networks of multispecies microbial systems using a diverse toolbox of AI-2 analogues. ACS Chem Biol 7:1023-30.
117. Roy V, Adams BL, Bentley WE. 2011. Developing next generation antimicrobials by intercepting AI-2 mediated quorum sensing. Enzyme Microb Technol 49:113-23.
118. Roy V, Meyer MT, Smith JA, Gamby S, Sintim HO, Ghodssi R, Bentley WE. 2013. AI-2 analogs and antibiotics: a synergistic approach to reduce bacterial biofilms. Appl Microbiol Biotechnol 97:2627-38.
119. Zhang C, Parrello D, Brown PJB, Wall JD, Hu Z. 2018. A novel whole-cell biosensor of Pseudomonas aeruginosa to monitor the expression of quorum sensing genes. Appl Microbiol Biotechnol 102:6023-6038.
120. Saeidi N, Wong CK, Lo TM, Nguyen HX, Ling H, Leong SS, Poh CL, Chang MW. 2011. Engineering microbes to sense and eradicate Pseudomonas aeruginosa, a human pathogen. Mol Syst Biol 7:521.

121. Fletcher MP, Diggle SP, Camara M, Williams P. 2007. Biosensor-based assays for PQS, HHQ and related 2-alkyl-4-quinolone quorum sensing signal molecules. Nat Protoc 2:1254-62.
122. Ripp S, Jegier P, Birmele M, Johnson CM, Daumer KA, Garland JL, Sayler GS. 2006. Linking bacteriophage infection to quorum sensing signalling and bioluminescent bioreporter monitoring for direct detection of bacterial agents. J Appl Microbiol 100:488-99.
123. Stephens K, Zargar A, Emamian M, Abutaleb N, Choi E, Quan DN, Payne G, Bentley WE. 2019. Engineering Escherichia coli for enhanced sensitivity to the autoinducer-2 quorum sensing signal. Biotechnol Prog doi:10.1002/btpr.2881:e2881.
124. Hsu CY, Chen BK, Hu RH, Chen BS. 2016. Systematic Design of a Quorum Sensing-Based Biosensor for Enhanced Detection of Metal Ion in Escherichia Coli. IEEE Trans Biomed Circuits Syst 10:593-601.
125. Cai S, Shen Y, Zou Y, Sun P, Wei W, Zhao J, Zhang C. 2018. Engineering highly sensitive whole-cell mercury biosensors based on positive feedback loops from quorum-sensing systems. Analyst 143:630-634.
126. Ozbudak EM, Thattai M, Kurtser I, Grossman AD, van Oudenaarden A. 2002. Regulation of noise in the expression of a single gene. Nat Genet 31:69-73.
127. Elowitz MB, Levine AJ, Siggia ED, Swain PS. 2002. Stochastic gene expression in a single cell. Science 297:1183-6.
128. Servinsky MD, Terrell JL, Tsao CY, Wu HC, Quan DN, Zargar A, Allen PC, Byrd CM, Sund CJ, Bentley WE. 2016. Directed assembly of a bacterial quorum. ISME J 10:158-69.
129. Hwang IY, Tan MH, Koh E, Ho CL, Poh CL, Chang MW. 2014. Reprogramming microbes to be pathogen-seeking killers. ACS Synth Biol 3:228-37.
130. Hwang IY, Koh E, Wong A, March JC, Bentley WE, Lee YS, Chang MW. 2017. Engineered probiotic Escherichia coli can eliminate and prevent Pseudomonas aeruginosa gut infection in animal models. Nat Commun 8:15028.
131. Riangrungroj P, Polizzi KM. 2019. BeQuIK (Biosensor Engineered Quorum Induced Killing): designer bacteria for destroying recalcitrant biofilms. Microb Biotechnol doi:10.1111/1751-7915.13465.
132. Hoiby N, Bjarnsholt T, Moser C, Bassi GL, Coenye T, Donelli G, Hall-Stoodley L, Hola V, Imbert C, Kirketerp-Moller K, Lebeaux D, Oliver A, Ullmann AJ, Williams C, Biofilms ESGf, Consulting External Expert Werner Z. 2015. ESCMID guideline for the diagnosis and treatment of biofilm infections 2014. Clin Microbiol Infect 21 Suppl 1:S1-25.
133. Muyldermans S. 2013. Nanobodies: natural single-domain antibodies. Annu Rev Biochem 82:775-97.
134. Pawelek JM, Low KB, Bermudes D. 1997. Tumor-targeted Salmonella as a novel anticancer vector. Cancer Res 57:4537-44.
135. Ruder WC, Lu T, Collins JJ. 2011. Synthetic biology moving into the clinic. Science 333:1248-52.

136. Weber W, Fussenegger M. 2011. Emerging biomedical applications of synthetic biology. Nat Rev Genet 13:21-35.
137. Kasinskas RW, Forbes NS. 2006. Salmonella typhimurium specifically chemotax and proliferate in heterogeneous tumor tissue in vitro. Biotechnol Bioeng 94:710-21.
138. Ganai S, Arenas RB, Sauer JP, Bentley B, Forbes NS. 2011. In tumors Salmonella migrate away from vasculature toward the transition zone and induce apoptosis. Cancer Gene Ther 18:457-66.
139. Ganai S, Arenas RB, Forbes NS. 2009. Tumour-targeted delivery of TRAIL using Salmonella typhimurium enhances breast cancer survival in mice. Br J Cancer 101:1683-91.
140. Loeffler M, Le'Negrate G, Krajewska M, Reed JC. 2008. IL-18-producing Salmonella inhibit tumor growth. Cancer Gene Ther 15:787-94.
141. Swofford CA, Van Dessel N, Forbes NS. 2015. Quorum-sensing Salmonella selectively trigger protein expression within tumors. Proc Natl Acad Sci U S A 112:3457-62.
142. Davila ML, Riviere I, Wang X, Bartido S, Park J, Curran K, Chung SS, Stefanski J, Borquez-Ojeda O, Olszewska M, Qu J, Wasielewska T, He Q, Fink M, Shinglot H, Youssif M, Satter M, Wang Y, Hosey J, Quintanilla H, Halton E, Bernal Y, Bouhassira DC, Arcila ME, Gonen M, Roboz GJ, Maslak P, Douer D, Frattini MG, Giralt S, Sadelain M, Brentjens R. 2014. Efficacy and toxicity management of 19-28z CAR T cell therapy in B cell acute lymphoblastic leukemia. Sci Transl Med 6:224ra25.
143. Dang LH, Bettegowda C, Huso DL, Kinzler KW, Vogelstein B. 2001. Combination bacteriolytic therapy for the treatment of experimental tumors. Proc Natl Acad Sci U S A 98:15155-60.
144. Prindle A, Samayoa P, Razinkov I, Danino T, Tsimring LS, Hasty J. 2011. A sensing array of radically coupled genetic 'biopixels'. Nature 481:39-44.
145. Din MO, Danino T, Prindle A, Skalak M, Selimkhanov J, Allen K, Julio E, Atolia E, Tsimring LS, Bhatia SN, Hasty J. 2016. Synchronized cycles of bacterial lysis for in vivo delivery. Nature 536:81-85.
146. Wu HC, Tsao CY, Quan DN, Cheng Y, Servinsky MD, Carter KK, Jee KJ, Terrell JL, Zargar A, Rubloff GW, Payne GF, Valdes JJ, Bentley WE. 2013. Autonomous bacterial localization and gene expression based on nearby cell receptor density. Mol Syst Biol 9:636.
147. Soma Y, Hanai T. 2015. Self-induced metabolic state switching by a tunable cell density sensor for microbial isopropanol production. Metab Eng 30:7-15.
148. Kim EM, Woo HM, Tian T, Yilmaz S, Javidpour P, Keasling JD, Lee TS. 2017. Autonomous control of metabolic state by a quorum sensing (QS)-mediated regulator for bisabolene production in engineered E. coli. Metab Eng 44:325-336.
149. West SA, Griffin AS, Gardner A, Diggle SP. 2006. Social evolution theory for microorganisms. Nat Rev Microbiol 4:597-607.
150. Darch SE, West SA, Winzer K, Diggle SP. 2012. Density-dependent fitness benefits in quorum-sensing bacterial populations. Proc Natl Acad Sci U S A 109:8259-63.

151. De Vadder F, Grasset E, Manneras Holm L, Karsenty G, Macpherson AJ, Olofsson LE, Backhed F. 2018. Gut microbiota regulates maturation of the adult enteric nervous system via enteric serotonin networks. Proc Natl Acad Sci U S A 115:6458-6463.
152. Clemente JC, Ursell LK, Parfrey LW, Knight R. 2012. The impact of the gut microbiota on human health: an integrative view. Cell 148:1258-70.
153. Tsoi R, Dai Z, You L. 2019. Emerging strategies for engineering microbial communities. Biotechnol Adv doi:10.1016/j.biotechadv.2019.03.011.
154. Zargar A, Payne GF, Bentley WE. 2015. A 'bioproduction breadboard': programming, assembling, and actuating cellular networks. Curr Opin Biotechnol 36:154-60.
155. Brenner K, Karig DK, Weiss R, Arnold FH. 2007. Engineered bidirectional communication mediates a consensus in a microbial biofilm consortium. Proc Natl Acad Sci U S A 104:17300-4.
156. Balagadde FK, Song H, Ozaki J, Collins CH, Barnet M, Arnold FH, Quake SR, You L. 2008. A synthetic Escherichia coli predator-prey ecosystem. Mol Syst Biol 4:187.
157. McCardell RD, Huang S, Green LN, Murray RM. 2017. Control of bacterial population density with population feedback and molecular sequestration., abstr bioRxiv
158. Wu F, Lopatkin AJ, Needs DA, Lee CT, Mukherjee S, You L. 2019. A unifying framework for interpreting and predicting mutualistic systems. Nat Commun 10:242.
159. Wang EX, Liu Y, Ma Q, Dong XT, Ding MZ, Yuan YJ. 2019. Synthetic cell-cell communication in a three-species consortium for one-step vitamin C fermentation. Biotechnol Lett 41:951-961.
160. Hu B, Du J, Zou RY, Yuan YJ. 2010. An environment-sensitive synthetic microbial ecosystem. PLoS One 5:e10619.
161. Chen Y, Kim JK, Hirning AJ, Josic K, Bennett MR. 2015. SYNTHETIC BIOLOGY. Emergent genetic oscillations in a synthetic microbial consortium. Science 349:986-9.
162. Stephens K, Pozo M, Tsao C-Y, Hauk P, Bentley WE. 2019. Bacterial co-culture with cell signaling translator and growth controller modules for autonomously regulated culture composition. Nature Communications 10:4129.
163. Terrell JL, Wu HC, Tsao CY, Barber NB, Servinsky MD, Payne GF, Bentley WE. 2015. Nano-guided cell networks as conveyors of molecular communication. Nat Commun 6:8500.
164. Scott SR, Hasty J. 2016. Quorum Sensing Communication Modules for Microbial Consortia. ACS Synth Biol 5:969-77.
165. Kylilis N, Tuza ZA, Stan GB, Polizzi KM. 2018. Tools for engineering coordinated system behaviour in synthetic microbial consortia. Nat Commun 9:2677.
166. Marchand N, Collins CH. 2013. Peptide-based communication system enables Escherichia coli to Bacillus megaterium interspecies signaling. Biotechnol Bioeng 110:3003-12.

167. Stump SM, Johnson EC, Klausmeier CA. 2018. Local interactions and self-organized spatial patterns stabilize microbial cross-feeding against cheaters. J R Soc Interface 15.
168. Travisano M, Velicer GJ. 2004. Strategies of microbial cheater control. Trends Microbiol 12:72-8.
169. Diggle SP, Griffin AS, Campbell GS, West SA. 2007. Cooperation and conflict in quorum-sensing bacterial populations. Nature 450:411-4.
170. Sandoz KM, Mitzimberg SM, Schuster M. 2007. Social cheating in Pseudomonas aeruginosa quorum sensing. Proc Natl Acad Sci U S A 104:15876-81.
171. Wang M, Schaefer AL, Dandekar AA, Greenberg EP. 2015. Quorum sensing and policing of Pseudomonas aeruginosa social cheaters. Proc Natl Acad Sci U S A 112:2187-91.
172. Majerczyk C, Schneider E, Greenberg EP. 2016. Quorum sensing control of Type VI secretion factors restricts the proliferation of quorum-sensing mutants. Elife 5.
173. Hung DT, Shakhnovich EA, Pierson E, Mekalanos JJ. 2005. Small-molecule inhibitor of Vibrio cholerae virulence and intestinal colonization. Science 310:670-4.
174. Roy V, Smith JA, Wang J, Stewart JE, Bentley WE, Sintim HO. 2010. Synthetic analogs tailor native AI-2 signaling across bacterial species. J Am Chem Soc 132:11141-50.
175. Thompson JA, Oliveira RA, Djukovic A, Ubeda C, Xavier KB. 2015. Manipulation of the quorum sensing signal AI-2 affects the antibiotic-treated gut microbiota. Cell Rep 10:1861-71.
176. Hsiao A, Ahmed AM, Subramanian S, Griffin NW, Drewry LL, Petri WA, Jr., Haque R, Ahmed T, Gordon JI. 2014. Members of the human gut microbiota involved in recovery from Vibrio cholerae infection. Nature 515:423-6.
177. Kim S, Kerns SJ, Ziesack M, Bry L, Gerber GK, Way JC, Silver PA. 2018. Quorum Sensing Can Be Repurposed To Promote Information Transfer between Bacteria in the Mammalian Gut. ACS Synth Biol 7:2270-2281.
178. Hughes DT, Terekhova DA, Liou L, Hovde CJ, Sahl JW, Patankar AV, Gonzalez JE, Edrington TS, Rasko DA, Sperandio V. 2010. Chemical sensing in mammalian host-bacterial commensal associations. Proc Natl Acad Sci U S A 107:9831-6.
179. Gonzalez JF, Venturi V. 2013. A novel widespread interkingdom signaling circuit. Trends Plant Sci 18:167-74.
180. Zargar A, Quan DN, Carter KK, Guo M, Sintim HO, Payne GF, Bentley WE. 2015. Bacterial secretions of nonpathogenic Escherichia coli elicit inflammatory pathways: a closer investigation of interkingdom signaling. MBio 6:e00025.
181. Silpe JE, Bassler BL. 2019. A Host-Produced Quorum-Sensing Autoinducer Controls a Phage Lysis-Lysogeny Decision. Cell 176:268-280 e13.
182. Fernandes R, Bentley WE. 2009. AI-2 biosynthesis module in a magnetic nanofactory alters bacterial response via localized synthesis and delivery. Biotechnol Bioeng 102:390-9.

183. Fernandes R, Roy V, Wu HC, Bentley WE. 2010. Engineered biological nanofactories trigger quorum sensing response in targeted bacteria. Nat Nanotechnol 5:213-7.
184. Hebert CG, Gupta A, Fernandes R, Tsao CY, Valdes JJ, Bentley WE. 2010. Biological nanofactories target and activate epithelial cell surfaces for modulating bacterial quorum sensing and interspecies signaling. ACS Nano 4:6923-31.
185. Wu HC, Quan DN, Tsao CY, Liu Y, Terrell JL, Luo X, Yang JC, Payne GF, Bentley WE. 2017. Conferring biological activity to native spider silk: A biofunctionalized protein-based microfiber. Biotechnol Bioeng 114:83-95.
186. Lentini R, Martin NY, Forlin M, Belmonte L, Fontana J, Cornella M, Martini L, Tamburini S, Bentley WE, Jousson O, Mansy SS. 2017. Two-Way Chemical Communication between Artificial and Natural Cells. ACS Cent Sci 3:117-123.
187. Gordonov T, Kim E, Cheng Y, Ben-Yoav H, Ghodssi R, Rubloff G, Yin JJ, Payne GF, Bentley WE. 2014. Electronic modulation of biochemical signal generation. Nat Nanotechnol 9:605-10.
188. Finkel SE. 2006. Long-term survival during stationary phase: evolution and the GASP phenotype. Nat Rev Microbiol 4:113-20.
189. Lu J, Peng W, Lv Y, Jiang Y, Xu B, Zhang W, Zhou J, Dong W, Xin F, Jiang M. 2020. Application of Cell Immobilization Technology in Microbial Cocultivation Systems for Biochemicals Production. Industrial & Engineering Chemistry Research 59:17026-17034.
190. Diep E, Schiffman JD. 2023. Electrospinning Living Bacteria: A Review of Applications from Agriculture to Health Care. ACS Appl Bio Mater doi:10.1021/acsabm.2c01055.
191. Vallee A, Humblot V, Pradier CM. 2010. Peptide interactions with metal and oxide surfaces. Acc Chem Res 43:1297-306.
192. Acres RG, Feyer V, Tsud N, Carlino E, Prince KC. 2014. Mechanisms of Aggregation of Cysteine Functionalized Gold Nanoparticles. The Journal of Physical Chemistry C 118:10481-10487.
193. Saha K, Agasti SS, Kim C, Li X, Rotello VM. 2012. Gold nanoparticles in chemical and biological sensing. Chem Rev 112:2739-79.
194. Dong H, Sarkes DA, Rice JJ, Hurley MM, Fu AJ, Stratis-Cullum DN. 2018. Living Bacteria-Nanoparticle Hybrids Mediated through Surface-Displayed Peptides. Langmuir 34:5837-5848.
195. Li J, Wu S, Kim E, Yan K, Liu H, Liu C, Dong H, Qu X, Shi X, Shen J, Bentley WE, Payne GF. 2019. Electrobiofabrication: electrically based fabrication with biologically derived materials. Biofabrication 11:032002.
196. Leisk GG, Lo TJ, Yucel T, Lu Q, Kaplan DL. 2010. Electrogelation for protein adhesives. Adv Mater 22:711-5.
197. Maerten C, Jierry L, Schaaf P, Boulmedais F. 2017. Review of Electrochemically Triggered Macromolecular Film Buildup Processes and Their Biomedical Applications. ACS Appl Mater Interfaces 9:28117-28138.
198. Rydzek G, Jierry L, Parat A, Thomann JS, Voegel JC, Senger B, Hemmerle J, Ponche A, Frisch B, Schaaf P, Boulmedais F. 2011. Electrochemically

triggered assembly of films: a one-pot morphogen-driven buildup. Angew Chem Int Ed Engl 50:4374-7.
199. El-Maiss J, Cuccarese M, Maerten C, Lupattelli P, Chiummiento L, Funicello M, Schaaf P, Jierry L, Boulmedais F. 2018. Mussel-Inspired Electro-Cross-Linking of Enzymes for the Development of Biosensors. ACS Appl Mater Interfaces 10:18574-18584.
200. Muskovich M, Bettinger CJ. 2012. Biomaterials-based electronics: polymers and interfaces for biology and medicine. Adv Healthc Mater 1:248-66.
201. Bettinger CJ. 2018. Advances in Materials and Structures for Ingestible Electromechanical Medical Devices. Angew Chem Int Ed Engl 57:16946-16958.
202. Wu J, Cao L, Liu Y, Zheng A, Jiao D, Zeng D, Wang X, Kaplan DL, Jiang X. 2019. Functionalization of Silk Fibroin Electrospun Scaffolds via BMSC Affinity Peptide Grafting through Oxidative Self-Polymerization of Dopamine for Bone Regeneration. ACS Appl Mater Interfaces 11:8878-8895.
203. Zhang J, Skardal A, Prestwich GD. 2008. Engineered extracellular matrices with cleavable crosslinkers for cell expansion and easy cell recovery. Biomaterials 29:4521-31.
204. Joyner K, Song D, Hawkins RF, Silcott RD, Duncan GA. 2019. A rational approach to form disulfide linked mucin hydrogels. Soft Matter 15:9632-9639.
205. Horner M, Raute K, Hummel B, Madl J, Creusen G, Thomas OS, Christen EH, Hotz N, Gubeli RJ, Engesser R, Rebmann B, Lauer J, Rolauffs B, Timmer J, Schamel WWA, Pruszak J, Romer W, Zurbriggen MD, Friedrich C, Walther A, Minguet S, Sawarkar R, Weber W. 2019. Phytochrome-Based Extracellular Matrix with Reversibly Tunable Mechanical Properties. Adv Mater 31:e1806727.
206. Pinnaratip R, Bhuiyan MSA, Meyers K, Rajachar RM, Lee BP. 2019. Multifunctional Biomedical Adhesives. Adv Healthc Mater 8:e1801568.
207. Neish AS. 2013. Redox signaling mediated by the gut microbiota. Free Radic Res 47:950-7.
208. Neish AS, Jones RM. 2014. Redox signaling mediates symbiosis between the gut microbiota and the intestine. Gut Microbes 5:250-3.
209. Taran O, Patel V, Lynn DG. 2019. Small molecule reaction networks that model the ROS dynamics of the rhizosphere. Chem Commun (Camb) 55:3602-3605.
210. Faure D, Vereecke D, Leveau JHJ. 2009. Molecular communication in the rhizosphere. Plant and Soil 321:279-303.
211. Mendes R, Kruijt M, de Bruijn I, Dekkers E, van der Voort M, Schneider JH, Piceno YM, DeSantis TZ, Andersen GL, Bakker PA, Raaijmakers JM. 2011. Deciphering the rhizosphere microbiome for disease-suppressive bacteria. Science 332:1097-100.
212. Zhang W, Wang R, Sun Z, Zhu X, Zhao Q, Zhang T, Cholewinski A, Yang FK, Zhao B, Pinnaratip R, Forooshani PK, Lee BP. 2020. Catechol-functionalized hydrogels: biomimetic design, adhesion mechanism, and biomedical applications. Chem Soc Rev 49:433-464.

213. Silva TL, de Azevedo MdLSG, Ferreira FR, Santos DC, Amatore C, Goulart MOF. 2020. Quinone-based molecular electrochemistry and their contributions to medicinal chemistry: A look at the present and future. Current Opinion in Electrochemistry 24:79-87.
214. Kim HS, Ham HO, Son YJ, Messersmith PB, Yoo HS. 2013. Electrospun catechol-modified poly(ethyleneglycol) nanofibrous mesh for anti-fouling properties. Journal of Materials Chemistry B 1:3940-3949.
215. Aruffo A, Stamenkovic I, Melnick M, Underhill CB, Seed B. 1990. CD44 is the principal cell surface receptor for hyaluronate. Cell 61:1303-13.
216. Raoof JB, Ojani R, Amiri-Aref M, Chekin F. 2010. Catechol as an electrochemical indicator for voltammetric determination of N-acetyl-l-cysteine in aqueous media at the surface of carbon paste electrode. Journal of Applied Electrochemistry 40:1357-1363.
217. Lee PT, Compton RG. 2015. Selective electrochemical detection of thiol biomarkers in saliva using multiwalled carbon nanotube screen-printed electrodes. Sensors and Actuators B: Chemical 209:983-988.
218. Li WW, Heinze J, Haehnel W. 2005. Site-specific binding of quinones to proteins through thiol addition and addition-elimination reactions. J Am Chem Soc 127:6140-1.
219. Ichitani M, Okumura H, Nakashima Y, Kinugasa H, Honda M, Kunimoto K-K. 2018. Spectroscopic characterization of thiol adducts formed in the reaction of 4-methylcatechol with DPPH in the presence of N-acetylcysteine. European Journal of Chemistry 9:386-393.
220. Manini P, Napolitano A, Westerhof W, Riley PA, d'Ischia M. 2009. A reactive ortho-quinone generated by tyrosinase-catalyzed oxidation of the skin depigmenting agent monobenzone: self-coupling and thiol-conjugation reactions and possible implications for melanocyte toxicity. Chem Res Toxicol 22:1398-405.
221. Menyo MS, Hawker CJ, Waite JH. 2013. Versatile tuning of supramolecular hydrogels through metal complexation of oxidation-resistant catechol-inspired ligands. Soft Matter 9.
222. Mijangos F, Varona F, Villota N. 2006. Changes in solution color during phenol oxidation by Fenton reagent. Environ Sci Technol 40:5538-43.
223. Kim E, Liu Y, Baker CJ, Owens R, Xiao S, Bentley WE, Payne GF. 2011. Redox-cycling and H2O2 generation by fabricated catecholic films in the absence of enzymes. Biomacromolecules 12:880-8.
224. Rhee SG. 2006. Cell signaling. H2O2, a necessary evil for cell signaling. Science 312:1882-3.
225. Virgile C, Hauk P, Wu HC, Shang W, Tsao CY, Payne GF, Bentley WE. 2018. Engineering bacterial motility towards hydrogen-peroxide. PLoS One 13:e0196999.
226. Saunders SH, Tse ECM, Yates MD, Otero FJ, Trammell SA, Stemp EDA, Barton JK, Tender LM, Newman DK. 2020. Extracellular DNA Promotes Efficient Extracellular Electron Transfer by Pyocyanin in Pseudomonas aeruginosa Biofilms. Cell 182:919-932 e19.

227. Costa KC, Glasser NR, Conway SJ, Newman DK. 2017. Pyocyanin degradation by a tautomerizing demethylase inhibits Pseudomonas aeruginosa biofilms. Science 355:170-173.
228. Glasser NR, Saunders SH, Newman DK. 2017. The Colorful World of Extracellular Electron Shuttles. Annu Rev Microbiol 71:731-751.
229. Lemire J, Alhasawi A, Appanna VP, Tharmalingam S, Appanna VD. 2017. Metabolic defence against oxidative stress: the road less travelled so far. J Appl Microbiol 123:798-809.
230. Rada B, Leto TL. 2013. Pyocyanin effects on respiratory epithelium: relevance in Pseudomonas aeruginosa airway infections. Trends Microbiol 21:73-81.
231. VanArsdale E, Pitzer J, Wang S, Stephens K, Chen CY, Payne GF, Bentley WE. 2022. Electrogenetic Signal Transmission and Propagation in Coculture to Guide Production of a Small Molecule, Tyrosine. ACS Synth Biol 11:877-887.
232. Li J, Wang SP, Zong G, Kim E, Tsao C-Y, VanArsdale E, Wang L-X, Bentley WE, Payne GF. 2021. Interactive Materials for Bidirectional Redox-Based Communication. Advanced Materials 33:2007758.
233. Wu G, Yan Q, Jones JA, Tang YJ, Fong SS, Koffas MAG. 2016. Metabolic Burden: Cornerstones in Synthetic Biology and Metabolic Engineering Applications. Trends Biotechnol 34:652-664.
234. Shang W, Liu Y, Kim E, Tsao CY, Payne GF, Bentley WE. 2018. Selective assembly and functionalization of miniaturized redox capacitor inside microdevices for microbial toxin and mammalian cell cytotoxicity analyses. Lab Chip 18:3578-3587.
235. Shin M, Lim J, An J, Yoon J, Choi JW. 2023. Nanomaterial-based biohybrid hydrogel in bioelectronics. Nano Converg 10:8.
236. Liu H, Qu X, Kim E, Lei M, Dai K, Tan X, Xu M, Li J, Liu Y, Shi X, Li P, Payne GF, Liu C. 2018. Bio-inspired redox-cycling antimicrobial film for sustained generation of reactive oxygen species. Biomaterials 162:109-122.
237. Napolitano A, Panzella L, Monfrecola G, d'Ischia M. 2014. Pheomelanin-induced oxidative stress: bright and dark chemistry bridging red hair phenotype and melanoma. Pigment Cell Melanoma Res 27:721-33.
238. Panzella L, Leone L, Greco G, Vitiello G, D'Errico G, Napolitano A, d'Ischia M. 2014. Red human hair pheomelanin is a potent pro-oxidant mediating UV-independent contributory mechanisms of melanomagenesis. Pigment Cell Melanoma Res 27:244-52.
239. Kimple ME, Brill AL, Pasker RL. 2013. Overview of affinity tags for protein purification. Curr Protoc Protein Sci 73:9 9 1-9 9 23.
240. Terpe K. 2003. Overview of tag protein fusions: from molecular and biochemical fundamentals to commercial systems. Appl Microbiol Biotechnol 60:523-33.
241. Wu HC, Shi XW, Tsao CY, Lewandowski AT, Fernandes R, Hung CW, DeShong P, Kobatake E, Valdes JJ, Payne GF, Bentley WE. 2009. Biofabrication of antibodies and antigens via IgG-binding domain engineered with activatable pentatyrosine pro-tag. Biotechnol Bioeng 103:231-40.

242. Wu SR, Chen JL, Wu HC. 2020. Biofabricating a Silk Scaffold as a Functional Microbial Trap. ACS Biomater Sci Eng 6:7041-7050.
243. Liu Y, Wu HC, Chhuan M, Terrell JL, Tsao CY, Bentley WE, Payne GF. 2015. Functionalizing Soft Matter for Molecular Communication. ACS Biomater Sci Eng 1:320-328.
244. Bhokisham N, Liu Y, Brown AD, Payne GF, Culver JN, Bentley WE. 2020. Transglutaminase-mediated assembly of multi-enzyme pathway onto TMV brush surfaces for synthesis of bacterial autoinducer-2. Biofabrication 12:045017.
245. Tamerler C, Duman M, Oren EE, Gungormus M, Xiong X, Kacar T, Parviz BA, Sarikaya M. 2006. Materials specificity and directed assembly of a gold-binding peptide. Small 2:1372-8.
246. Sedlak RH, Hnilova M, Grosh C, Fong H, Baneyx F, Schwartz D, Sarikaya M, Tamerler C, Traxler B. 2012. Engineered Escherichia coli silver-binding periplasmic protein that promotes silver tolerance. Appl Environ Microbiol 78:2289-96.
247. Zhou S, Huang W, Belton DJ, Simmons LO, Perry CC, Wang X, Kaplan DL. 2015. Control of silicification by genetically engineered fusion proteins: silk-silica binding peptides. Acta Biomater 15:173-80.
248. Kim SG, Min WK, Rho YT, Seo JH. 2012. Electrostatic interaction-induced inclusion body formation of glucagon-like peptide-1 fused with ubiquitin and cationic tag. Protein Expr Purif 84:38-46.
249. Lilie H, Richter S, Bergelt S, Frost S, Gehle F. 2013. Polyionic and cysteine-containing fusion peptides as versatile protein tags. Biol Chem 394:995-1004.
250. Li J, Kim E, Gray KM, Conrad C, Tsao C-Y, Wang SP, Zong G, Scarcelli G, Stroka KM, Wang L-X, Bentley WE, Payne GF. 2020. Mediated Electrochemistry to Mimic Biology's Oxidative Assembly of Functional Matrices. Advanced Functional Materials 30:2001776.
251. Motabar D, Li J, Wang S, Tsao CY, Tong X, Wang LX, Payne GF, Bentley WE. 2021. Simple, rapidly electroassembled thiolated PEG-based sensor interfaces enable rapid interrogation of antibody titer and glycosylation. Biotechnol Bioeng 118:2744-2758.
252. Kiedzierska A, Czepczynska H, Smietana K, Otlewski J. 2008. Expression, purification and crystallization of cysteine-rich human protein muskelin in Escherichia coli. Protein Expr Purif 60:82-8.
253. Singh A, Upadhyay V, Upadhyay AK, Singh SM, Panda AK. 2015. Protein recovery from inclusion bodies of Escherichia coli using mild solubilization process. Microb Cell Fact 14:41.
254. Ban B, Sharma M, Shetty J. 2020. Optimization of Methods for the Production and Refolding of Biologically Active Disulfide Bond-Rich Antibody Fragments in Microbial Hosts. Antibodies (Basel) 9.
255. Bentley WE, Mirjalili N, Andersen DC, Davis RH, Kompala DS. 1990. Plasmid-encoded protein: the principal factor in the "metabolic burden" associated with recombinant bacteria. Biotechnol Bioeng 35:668-81.

256. Ramirez DM, Bentley WE. 1995. Fed-batch feeding and induction policies that improve foreign protein synthesis and stability by avoiding stress responses. Biotechnol Bioeng 47:596-608.
257. DeLisa MP, Valdes JJ, Bentley WE. 2001. Mapping stress-induced changes in autoinducer AI-2 production in chemostat-cultivated Escherichia coli K-12. J Bacteriol 183:2918-28.
258. Harcum SW, Bentley WE. 1993. Response dynamics of 26-, 34-, 39-, 54-, and 80-kDa proteases in induced cultures of recombinant Escherichia coli. Biotechnol Bioeng 42:675-85.
259. Wang S, Payne GF, Bentley WE. 2020. Quorum Sensing Communication: Molecularly Connecting Cells, Their Neighbors, and Even Devices. Annu Rev Chem Biomol Eng 11:447-468.
260. Xavier KB, Miller ST, Lu W, Kim JH, Rabinowitz J, Pelczer I, Semmelhack MF, Bassler BL. 2007. Phosphorylation and processing of the quorum-sensing molecule autoinducer-2 in enteric bacteria. ACS Chem Biol 2:128-36.
261. Vendeville A, Winzer K, Heurlier K, Tang CM, Hardie KR. 2005. Making 'sense' of metabolism: autoinducer-2, LuxS and pathogenic bacteria. Nat Rev Microbiol 3:383-96.
262. Tsao CY, Wang L, Hashimoto Y, Yi H, March JC, DeLisa MP, Wood TK, Valdes JJ, Bentley WE. 2011. LuxS coexpression enhances yields of recombinant proteins in Escherichia coli in part through posttranscriptional control of GroEL. Appl Environ Microbiol 77:2141-52.
263. Bessette PH, Aslund F, Beckwith J, Georgiou G. 1999. Efficient folding of proteins with multiple disulfide bonds in the Escherichia coli cytoplasm. Proc Natl Acad Sci U S A 96:13703-8.
264. Faulkner MJ, Veeravalli K, Gon S, Georgiou G, Beckwith J. 2008. Functional plasticity of a peroxidase allows evolution of diverse disulfide-reducing pathways. Proc Natl Acad Sci U S A 105:6735-40.
265. Becker-Hapak M, Eisenstark A. 1995. Role of rpoS in the regulation of glutathione oxidoreductase (gor) in Escherichia coli. FEMS Microbiol Lett 134:39-44.
266. Seaver LC, Imlay JA. 2001. Alkyl hydroperoxide reductase is the primary scavenger of endogenous hydrogen peroxide in Escherichia coli. J Bacteriol 183:7173-81.
267. Storz G, Tartaglia LA, Ames BN. 1990. Transcriptional regulator of oxidative stress-inducible genes: direct activation by oxidation. Science 248:189-94.
268. Gonzalez-Flecha B, Demple B. 1999. Role for the oxyS gene in regulation of intracellular hydrogen peroxide in Escherichia coli. J Bacteriol 181:3833-6.
269. Lee JM, Park HK, Jung Y, Kim JK, Jung SO, Chung BH. 2007. Direct immobilization of protein g variants with various numbers of cysteine residues on a gold surface. Anal Chem 79:2680-7.
270. Marques JC, Lamosa P, Russell C, Ventura R, Maycock C, Semmelhack MF, Miller ST, Xavier KB. 2011. Processing the interspecies quorum-sensing signal autoinducer-2 (AI-2): characterization of phospho-(S)-4,5-dihydroxy-2,3-pentanedione isomerization by LsrG protein. J Biol Chem 286:18331-43.

271. Marques JC, Oh IK, Ly DC, Lamosa P, Ventura MR, Miller ST, Xavier KB. 2014. LsrF, a coenzyme A-dependent thiolase, catalyzes the terminal step in processing the quorum sensing signal autoinducer-2. Proc Natl Acad Sci U S A 111:14235-40.
272. Di Felice R, Selloni A, Molinari E. 2003. DFT Study of Cysteine Adsorption on Au(111). The Journal of Physical Chemistry B 107:1151-1156.
273. Varshavsky A. 2019. N-degron and C-degron pathways of protein degradation. Proc Natl Acad Sci U S A 116:358-366.
274. Studier FW. 2014. Stable expression clones and auto-induction for protein production in E. coli. Methods Mol Biol 1091:17-32.
275. Gonzalez-Flecha B, Demple B. 1997. Homeostatic regulation of intracellular hydrogen peroxide concentration in aerobically growing Escherichia coli. J Bacteriol 179:382-8.
276. Thomas JA, Mallis RJ. 2001. Aging and oxidation of reactive protein sulfhydryls. Exp Gerontol 36:1519-26.
277. Tanaka G, Funabashi H, Mie M, Kobatake E. 2006. Fabrication of an antibody microwell array with self-adhering antibody binding protein. Anal Biochem 350:298-303.
278. Datsenko KA, Wanner BL. 2000. One-step inactivation of chromosomal genes in Escherichia coli K-12 using PCR products. Proc Natl Acad Sci U S A 97:6640-5.
279. Stephens K, Zakaria FR, VanArsdale E, Payne GF, Bentley WE. 2021. Electronic signals are electrogenetically relayed to control cell growth and co-culture composition. Metab Eng Commun 13:e00176.
280. Sultana ST, Atci E, Babauta JT, Falghoush AM, Snekvik KR, Call DR, Beyenal H. 2015. Electrochemical scaffold generates localized, low concentration of hydrogen peroxide that inhibits bacterial pathogens and biofilms. Sci Rep 5:14908.
281. Wang S, Payne GF, Bentley WE. 2022. Quorum sensing componentry opens new lines of communication. EMBO J 41:e112162.
282. Surette MG, Miller MB, Bassler BL. 1999. Quorum sensing in *Escherichia coli, Salmonella typhimurium*, and *Vibrio harveyi*: a new family of genes responsible for autoinducer production. Proc Natl Acad Sci U S A 96:1639-44.
283. Altuvia S, Zhang A, Argaman L, Tiwari A, Storz G. 1998. The Escherichia coli OxyS regulatory RNA represses fhlA translation by blocking ribosome binding. EMBO J 17:6069-75.
284. De Lay N, Gottesman S. 2012. A complex network of small non-coding RNAs regulate motility in Escherichia coli. Mol Microbiol 86:524-38.
285. McCarty NS, Graham AE, Studena L, Ledesma-Amaro R. 2020. Multiplexed CRISPR technologies for gene editing and transcriptional regulation. Nat Commun 11:1281.
286. Liao C, Ttofali F, Slotkowski RA, Denny SR, Cecil TD, Leenay RT, Keung AJ, Beisel CL. 2019. Modular one-pot assembly of CRISPR arrays enables library generation and reveals factors influencing crRNA biogenesis. Nat Commun 10:2948.

287. Barrangou R, Fremaux C, Deveau H, Richards M, Boyaval P, Moineau S, Romero DA, Horvath P. 2007. CRISPR provides acquired resistance against viruses in prokaryotes. Science 315:1709-12.
288. Deltcheva E, Chylinski K, Sharma CM, Gonzales K, Chao Y, Pirzada ZA, Eckert MR, Vogel J, Charpentier E. 2011. CRISPR RNA maturation by trans-encoded small RNA and host factor RNase III. Nature 471:602-7.
289. Chalfie M, Tu Y, Euskirchen G, Ward WW, Prasher DC. 1994. Green fluorescent protein as a marker for gene expression. Science 263:802-5.
290. March JC, Rao G, Bentley WE. 2003. Biotechnological applications of green fluorescent protein. Appl Microbiol Biotechnol 62:303-15.
291. VanArsdale E, Navid A, Chu MJ, Halvorsen TM, Payne GF, Jiao Y, Bentley WE, Yung MC. 2023. Electrogenetic signaling and information propagation for controlling microbial consortia via programmed lysis. Biotechnol Bioeng doi:10.1002/bit.28337.
292. Gargalo CL, Udugama I, Pontius K, Lopez PC, Nielsen RF, Hasanzadeh A, Mansouri SS, Bayer C, Junicke H, Gernaey KV. 2020. Towards smart biomanufacturing: a perspective on recent developments in industrial measurement and monitoring technologies for bio-based production processes. J Ind Microbiol Biotechnol 47:947-964.
293. Akyildiz IF, Pierobon M, Balasubramaniam S, Koucheryavy Y. 2015. The internet of Bio-Nano things. IEEE Communications Magazine 53:32-40.
294. Krawczyk K, Xue S, Buchmann P, Charpin-El-Hamri G, Saxena P, Hussherr MD, Shao J, Ye H, Xie M, Fussenegger M. 2020. Electrogenetic cellular insulin release for real-time glycemic control in type 1 diabetic mice. Science 368:993-1001.
295. Senturk S, Kok I, Şentürk F. 2022. Internet of Nano, Bio-Nano, Biodegradable and Ingestible Things: A Survey. ArXiv abs/2202.12409.
296. Afridi MS, Fakhar A, Kumar A, Ali S, Medeiros FHV, Muneer MA, Ali H, Saleem M. 2022. Harnessing microbial multitrophic interactions for rhizosphere microbiome engineering. Microbiol Res 265:127199.
297. Lindsay A, Ahmer BM. 2005. Effect of sdiA on biosensors of N-acylhomoserine lactones. J Bacteriol 187:5054-8.
298. Bikard D, Jiang W, Samai P, Hochschild A, Zhang F, Marraffini LA. 2013. Programmable repression and activation of bacterial gene expression using an engineered CRISPR-Cas system. Nucleic Acids Res 41:7429-37.
299. Sunwoo SH, Ha KH, Lee S, Lu N, Kim DH. 2021. Wearable and Implantable Soft Bioelectronics: Device Designs and Material Strategies. Annu Rev Chem Biomol Eng 12:359-391.
300. Paulsen CE, Carroll KS. 2013. Cysteine-mediated redox signaling: chemistry, biology, and tools for discovery. Chem Rev 113:4633-79.